THE
BENDIX
CORPORATION

GUIDANCE SYSTEMS
DIVISION
DENVER OPERATIONS

Prepared by:

The Guidance and Control Group
The Bendix Corporation

Approved by:

S. Calvin Rybak
Program Manager

O. Taylor
Technical Manager

M. Brown
Manager,
Denver Operations

FLOATED PALLET DEFINITION STUDY

FINAL REPORT

MAY 1975

VOLUME I
EVALUATION OF ALTERNATE TELESCOPE POINTING SCHEMES

PREPARED FOR:

GEORGE C. MARSHALL
SPACE FLIGHT CENTER
HUNTSVILLE, ALABAMA

NASA CONTRACT NO.
NAS8-30889

FOREWORD

This final report is submitted in accordance with the requirements of NASA-GSFC, Contract No. NAS8-30889. The report includes:

Volume I - Evaluation of Alternate Telescope Pointing Schemes

Volume II - Suspended Pallet Pointing Performance Study

Volume III - Retention/Suspension Systems, Pallet Common Module Configuration Study

Volume IV - Summary Volume

CONTENTS

CONTENTS (Continued)

CONTENTS (Concluded)

1. INTRODUCTION

With the maturation of the space shuttle concept of a reusable launch vehicle for earth orbital missions, two divergent modes of operation have been defined. One mode involves the use of the shuttle as a logistics vehicle placing free flying experiment packages in orbit and replacing, repairing or servicing existing packages. In addition it will perform a crucial role as a manned experiment base, remaining in earth orbit from 7 to 30 days performing various experiments with equipment mounted in the payload bay.

Current assessments of the experiments proposed for operation in low earth orbit in conjunction with a manned vehicle indicate that nearly 45 percent of the payloads require pointing accuracy greater than that afforded by the orbiter capability using the Reaction Control System (RCS). It is therefore apparent that a second level of control or alternately, an Instrument Pointing System (IPS), is required to meet the precise pointing accuracies required by a substantial percentage of experiments that can fly on the orbiter.

There are presently three concepts that have been proposed for the Instrument Pointing System. They are the Inside-Out Gimbal (IOG) system proposed by the European Spacelab project, the Standard Experiment Pointing Base (SEPB), and the Floated Pallet. The latter two concepts were developed by Marshall Space Flight Center (MSFC) personnel. The purpose of this portion of the study is to evaluate the operation of these three concepts and to determine the relative advantages and disadvantages of the three proposed Instrument Pointing Systems. Of particular interest was the effect of structural flexibility on the performance of each of the proposed concepts. The approach taken in evaluating these effects was to assure a rigid structure for determining the control loop bandwidths and other system parameters (i.e., suspension characteristics, sensor characteristics, etc.) required to meet a pointing stability performance of ± 1 $\widehat{\text{sec}}$ for all of the proposed systems in the presence of crew motion disturbances. Crew motion disturbances are projected to be the most severe disturbance presented to the IPS. Once these parameters were identified, structural flexibility was inserted and its effect on overall system stability and performance was determined for each of the proposed concepts.

This volume (one of four) describes the results and the conclusions obtained during this portion of the study. The computer models used are presented in great detail in order to make the reader aware of the assumptions made and the implied limitations of the results obtained and described in this volume.

2. MODEL DESCRIPTION

Two modes of Instrument Pointing System operation were investigated from the standpoint of stability and performance. These were the pointing and slewing modes. In order to investigate these two modes of system operation two mathematical models were defined, one for use in system pointing performance evaluations, the other to be used to determine the slewing capability and performance of the IOG.

The mathematical model employed for the determination of system pointing performance is linear consisting of six bodies. These bodies are distributed in the following manner: one body represents the orbiter; two bodies represent the pallet; one body represents a gimbal base or pedestal; one body represents the inner gimbal or inertial gimbal of a proposed gimballing system; one body represents the telescope or instrument to be pointed. Features of this model include the following:

a. Six degree of freedom suspension dynamics between pallet and orbiter.

b. Pallet flexibility.

c. Six degree of freedom suspension dynamics between the pallet and the gimbal pedestal.

d. Gimbal and telescope interface flexibility.

e. Sensor and actuator dynamics.

By proper initialization this model can be made to represent any of the three (i.e., IOG, SEPB, or Floated Pallet) IPS evaluated during the course of this study. A schematic representation of the linear pointing performance model is shown in figure 2-1.

The slewing model is nonlinear and consists of three bodies. One body represents the orbiter and pallet, the second represents the gimbal pedestal, and the third represents the telescope inner gimbal plus instrument. Features of this model include the following:

a. Full strapdown equations of motion for the telescope.

b. Nonlinear Euler terms due to telescope motion.

c. Six degree of freedom suspension dynamics between pallet and gimbal pedestal.

d. Quaternion type slew command logic.

e. Sensor and actuator dynamics.

A schematic representation of the slewing model is shown in figure 2-2.

In the paragraphs that follow the mathematical derivation of both the pointing performance and slewing models will be outlined.

2.1 Linear Pointing Performance Model

2.1.1 Translational Equations of Motion - Referring to figure 2-3 the following translational equations of motion can be written for the six bodies depicted.

$$F_{1e}+F_{c12}=m_1\ddot{\rho}_1 \tag{1}$$

$$F_{2e}-F_{c12}+F_{c23}=m_2\ddot{\rho}_2 \tag{2}$$

$$F_{3e}-F_{c23}+F_{c34}=m_3\ddot{\rho}_3 \tag{3}$$

$$F_{4e}-F_{c34}+F_H=m_4\ddot{\rho}_4 \tag{4}$$

$$F_{5e}-F_H+F_I=m_5\ddot{\rho}_5 \tag{5}$$

$$F_{6e}-F_I=m_6\ddot{\rho}_6 \tag{6}$$

where:

$F_{je}(j=1,\ldots,6)$ = external forces applied to bodies 1 thru 6 respectively

$F_{c12}, F_{c23}, F_{c34}$ = compliance forces between bodies 1 and 2, 2 and 3, and 3 and 4, respectively

F_H = hinge force between bodies 4 and 5

F_I = interface force between bodies 5 and 6

$m_j(j=1,\ldots,6)$ = mass of bodies 1 thru 6

$\rho_j(j=1,\ldots,6)$ = distance from origin of arbitrary inertial coordinate frame to center of mass of bodies 1 thru 6

In addition the following equation applies

$$\sum_{j=1}^{6} F_{je} = M\ddot{\rho}_o \tag{7}$$

where:

$$M = \sum_{j=1}^{6} m_j \tag{8}$$

and

ρ_o = distance from origin of arbitrary inertial coordinate frame to the composite center of mass of the system shown in figure 2-3.

Examination of figure 2-3 allows the following geometrical relationship to be written for the six bodies depicted.

$$\rho_j = \rho_o + R_j \quad j=1,\ldots,6 \tag{9}$$

where:

R_j = distance from composite center of mass to the center of mass of bodies 1 thru 6

Additionally from geometric considerations

$$R_2 = R_1 + R_{120} + \varepsilon_{12} \tag{10}$$

$$R_3 = R_1 + R_{120} + \varepsilon_{12} + R_{230} + \varepsilon_{23} \tag{11}$$

$$R_4 = R_1 + R_{120} + \varepsilon_{12} + R_{230} + \varepsilon_{23} + R_{340} + \varepsilon_{34} \tag{12}$$

$$R_5 = R_1 + R_{120} + \varepsilon_{12} + R_{230} + \varepsilon_{23} + R_{340} + \varepsilon_{34} + r_1 + r_2 \tag{13}$$

$$R_6 = R_1 + R_{120} + \varepsilon_{12} + R_{230} + \varepsilon_{23} + R_{340} + \varepsilon_{34} + r_1 + r_2 + r_3 + r_4 \tag{14}$$

From the definition of the system composite CM the following results

$$\sum_{j=1}^{6} m_j R_j = 0 \tag{15}$$

where:

R_{120} = inertially fixed vector directed from the CM of body 1 to body 2 when the system is in an unstressed state

R_{230} = inertially fixed vector directed from the CM of body 2 to the CM of body 3 when the system is in an unstressed state

R_{340} = inertially fixed vector directed from the CM of body 3 to the CM of body 4 when the system is in an unstressed state

ε_{12} = relative linear displacement between bodies 1 and 2 measured with respect to R_{120}

ε_{23} = relative linear displacement between bodies 2 and 3 measured with respect to R_{230}

ε_{34} = relative linear displacement between bodies 3 and 4 measured with respect to R_{340}

Substituting equations (10) thru (13) into equation (15) keeping in mind the R_{120}, R_{230}, and R_{340} are inertially fixed vectors yields the following

$$\ddot{R}_1 = -\frac{1}{M}\left[(m_2+m_3+m_4+m_5+m_6)\ddot{\varepsilon}_{12}+(m_3+m_4+m_5+m_6)\ddot{\varepsilon}_{23}+(m_4+m_5+m_6)\ddot{\varepsilon}_{34} + (m_5+m_6)(\ddot{r}_1+\ddot{r}_2)+m_6(\ddot{r}_3+\ddot{r}_4)\right] \tag{16}$$

Substituting equations (10) thru (13) in conjunction with equation (16) into equation (9) gives

$$\ddot{\rho}_1 = \frac{1}{M}\left\{\sum_{j=1}^{6} F_{je} - \left[(m_2+m_3+m_4+m_5+m_6)\ddot{\varepsilon}_{12}+(m_3+m_4+m_5+m_6)\ddot{\varepsilon}_{23}+(m_4+m_5+m_6)\ddot{\varepsilon}_{34} + (m_5+m_6)(\ddot{r}_1+\ddot{r}_2)+m_6(\ddot{r}_3+\ddot{r}_4)\right]\right\} \tag{17}$$

$$\ddot{\rho}_2 = \frac{1}{M}\left\{\sum_{j=1}^{6} F_{je} + m_1\ddot{\varepsilon}_{12} - (m_3+m_4+m_5+m_6)\ddot{\varepsilon}_{23} - (m_4+m_5+m_6)\ddot{\varepsilon}_{34} - (m_5+m_6)(\ddot{r}_1+\ddot{r}_2) - m_6(\ddot{r}_3+\ddot{r}_4)\right\} \tag{18}$$

$$\ddot{\rho}_3 = \frac{1}{M}\left\{\sum_{j=1}^{6} F_{je} + m_1\ddot{\varepsilon}_{12} + (m_1+m_2)\ddot{\varepsilon}_{23} - (m_4+m_5+m_6)\ddot{\varepsilon}_{34} - (m_5+m_6)(\ddot{r}_1+\ddot{r}_2) - m_6(\ddot{r}_3+\ddot{r}_4)\right\} \tag{19}$$

$$\ddot{\rho}_4 = \frac{1}{M}\left\{\sum_{j=1}^{6} F_{je} + m_1\ddot{\varepsilon}_{12} + (m_1+m_2)\ddot{\varepsilon}_{23} + (m_1+m_2+m_3)\ddot{\varepsilon}_{34} - (m_5+m_6)(\ddot{r}_1+\ddot{r}_2) - m_6(\ddot{r}_3+\ddot{r}_4)\right\} \tag{20}$$

$$\ddot{\rho}_5 = \frac{1}{M}\left\{\sum_{j=1}^{6} F_{je} + m_1\ddot{\varepsilon}_{12} + (m_1+m_2)\ddot{\varepsilon}_{23} + (m_1+m_2+m_3)\ddot{\varepsilon}_{34} + (m_1+m_2+m_3+m_4)(\ddot{r}_1+\ddot{r}_2) - m_6(\ddot{r}_3+\ddot{r}_4)\right\} \tag{21}$$

$$\ddot{\rho}_6 = \frac{1}{M}\left\{\sum_{j=1}^{6} F_{je} + m_1\ddot{\varepsilon}_{12} + (m_1+m_2)\ddot{\varepsilon}_{23} + (m_1+m_2+m_3)\ddot{\varepsilon}_{34} + (m_1+m_2+m_3+m_4)(\ddot{r}_1+\ddot{r}_2) + (m_1+m_2+m_3+m_4+m_5)(\ddot{r}_3+\ddot{r}_4)\right\} \tag{22}$$

Substitution of equation (22) into equation (6) yields

$$F_I = \frac{1}{M}\left\{(m_1+m_2+m_3+m_4+m_5)F_{6e} - m_6(F_{1e}+F_{2e}+F_{3e}+F_{4e}+F_{5e}) - m_1m_6\ddot{\varepsilon}_{12} - m_6(m_1+m_2)\ddot{\varepsilon}_{23} - m_6(m_1+m_2+m_3)\ddot{\varepsilon}_{34} - m_6(m_1+m_2+m_3+m_4)(\ddot{r}_1+\ddot{r}_2) - m_6(m_1+m_2+m_3+m_4+m_5)(\ddot{r}_3+\ddot{r}_4)\right\} \tag{23}$$

Substitution of equations (21) and (23) into equation (5) results in

$$F_H = \frac{1}{M}\left\{(m_1+m_2+m_3+m_4)(F_{5e}+F_{6e}) - (m_5+m_6)(F_{1e}+F_{2e}+F_{3e}+F_{4e}) - m_1(m_5+m_6)\ddot{\varepsilon}_{12} - (m_1+m_2)(m_5+m_6)\ddot{\varepsilon}_{23} - (m_1+m_2+m_3)(m_5+m_6)\ddot{\varepsilon}_{34} - (m_1+m_2+m_3+m_4)(m_5+m_6)(\ddot{r}_1+\ddot{r}_2) - m_6(m_1+m_2+m_3+m_4)(\ddot{r}_3+\ddot{r}_4)\right\} \tag{24}$$

It now becomes necessary to specify the compliance forces that act on the various bodies which will then result in the complete specification of the linear equations of motion of the six body system shown in figure 2-3.

The compliance force between bodies 1 and 2 can be written as

$$F_{c12}=K_{12}\cdot\left[\varepsilon_{12}+(\beta^{12}_{12}-\beta^{12}_{120})-(\beta^{12}_{11}-\beta^{12}_{110})\right]+K_{12}\cdot\left[\varepsilon_{12}+(\beta^{12}_{22}-\beta^{12}_{220})-(\beta^{12}_{21}-\beta^{12}_{210})\right]$$
$$+K_{12}\cdot\left[\varepsilon_{12}+(\beta^{12}_{32}-\beta^{12}_{320})-(\beta^{12}_{31}-\beta^{12}_{310})\right]+K_{12}\cdot\left[\varepsilon_{12}+(\beta^{12}_{42}-\beta^{12}_{420})-(\beta^{12}_{41}-\beta^{12}_{410})\right]$$
$$+D_{12}\cdot\left[\dot{\varepsilon}_{12}+\dot{\beta}^{12}_{12}-\dot{\beta}^{12}_{11}\right]+D_{12}\cdot\left[\dot{\varepsilon}_{12}+\dot{\beta}^{12}_{22}-\dot{\beta}^{12}_{21}\right]+D_{12}\cdot\left[\dot{\varepsilon}_{12}+\dot{\beta}^{12}_{32}-\dot{\beta}^{12}_{31}\right]$$
$$+D_{12}\cdot\left[\dot{\varepsilon}_{12}+\dot{\beta}^{12}_{42}-\dot{\beta}^{12}_{41}\right] \qquad (25)$$

where:

$\beta^{12}_{k1}(k=1,\ldots,4)$ = distance from CM of body 1 to the k^{th} lumped spring damper between bodies 1 and 2 on the body 1 side of the k^{th} spring damper system. This vector is fixed in body 1.

$\beta^{12}_{k2}(k=1,\ldots,4)$ = distance from CM of body 2 to the k^{th} lumped spring damper between bodies 1 and 2 on the body 2 side of the k^{th} spring damper system. This vector is fixed in body 2.

$\beta^{12}_{k10}(k=1,\ldots,4)$ = value of β^{12}_{k1} when system is unstressed.

$\beta^{12}_{k20}(k=1,\ldots,4)$ = value of β^{12}_{k2} when system is unstressed.

K_{12} = spring constant between bodies 1 and 2.

D_{12} = damping constant of spring damper between bodies 1 and 2.

The damping and spring constants are defined as diagonal matrices in the following manner

$$K_{12}=\text{diag}\left[K_{12x};K_{12y};K_{12z}\right] \tag{27}$$

$$D_{12}=\text{diag}\left[D_{12x};D_{12y};D_{12z}\right] \tag{28}$$

For small angular rotations of bodies 1 and 2 the following relations apply

$$\beta_{k1}^{12}=\beta_{k10}^{12}+\theta_1 x\beta_{k10}^{12} \tag{29}$$

$$\beta_{k2}^{12}=\beta_{k20}^{12}+\theta_2 x\beta_{k20}^{12} \tag{30}$$

$$\dot{\beta}_{k1}^{12}=\omega_1 x\beta_{k10}^{12} \tag{31}$$

$$\dot{\beta}_{k2}^{12}=\omega_2 x\beta_{k20}^{12} \tag{32}$$

In addition

$$\beta_{k10}^{12}=R_{120}+R_{E20}+\alpha_{k20}^{12} \tag{33}$$

$$\beta_{k20}^{12}=R_{E20}+\alpha_{k20}^{12} \tag{34}$$

where:

R_{E20} = inertial vector equal to the distance from CM of body 2 to center of elasticity of spring damper system between bodies 1 and 2 when the system is unstressed

$\alpha_{k20}^{12}(k=1,\ldots,4)$ = inertial vector equal to the distance from the center of elasticity of the spring damper system between bodies 1 and 2 to the k^{th} spring damper of that system

Equation (25) can also be written as

$$F_{c12}=\sum_{k=1}^{4} F_{c12k} \tag{35}$$

where:

$$F_{c12k}=K_{12}\cdot\left[\varepsilon_{12}+(\beta_{k2}^{12}-\beta_{k20}^{12})-(\beta_{k1}^{12}-\beta_{k10}^{12})\right]+D_{12}\cdot\left[\dot{\varepsilon}_{12}+\dot{\beta}_{k2}^{12}-\dot{\beta}_{k1}^{12}\right] \quad (36)$$

Substituting equations (29) thru (34) into equation (36) and rearranging terms yields

$$F_{c12k}=K_{12}\cdot\left[\varepsilon_{12}+(\theta_2-\theta_1)xR_{E20}-\theta_1xR_{120}+(\theta_2-\theta_1)x\alpha_{k20}^{12}\right]$$
$$+D_{12}\cdot\left[\dot{\varepsilon}_{12}+(\omega_2-\omega_1)xR_{E20}+(\omega_2-\omega_1)x\alpha_{k20}^{12}-\omega_1xR_{120}\right] \quad (37)$$

Substituting equation (37) into equation (35) and performing the indicated summations yields

$$F_{c12}=K_{12}\cdot\left[4\varepsilon_{12}+4(\theta_2-\theta_1)xR_{E20}-4\theta_1xR_{120}+(\theta_2-\theta_1)x\sum_{k=1}^{4}\alpha_{k20}^{12}\right]$$

$$+D_{12}\cdot\left[4\dot{\varepsilon}_{12}+4(\omega_2-\omega_1)xR_{E20}-4\omega_1xR_{120}+(\omega_2-\omega_1)x\sum_{k=1}^{4}\alpha_{k20}^{12}\right] \quad (38)$$

However, by the definition of center of elasticity

$$\sum_{k=1}^{4}\alpha_{K20}^{12}=0 \quad (39)$$

Therefore

$$F_{c12}=4K_{12}\cdot\left[\varepsilon_{12}+(\theta_2-\theta_1)xR_{E20}-\theta_1xR_{120}\right]$$
$$+4D_{12}\cdot\left[\dot{\varepsilon}_{12}+(\omega_2-\omega_1)xR_{E20}-\omega_1xR_{120}\right] \quad (40)$$

Using the same procedure as outlined above the compliance forces between bodies 2 and 3 and 3 and 4 can be written as

$$F_{c23}=\sum_{k=1}^{4}F_{c23k} \quad (41)$$

$$F_{c23k}=K_{23}\cdot\left[\varepsilon_{23}+(\theta_3-\theta_2)\times R_{E30}-\theta_2\times R_{230}+(\theta_3-\theta_2)\times\alpha_{k30}^{23}\right]$$
$$+D_{23}\cdot\left[\dot{\varepsilon}_{23}+(\omega_3-\omega_2)\times R_{E30}+(\omega_3-\omega_2)\times\alpha_{k30}^{23}-\omega_2\times R_{230}\right] \quad (42)$$

$$F_{c23}=4K_{23}\cdot\left[\varepsilon_{20}+(\theta_3-\theta_2)\times R_{E30}-\theta_2\times R_{230}\right]$$
$$+4D_{23}\cdot\left[\dot{\varepsilon}_{23}+(\omega_3-\omega_2)\times R_{E30}-\omega_2\times R_{230}\right] \quad (43)$$

$$F_{c34}=\sum_{k=1}^{4}F_{c34k} \quad (44)$$

$$F_{c34k}=K_{34}\cdot\left[\varepsilon_{34}+(\theta_4-\theta_3)\times R_{E40}-\theta_3\times R_{340}+(\theta_4-\theta_3)\times\alpha_{k40}^{34}\right]$$
$$+D_{34}\cdot\left[\dot{\varepsilon}_{34}+(\omega_4-\omega_3)\times R_{E40}+(\omega_4-\omega_3)\times\alpha_{k40}^{34}-\omega_3\times R_{340}\right] \quad (45)$$

$$F_{c34}=4K_{34}\cdot\left[\varepsilon_{34}+(\theta_4-\theta_3)\times R_{E40}+\theta_3\times R_{340}\right]$$
$$+4D_{34}\cdot\left[\dot{\varepsilon}_{34}+(\omega_4-\omega_3)\times R_{E40}-\omega_3\times R_{340}\right] \quad (46)$$

where:

K_{23} = spring constant of spring damper system between bodies 2 and 3

D_{23} = damping constant of spring damper system between bodies 2 and 3

K_{34} = spring constant of spring damper system between bodies 3 and 4

D_{34} = damping constant of spring damper system between bodies 3 and 4

$\alpha_{k30}^{23}(k=1,\ldots,4)$ = inertial vector equal to the distance from the center of elasticity of the spring damper system between bodies 2 and 3 to the k^{th} spring damper of that system

$\alpha^{34}_{k40}(k=1,\ldots,4)$ = inertial vector equal to the distance from the center of elasticity of the spring damper system between bodies 3 and 4 to the k^{th} spring damper of that system

$K_{23}, K_{34}, D_{23}, D_{34}$ are defined as diagonal matrices in the following manner

$$K_{23}=\text{diag}\left[K_{23x};K_{23y};K_{23z}\right] \tag{47}$$

$$K_{34}=\text{diag}\left[K_{34x};K_{34y};K_{34z}\right] \tag{48}$$

$$D_{23}=\text{diag}\left[D_{23x};D_{23y};D_{23z}\right] \tag{49}$$

$$D_{34}=\text{diag}\left[D_{34x};D_{34y};D_{34z}\right] \tag{50}$$

The above equations completely define the translational equations of motion of the six body system shown in figure 2-3.

It is now necessary to derive the rotational equations of motion for the six body system shown in figure 2-3. This is outlined in what follows.

2.1.2 Rotational Equations of Motion

Body 1 - The rotational equation of motion for body 1 can be written as

$$T_{1e}+T_{1c}+R_{11}\times F_{1e}+\beta^{12}_{11}\times(F_{c121})+\beta^{12}_{21}\times F_{c122}+\beta^{12}_{31}\times F_{c123}+\beta^{12}_{41}\times(F_{c124})=\frac{d}{dt}(J_1\cdot\omega_1) \tag{51}$$

But upon substitution of equations (29), (33), and (37) into $B^{12}_{11}\times(F_{c121})$ and eliminating second order terms the following results.

$$\begin{aligned}\beta^{12}_{11}\times F_{c121}=&(R_{120}+R_{E20})\times\left\{K_{12}\cdot\left[\varepsilon_{12}+(\theta_2-\theta_1)\times R_{E20}-\theta_1\times R_{120}\right]\right.\\&\left.+D_{12}\cdot\left[\dot{\varepsilon}_{12}+(\omega_2-\omega_1)\times R_{E20}-\omega_1\times R_{120}\right]\right\}\\&+(R_{120}+R_{E20})\times\left\{K_{12}\cdot\left[(\theta_2-\theta_1)\times\alpha^{12}_{120}\right]+D_{12}\cdot\left[(\omega_2-\omega_1)\times\alpha^{12}_{120}\right]\right\}\\&+\alpha^{12}_{120}\times\left\{K_{12}\cdot\left[\varepsilon_{12}+(\theta_2-\theta_1)\times R_{E20}-\theta_1\times R_{120}\right]\right\}\\&+\alpha^{12}_{120}\times\left\{D_{12}\cdot\left[\dot{\varepsilon}_{12}+(\omega_2-\omega_1)\times R_{E20}-\omega_1\times R_{120}\right]\right\}\\&+\alpha^{12}_{120}\times\left\{K_{12}\cdot\left[(\theta_2-\theta_1)\times\alpha^{12}_{120}\right]\right\}\\&+\alpha^{12}_{120}\times\left\{D_{12}\cdot\left[(\omega_2-\omega_1)\times\alpha^{12}_{120}\right]\right\}\end{aligned} \tag{52}$$

Evaluating the other terms in equation (51) similarly and performing the indicated summation results in the following

$$T_{1e}+T_{1c}+R_{11}xF_{1e}=\frac{d}{dt}(J_1\cdot\omega_1)-4(R_{120}+R_{E20})x\left\{K_{12}\cdot\left[\varepsilon_{12}+(\theta_2-\theta_1)xR_{E20}-\theta_1xR_{120}\right]\right.$$
$$\left.+D_{12}\cdot\left[\dot{\varepsilon}_{12}+(\omega_2-\omega_1)xR_{E20}-\omega_1xR_{120}\right]\right\}$$
$$-\sum_{k=1}^{4}\alpha_{k20}^{12}x\left[K_{12}\cdot(\theta_2-\theta_1)x\alpha_{k20}^{12}\right]$$
$$-\sum_{k=1}^{4}\alpha_{k20}^{12}x\left[D_{12}\cdot(\omega_2-\omega_1)x\alpha_{120}^{12}\right] \qquad (53)$$

Equation (53) can be rewritten as

$$T_{1e}+T_{1c}+R_{11}xF_{1e}=\frac{d}{dt}(J_1\cdot\omega_1)+d_{12}\cdot(\omega_1-\omega_2)+k_{12}\cdot(\theta_1-\theta_2)$$
$$+4(R_{120}+R_{E20})x\left\{D_{12}\cdot\left[(\omega_1-\omega_2)xR_{E20}+\omega_1xR_{120}\right]\right.$$
$$\left.+K_{12}\cdot\left[(\theta_1-\theta_2)xR_{E20}+\theta_1xR_{120}\right]\right\}$$
$$-4(R_{120}+R_{E20})x\left[D_{12}\cdot\dot{\varepsilon}_{12}+K_{12}\cdot\varepsilon_{12}\right] \qquad (54)$$

where:

$$k_{12}=\mathrm{diag}\left\{4K_{12z}(\alpha_{120y}^{12})^2;4K_{12z}(\alpha_{120x}^{12})^2;4\left[K_{12y}(\alpha_{120x}^{12})^2+K_{12x}(\alpha_{120y}^{12})^2\right]\right\} \qquad (55)$$

$$d_{12}=\mathrm{diag}\left\{4D_{12z}(\alpha_{120y}^{12})^2;4D_{12z}(\alpha_{120x}^{12})^2;4\left[D_{12z}(\alpha_{120x}^{12})^2+D_{12x}(\alpha_{120y}^{12})^2\right]\right\} \qquad (56)$$

and

T_{1e} = external torque applied to body 1

T_{1c} = control torque applied to body 1

R_{11} = distance from CM of body 1 to the external force application on body 1

Body 2 - The rotational equation of motion for body 2 can be written as

$$T_{2e}+T_{2c}+R_{22}xF_{2e}-\beta_{12}^{12}xF_{c121}-\beta_{22}^{12}xF_{c122}-\beta_{32}^{12}xF_{c123}-\beta_{42}^{12}xF_{c124}+\beta_{12}^{23}xF_{c231}$$
$$+\beta_{22}^{23}xF_{c232}+\beta_{32}^{23}xF_{c233}+\beta_{42}^{23}xF_{c234}=\frac{d}{dt}(J_2\cdot\omega_2) \qquad (57)$$

Using the same approach as outlined for body 1 in conjunction with the following relationships

$$\beta_{k2}^{12}=\beta_{k20}^{12}+\theta_2x\beta_{k20}^{12} \qquad k=1,\ldots,4 \qquad (58)$$

$$\beta_{k20}^{12}=R_{E20}+\alpha_{k20}^{12} \qquad k=1,\ldots,4 \qquad (59)$$

$$\beta_{k2}^{23}=\beta_{k20}^{23}+\theta_2x\beta_{k20}^{23} \qquad k=1,\ldots,4 \qquad (60)$$

$$\beta_{k20}^{23}=R_{230}+R_{E30}+\alpha_{k30}^{23} \qquad k=1,\ldots,4 \qquad (61)$$

results in

$$T_{2e}+T_{2c}+R_{22}xF_{2e}=\frac{d}{dt}(J_2\cdot\omega_2)+d_{12}\cdot(\omega_2-\omega_1)+k_{12}(\theta_2-\theta_1)$$
$$+4R_{E20}x\left\{D_{12}\cdot\left[\dot{\varepsilon}_{12}+(\omega_2-\omega_1)xR_{E20}-\omega_1xR_{120}\right]\right.$$
$$\left.+K_{12}\cdot\left[\varepsilon_{12}+(\theta_2-\theta_1)xR_{E20}-\theta_1xR_{120}\right]\right\}+d_{23}\cdot(\omega_2-\omega_3)$$
$$+k_{23}\cdot(\theta_2-\theta_3)+4(R_{230}+R_{E30})x\left\{K_{23}\cdot\left[(\theta_2-\theta_3)xR_{E30}+\theta_2xR_{230}\right]\right.$$
$$\left.+D_{23}\cdot\left[(\omega_2-\omega_3)xR_{E30}+\omega_2xR_{230}\right]\right\}$$
$$-4(R_{230}+R_{E30})x\left[K_{23}\cdot\varepsilon_{23}+D_{23}\cdot\dot{\varepsilon}_{23}\right] \qquad (62)$$

where:

$$d_{23}=\mathrm{diag}\left\{4D_{23z}(\alpha_{130y}^{23})^2;4D_{23z}(\alpha_{130x}^{23})^2;4\left[D_{23y}(\alpha_{130x}^{23})^2+D_{23x}(\alpha_{130y}^{23})^2\right]\right\} \qquad (63)$$

$$k_{23}=\mathrm{diag}\left\{4K_{23z}(\alpha_{130y}^{23})^2;4K_{23z}(\alpha_{130x}^{23})^2;4\left[K_{23y}(\alpha_{130x}^{23})^2+K_{23x}(\alpha_{130y}^{23})^2\right]\right\} \qquad (64)$$

and

T_{2e} = external torque applied to body 2

T_{2c} = control torque applied to body 2

R_{22} = distance from CM of body 2 to the point of external force application on body 2

Body 3 - The rotational equation of motion for body 3 can be written as

$$T_{3e}+T_{3c}+R_{33}xF_{3e}-\beta_{13}^{23}xF_{c231}-\beta_{23}^{23}xF_{c232}-\beta_{33}^{23}xF_{c233}-\beta_{43}^{23}xF_{c234}+\beta_{13}^{34}xF_{c341}$$
$$+\beta_{23}^{34}xF_{c342}+\beta_{33}^{34}xF_{c343}+\beta_{43}^{34}xF_{c344}=\frac{d}{dt}(J_3\cdot\omega_3) \qquad (65)$$

Using the same approach as outlined for body 1 in conjunction with the following relationships

$$\beta_{k3}^{23}=\beta_{k30}^{23}+\theta_3x\beta_{k30}^{23} \qquad k=1,\ldots,4 \qquad (66)$$

$$\beta_{k30}^{23}=R_{E30}+\alpha_{k30}^{23} \qquad k=1,\ldots,4 \qquad (67)$$

$$\beta_{k3}^{34}=\beta_{k30}^{34}+\theta_3x\beta_{k30}^{34} \qquad k=1,\ldots,4 \qquad (68)$$

$$\beta_{k30}^{34}=R_{340}+R_{E40}+\alpha_{k40}^{34} \qquad k=1,\ldots,4 \qquad (69)$$

gives

$$T_{3e}+T_{3c}+R_{33}xF_{3e}=\frac{d}{dt}(J_3\cdot\omega_3)+d_{23}\cdot(\omega_3-\omega_2)+k_{23}\cdot(\theta_3-\theta_2)$$
$$+4R_{E30}x\Big\{D_{23}\cdot\Big[\dot{\varepsilon}_{23}+(\omega_3-\omega_2)xR_{E30}-\omega_2xR_{230}\Big]$$
$$+K_{23}\cdot\Big[\varepsilon_{23}+(\theta_3-\theta_2)xR_{E30}-\theta_2xR_{230}\Big]\Big\}$$
$$+d_{34}\cdot(\omega_3-\omega_4)+k_{34}\cdot(\theta_3-\theta_4)$$
$$+4(R_{340}+R_{E40})x\Big\{K_{34}\cdot\Big[(\theta_3-\theta_4)xR_{E40}+\theta_3xR_{340}\Big]$$
$$+D_{34}\cdot\Big[(\omega_3-\omega_4)xR_{E40}+\omega_3xR_{340}\Big]\Big\}$$
$$-4(R_{340}+R_{E40})x\Big[K_{34}\cdot\varepsilon_{34}+D_{34}\cdot\dot{\varepsilon}_{34}\Big] \qquad (70)$$

where:

$$d_{34}=\text{diag}\left\{4D_{34z}(\alpha^{34}_{140y})^2;4D_{34z}(\alpha^{34}_{140x})^2;4\left[D_{34y}(\alpha^{34}_{140x})^2+D_{34x}(\alpha^{34}_{140y})^2\right]\right\} \quad (71)$$

$$k_{34}=\text{diag}\left\{4K_{34z}(\alpha^{34}_{140y})^2;4K_{34z}(\alpha^{34}_{140x})^2;4\left[K_{34y}(\alpha^{34}_{140x})^2+K_{34x}(\alpha^{34}_{140y})^2\right]\right\} \quad (72)$$

and

T_{3e} = external torque applied to body 3

T_{3c} = control torque applied to body 3

R_{33} = distance from CM of body 3 to the point of external force application on body 2

Body 4 - The rotational equation of motion for body 4 can be written as

$$T_{4e}-T^4_H+R_{44}xF_{4e}+r_1xF_H-\beta^{34}_{14}xF_{c341}-\beta^{34}_{24}xF_{c342}-\beta^{34}_{34}xF_{c343}-\beta^{34}_{44}xF_{c344}=\frac{d}{dt}(J_4\cdot\omega_4) \quad (73)$$

Using the same approach outlined for body 1 in conjunction with equation (24) and the following relationships

$$\beta^{34}_{k4}=\beta^{34}_{k40}+\theta_4x\beta^{34}_{k40} \qquad k=1,\ldots,4 \quad (74)$$

$$\beta^{34}_{k40}=R_{E40}+\alpha^{34}_{k40} \qquad k=1,\ldots,4 \quad (75)$$

yields

$$T_{4e}-T_H+R_{44}xF_{4e}+\frac{(m_1+m_2+m_3+m_4)}{M}r^4_1x(F^4_{5e}+F^4_{6e})-\left[\frac{m_5+m_6}{M}\right]r^4_1x(F_{1e}+F_{2e}+F_{3e}+F_{4e})=$$
$$\frac{d}{dt}(J_4\cdot\omega_4)+d_{34}\cdot(\omega_4-\omega_3)+k_{34}\cdot(\theta_4-\theta_3)+4R_{E40}x\left\{D_{34}\cdot\left[\dot{\varepsilon}_{34}+(\omega_4-\omega_3)xR_{E40}-\omega_3xR_{340}\right]\right.$$
$$\left.+K_{34}\cdot\left[\varepsilon_{34}+(\theta_4-\theta_3)xR_{E40}-\theta_3xR_{340}\right]\right\}+\frac{m_1(m_5+m_6)}{M}r^4_1x\ddot{\varepsilon}_{12}+\frac{(m_1+m_2)(m_5+m_6)}{M}r_1x\ddot{\varepsilon}_{23}$$
$$+\frac{(m_1+m_2+m_3)(m_5+m_6)}{M}r_1x\ddot{\varepsilon}_{34}+\frac{(m_1+m_2+m_3+m_4)(m_5+m_6)}{M}r_1x(\ddot{r}_1+\ddot{r}^4_2)$$
$$+\frac{m_6(m_1+m_2+m_3+m_4)}{M}r_1x(\ddot{r}^4_3+\ddot{r}^4_4) \quad (76)$$

where:

T_{4e} = external torque applied to body 4

T_H^4 = hinge torque between bodies 4 and 5 written in body 4 coordinates

R_{44} = distance from CM of body 4 to the point of external force application on body 4

r_1 = distance from CM of body 4 to hinge point and is fixed in body 4

r_2^4 = distance from hinge point to CM of body 5 written in body 4 coordinates

r_3^4 = distance from CM of body 5 to telescope interface point written in body 4 coordinates

r_4^4 = distance from telescope interface to CM of body 6 written in body 4 coordinates

Body 5 - The rotational equation of motion for body 5 can be written as

$$R_{55}xF_{5e}+T_{5e}+T_H+r_2xF_H+r_3xF_I=\frac{d}{dt}(J_5\cdot\omega_5)+d_{56}\cdot(\omega_5-\omega_6)+k_{56}\cdot(\theta_5-\theta_6) \quad (77)$$

Substituting equations (23) and (24) into equation (77) results in

$$R_{55}xF_{5e}+T_{5e}+T_H+\frac{(m_1+m_2+m_3+m_4)}{M}r_2x(F_{5e}+F_{6e})-\frac{(m_5+m_6)}{M}r_2x(F_{1e}^5+F_{2e}^5+F_{3e}^5+F_{4e}^5)$$
$$+\frac{(m_1+m_2+m_3+m_4+m_5)}{M}r_3xF_{6e}-\frac{m_6}{M}r_3x(F_{1e}^5+F_{2e}^5+F_{3e}^5+F_{4e}^5+F_{5e})=\frac{d}{dt}(J_5\cdot\omega_5)$$
$$+d_{56}\cdot(\omega_5-\omega_6)+k_{56}\cdot(\theta_5-\theta_6)+\frac{m_1}{M}\left[(m_5+m_6)r_2+m_6r_3\right]x\ddot{\varepsilon}_{12}+\frac{(m_1+m_2)}{M}\left[(m_5+m_6)r_2+m_6r_3\right]x\ddot{\varepsilon}_{23}$$
$$+\frac{(m_1+m_2+m_3)}{M}\left[(m_5+m_6)r_2+m_6r_3\right]x\ddot{\varepsilon}_{34}+\frac{(m_1+m_2+m_3+m_4)}{M}\left[(m_5+m_6)r_2+m_6r_3\right]x(\ddot{r}_1^5+\ddot{r}_2)$$
$$+\frac{m_6}{M}\left[(m_1+m_2+m_3+m_4)r_2+(m_1+m_2+m_3+m_4+m_5)r_3\right]x(\ddot{r}_3+\ddot{r}_4) \quad (78)$$

where:

T_{5e} = external torque applied to body 5

R_{55} = distance from CM of body 5 to point of external force application on body 5

$F^5_{1e}, F^5_{2e}, F^5_{3e}, F^5_{4e}$ = external forces applied on bodies 1 thru 4, respectively, written in body 5 coordinates

r^5_1 = distance from CM of body 4 to hinge point written in body 5 coordinates

Body 6 - The rotational equation of motion for body 6 can be written as

$$R_{66}xF_{6e}+T_{6e}+r_4xF_I=\frac{d}{dt}(J_6\cdot\omega_6)+d_{56}\cdot(\omega_6-\omega_5)+k_{56}(\theta_6-\theta_5) \qquad (79)$$

Substituting equation (23) into equation (79) results in

$$T_{6e}+R_{66}xF_{6e}+\frac{(m_1+m_2+m_3+m_4+m_5)}{M}r_4xF_{6e}-\frac{m_6}{M}r_4x(F^6_{1e}+F^6_{2e}+F^6_{3e}+F^6_{4e}+F^6_{5e})=$$

$$\frac{d}{dt}(J_6\cdot\omega_6)+d_{56}\cdot(\omega_6-\omega_5)+k_{56}\cdot(\theta_6-\theta_5)+\frac{m_1m_6}{M}r_4x\ddot{\varepsilon}_{12}+\frac{m_6(m_1+m_2)}{M}r_4x\ddot{\varepsilon}_{23}$$

$$+\frac{m_6(m_1+m_2+m_3)}{M}r_4x\ddot{\varepsilon}_{34}+\frac{m_6(m_1+m_2+m_3+m_4)}{M}r_4x(\ddot{r}^5_1+\ddot{r}_2)$$

$$+\frac{m_6(m_1+m_2+m_3+m_4+m_5)}{M}r_4x(\ddot{r}_3+\ddot{r}_4) \qquad (80)$$

where:

T_{6e} = external torque acting on body 6

R_{66} = distance from CM of body 6 to the point of external force application on body 6

The assumption made in the derivation of the above rotational equations of motion is that coordinate frames fixed in bodies 1 thru 4 are co-aligned while the coordinate frames fixed in bodies 5 and 6 are co-aligned. Hence vectors fixed in bodies 1 thru 4 are expressed equally in any of the coordinate frames 1 thru 4. Vectors fixed in bodies 5 and 6 are expressed equally in either

body 5 or body 6 coordinates. The relationship between body 5 and 6 coordinates and the coordinates of bodies 1 thru 4 is given by the direction cosine transformation ${}_4T_5$ which describes the transformation from body 5 coordinates to body 4 coordinates and is given by

$$ {}_4T_5 = \begin{bmatrix} a_{11} & a_{12} & a_{13} \\ a_{21} & a_{22} & a_{23} \\ a_{31} & a_{32} & a_{33} \end{bmatrix} \tag{81} $$

In order to obtain a complete set of equations of motion for the six body system being considered three linear equations of motion are required in addition to the six rotational equations of motion derived above for each of the six bodies. These are needed to enable the solution of the relative linear displacements ε_{12}, ε_{23} and ε_{34} between bodies 1 and 2, 2 and 3, and 3 and 4, respectively. The three linear equations of motion chosen are equations (1), (2), and (3).

Substituting equations (17) and (40) into equation (1) yields

$$ \frac{(m_2+m_3+m_4+m_5+m_6)}{M} F_{1e} - \frac{m_1}{M}(F_{2e}+F_{3e}+F_{4e}+F^4_{5e}+F^4_{6e}) = -\left[\frac{m_1}{M}(m_2+m_3+m_4+m_5+m_6)\ddot{\varepsilon}_{12}\right. $$

$$ \left. +4D_{12}\cdot\dot{\varepsilon}_{12}+4K_{12}\cdot\varepsilon_{12}\right] - \frac{m_1}{M}\left[(m_3+m_4+m_5+m_6)\ddot{\varepsilon}_{23}+(m_4+m_5+m_6)\ddot{\varepsilon}_{34}\right] $$

$$ - \frac{m_1}{M}\left[(m_5+m_6)(\ddot{r}_1+\ddot{r}^4_2)+m_6(\ddot{r}^4_3+\ddot{r}^4_4)\right] +4D_{12}\cdot(\omega_1 x R_{120})+4K_{12}\cdot(\theta_1 x R_{120}) $$

$$ +4D_{12}\cdot\left[(\omega_1-\omega_2)xR_{E20}\right]+4K_{12}\cdot\left[(\theta_1-\theta_2)xR_{E20}\right] \tag{82} $$

Substituting equations (18), (40) and (43) into equation (2) results in

$$\frac{(m_1+m_3+m_4+m_5+m_6)}{M} F_{2e} - \frac{m_2}{M}(F_{1e}+F_{3e}+F_{4e}+F^4_{5e}+F^4_{6e}) = \frac{m_1 m_2}{M} \ddot{\varepsilon}_{12}+4D_{12}\cdot\dot{\varepsilon}_{12}$$
$$+4K_{12}\cdot\varepsilon_{12}-\left[\frac{m_2(m_3+m_4+m_5+m_6)}{M} \ddot{\varepsilon}_{23}+4D_{23}\cdot\dot{\varepsilon}_{23}+4K_{23}\cdot\varepsilon_{23}\right]-\frac{m_2}{M}(m_4+m_5+m_6)\ddot{\varepsilon}_{34}$$
$$-\frac{m_2}{M}\left[(m_5+m_6)(\ddot{r}_1+\ddot{r}^4_2)-m_6(\ddot{r}^4_3+\ddot{r}^4_4)\right]+4D_{12}\cdot\left[(\omega_2-\omega_1)xR_{E20}\right]+4K_{12}\cdot\left[(\theta_2-\theta_1)xR_{E20}\right]$$
$$-\left[4D_{12}\cdot(\omega_1 xR_{120})+4K_{12}\cdot(\theta_1 xR_{120})\right]+4D_{23}\cdot\left[(\omega_2-\omega_3)xR_{E30}\right]+4K_{23}\cdot\left[(\theta_2-\theta_3)xR_{E30}\right]$$
$$+4D_{23}\cdot(\omega_2 xR_{230})+4K_{23}\ (\theta_2 xR_{230}) \qquad (83)$$

Substituting equations (19), (43) and (46) into equation (3) gives

$$\frac{m_1+m_2+m_4+m_5+m_6}{M} F_{3e} - \frac{m_3}{M}(F_{1e}+F_{2e}+F_{4e}+F^4_{5e}+F^4_{6e}) = \frac{m_1 m_3}{M} \ddot{\varepsilon}_{12}+\left[\frac{m_3(m_1+m_2)}{M} \ddot{\varepsilon}_{23}\right.$$
$$\left.+4D_{23}\cdot\dot{\varepsilon}_{23}+4K_{23}\cdot\varepsilon_{23}\right]-\left[\frac{m_3(m_4+m_5+m_6)}{M} \ddot{\varepsilon}_{34}+4D_{34}\cdot\dot{\varepsilon}_{34}+4K_{34}\cdot\varepsilon_{34}\right]$$
$$-\frac{m_3}{M}\left[(m_5+m_6)(\ddot{r}_1+\ddot{r}^4_2)-m_6(\ddot{r}^4_3+\ddot{r}^4_4)\right]+4D_{23}\cdot\left[(\omega_3-\omega_2)xR_{E30}\right]+4K_{23}\cdot\left[(\theta_3-\theta_2)xR_{E30}\right]$$
$$-\left[4D_{23}\cdot(\omega_2 xR_{230})+4K_{23}\cdot(\theta_2 xR_{230})\right]+4D_{34}\cdot\left[(\omega_3-\omega_4)xR_{E40}\right]+4K_{34}\cdot\left[(\theta_3-\theta_4)xR_{E40}\right]$$
$$+4D_{34}\cdot(\omega_3 xR_{340})+4K_{34}\cdot(\theta_3 xR_{340}) \qquad (84)$$

Equations (54), (62), (70), (76), (78), (80), (82), (83) and (84) form the complete set of equations of motion for the six body system being considered. Linearizing these equations of motion and writing them in complete matrix format results in the following

$$T_{1e}+\bar{R}_{11}\cdot F_{1e}=J_1\cdot\dot{\omega}_1+\left[d_{12}-4(\bar{R}_{120}+\bar{R}_{E20})\cdot D_{12}\cdot(\bar{R}_{120}+\bar{R}_{E20})\right]\cdot\omega_1$$
$$+\left[k_{12}-4(\bar{R}_{120}+\bar{R}_{E20})\cdot K_{12}\cdot(\bar{R}_{120}+\bar{R}_{E20})\right]\cdot\theta_1+\left[4(\bar{R}_{120}+\bar{R}_{E20})\cdot D_{12}\cdot\bar{R}_{E20}-d_{12}\right]\cdot\omega_2$$
$$+\left[4(\bar{R}_{120}+\bar{R}_{E20})\cdot K_{12}\cdot\bar{R}_{E20}-k_{12}\right]\cdot\theta_2-T_{1c}-4(\bar{R}_{120}+\bar{R}_{E20})\cdot D_{12}\cdot\dot{\varepsilon}_{12}$$
$$-4(\bar{R}_{120}+\bar{R}_{E20})\cdot K_{12}\cdot\varepsilon_{12} \qquad (85)$$

$$T_{2e}+\bar{R}_{22}\cdot F_{2e}=\left[4R_{E20}\cdot D_{12}\cdot(\bar{R}_{120}+\bar{R}_{E20})-d_{12}\right]\cdot\omega_1+J_2\cdot\dot{\omega}_2$$
$$+\left[d_{12}-4\bar{R}_{E20}\cdot D_{12}\cdot\bar{R}_{E20}+d_{23}-4(\bar{R}_{230}+\bar{R}_{E30})\cdot D_{23}\cdot(\bar{R}_{230}+\bar{R}_{E30})\right]\cdot\omega_2$$
$$+\left[k_{12}-4\bar{R}_{E20}\cdot K_{12}\cdot\bar{R}_{E20}+k_{23}-4(\bar{R}_{230}+\bar{R}_{E30})\cdot K_{23}\cdot(\bar{R}_{230}+\bar{R}_{E30})\right]\cdot\theta_2$$
$$+\left[4(\bar{R}_{230}+\bar{R}_{E30})\cdot D_{23}\cdot R_{E30}-d_{23}\right]\cdot\omega_3+\left[4(\bar{R}_{230}+\bar{R}_{E30})\cdot K_{23}\cdot\bar{R}_{E30}-k_{23}\right]\cdot\theta_3$$
$$-T_{2c}+\left[4\bar{R}_{E20}\cdot K_{12}\cdot(\bar{R}_{120}+\bar{R}_{E30})-k_{12}\right]\cdot\theta_1+4\bar{R}_{E20}\cdot D_{12}\cdot\dot{\varepsilon}_{12}+4\bar{R}_{E20}\cdot K_{12}\cdot\varepsilon_{12}$$
$$-4(\bar{R}_{230}+\bar{R}_{E30})\cdot D_{23}\cdot\dot{\varepsilon}_{23}-4(\bar{R}_{230}+\bar{R}_{E30})\cdot K_{23}\cdot\varepsilon_{23} \qquad (86)$$

$$T_{3e}+\bar{R}_{33}\cdot F_{3e}=\left[4\bar{R}_{E30}\cdot D_{23}\cdot(\bar{R}_{230}+\bar{R}_{E30})-d_{23}\right]\cdot\omega_2+\left[4\bar{R}_{E30}\cdot K_{23}\cdot(\bar{R}_{230}+\bar{R}_{E30})-k_{23}\right]\cdot\theta_2$$
$$+J_3\cdot\dot{\omega}_3+\left[d_{23}-4\bar{R}_{E30}\cdot D_{23}\cdot\bar{R}_{E30}+d_{34}-4(\bar{R}_{340}+\bar{R}_{E40})\cdot D_{34}\cdot(\bar{R}_{340}-\bar{R}_{E40})\right]\cdot\omega_3$$
$$+\left[k_{23}-4\bar{R}_{E30}\cdot K_{23}\cdot\bar{R}_{E30}+k_{34}-4(\bar{R}_{340}+\bar{R}_{E40})\cdot K_{34}\cdot(\bar{R}_{340}+\bar{R}_{E40})\right]\cdot\theta_3-T_{3c}$$
$$+\left[4(\bar{R}_{340}+\bar{R}_{E40})\cdot D_{34}\cdot\bar{R}_{E40}-d_{34}\right]\cdot\omega_4+\left[4(\bar{R}_{340}+\bar{R}_{E40})\cdot K_{34}\cdot\bar{R}_{E40}-k_{34}\right]\cdot\theta_4$$
$$+4\bar{R}_{E30}\cdot D_{23}\cdot\dot{\varepsilon}_{23}+4\bar{R}_{E30}\cdot K_{23}\cdot\varepsilon_{23}-4(\bar{R}_{340}+\bar{R}_{E40})\cdot D_{34}\cdot\dot{\varepsilon}_{34}-4(\bar{R}_{340}+\bar{R}_{E40})\cdot K_{34}\cdot\varepsilon_{34} \qquad (87)$$

$$T_{4e}+\left(\bar{R}_{44}-\frac{m_5+m_6}{M}\bar{r}_1\right)\cdot F_{4e}+\left(\frac{m_1+m_2+m_3+m_4}{M}\right)\bar{r}_1\cdot{}^4T_5\cdot(F_{5e}+F_{6e})-\frac{m_5+m_6}{M}\bar{r}_1\cdot(F_{1e}+F_{2e}+F_{3e})=$$
$$\left[4\bar{R}_{E40}\cdot D_{34}\cdot(\bar{R}_{340}+\bar{R}_{E40})-d_{34}\right]\cdot\omega_3+\left[4\bar{R}_{E40}\cdot K_{34}\cdot(\bar{R}_{340}+\bar{R}_{E40})-k_{34}\right]\cdot\theta_3+J_4^*\cdot\dot{\omega}_4$$
$$+\left[d_{34}-4\bar{R}_{E40}\cdot D_{34}\cdot\bar{R}_{E40}\right]\cdot\omega_4+\left[k_{34}-4\bar{R}_{E40}\cdot K_{34}\cdot\bar{R}_{E40}\right]\cdot\theta_4$$
$$-\left[\frac{(m_1+m_2+m_3+m_4)(m_5+m_6)}{M}\bar{r}_1\cdot{}^4T_5\cdot\bar{r}_2+\frac{m_6(m_1+m_2+m_3+m_4)}{M}\bar{r}_1\cdot{}^4T_5\cdot\bar{r}_3\right]\cdot\dot{\omega}_5$$
$$-\left[\frac{m_6(m_1+m_2+m_3+m_4)}{M}\bar{r}_1\cdot{}^4T_5\cdot\bar{r}_4\right]\cdot\dot{\omega}_6+{}^4T_5\cdot T_H+\frac{m_1(m_5+m_6)}{M}\bar{r}_1\cdot\ddot{\varepsilon}_{12}+\frac{(m_1+m_2)(m_5+m_6)}{M}\bar{r}_1\cdot\ddot{\varepsilon}_{23}$$
$$+\frac{(m_1+m_2+m_3)(m_5+m_6)}{M}\bar{r}_1\cdot\ddot{\varepsilon}_{34}+4R_{E40}\cdot D_{34}\cdot\dot{\varepsilon}_{34}+4R_{E40}\cdot K_{34}\cdot\varepsilon_{34} \qquad (88)$$

$$T_{5e} - \frac{1}{M}\left[(m_5+m_6)\bar{r}_2+m_6\bar{r}_3\right]\cdot {}_4T_5^{-1}\cdot\left[F_{1e}+F_{2e}+F_{3e}+F_{4e}\right]+\left[\bar{R}_{55}+\frac{m_1+m_2+m_3+m_4}{M}\bar{r}_2\right.$$
$$\left.-\frac{m_6}{M}\bar{r}_3\right]\cdot F_{5e}+\left[\frac{(m_1+m_2+m_3+m_4)}{M}\bar{r}_2+\frac{(m_1+m_2+m_3+m_4+m_5)}{M}\bar{r}_3\right]\cdot F_{6e}=$$
$$-\frac{(m_1+m_2+m_3+m_4)}{M}\left[(m_5+m_6)\bar{r}_2+m_6\bar{r}_3\right]\cdot {}_4T_5^{-1}\cdot\bar{r}_1\cdot\dot{\omega}_4+J_5^*\cdot\dot{\omega}_5+d_{56}\cdot\omega_5+k_{56}\cdot\theta_5$$
$$+J_{56}\cdot\dot{\omega}_6-d_{56}\cdot\dot{\omega}_6-k_{56}\cdot\theta_6-T_H+\frac{m_1}{M}\left[(m_5+m_6)\bar{r}_2+m_6\bar{r}_3\right]\cdot {}_4T_5^{-1}\cdot\ddot{\varepsilon}_{12}$$
$$+\frac{(m_1+m_2)}{M}\left[(m_5+m_6)\bar{r}_2+m_6\bar{r}_3\right]\cdot {}_4T_5^{-1}\cdot\ddot{\varepsilon}_{23}$$
$$+\frac{(m_1+m_2+m_3)}{M}\left[(m_5+m_6)\bar{r}_2+m_6 r_3\right]\cdot {}_4T_5^{-1}\cdot\ddot{\varepsilon}_{34} \qquad (89)$$

$$T_{6e} - \frac{m_6}{M}\bar{r}_4\cdot\left[{}_4T_5^{-1}\cdot(F_{1e}+F_{2e}+F_{3e}+F_{4e})+F_{5e}\right]+\left[\bar{R}_{66}+\frac{(m_1+m_2+m_3+m_4+m_5)}{M}\bar{r}_4\right]\cdot F_{6e}=$$
$$-\frac{m_6(m_1+m_2+m_3+m_4)}{M}\bar{r}_4\cdot {}_4T_5^{-1}\cdot\bar{r}_1\cdot\dot{\omega}_4+J_{65}\cdot\dot{\omega}_5-d_{56}\cdot\omega_5-k_{56}\cdot\theta_5+J_6^*\cdot\dot{\omega}_6+d_{56}\cdot\omega_6+k_{56}\cdot\theta_6$$
$$+\frac{m_1m_6}{M}\bar{r}_4\cdot {}_4T_5^{-1}\cdot\ddot{\varepsilon}_{12}+\frac{m_6(m_1+m_2)}{M}\bar{r}_4\cdot {}_4T_5^{-1}\cdot\ddot{\varepsilon}_{23}+\frac{m_6(m_1+m_2+m_3)}{M}\bar{r}_4\cdot {}_4T_5^{-1}\cdot\ddot{\varepsilon}_{34} \qquad (90)$$

$$\frac{(m_2+m_3+m_4+m_5+m_6)}{M}F_{1e}-\frac{m_1}{M}\left[F_{2e}+F_{3e}+F_{4e}+{}_4T_5\cdot(F_{5e}+F_{6e})\right]=-4D_{12}\ (\bar{R}_{120}+\bar{R}_{E220})\cdot\omega_1$$
$$-4K_{12}\cdot(\bar{R}_{120}+\bar{R}_{E20})\cdot\theta_1+4D_{12}\cdot\bar{R}_{E20}\cdot\omega_2+4K_{12}\cdot\bar{R}_{E20}\cdot\theta_2+\frac{m_1}{M}(m_5+m_6)\bar{r}_1\cdot\dot{\omega}_4$$
$$+{}_4T_5\cdot\frac{m_1}{M}\left[(m_5+m_6)\bar{r}_2+m_6\bar{r}_3\right]\cdot\dot{\omega}_5+\frac{m_1m_6}{M}\ {}_4T_5\cdot\bar{r}_4\cdot\omega_4-\left[\frac{m_1}{M}(m_2+m_3+m_4+m_5+m_6)\ddot{\varepsilon}_{12}\right.$$
$$\left.+4D_{12}\cdot\dot{\varepsilon}_{12}+4K_{12}\cdot\varepsilon_{12}\right]-\left[\frac{m_1}{M}(m_3+m_4+m_5+m_6)\ddot{\varepsilon}_{23}+\frac{m_1}{M}(m_4+m_5+m_6)\ddot{\varepsilon}_{34}\right] \qquad (91)$$

$$\frac{m_1+m_3+m_4+m_5+m_6}{M} F_{2e} - \frac{m_2}{M}\left[F_{1e}+F_{3e}+F_{4e}+{}_4T_5\cdot(F_{5e}+F_{6e})\right] = 4D_{12}\cdot(\bar{R}_{E20}+\bar{R}_{120})\cdot\omega_1$$
$$+4K_{12}\cdot(\bar{R}_{E20}+\bar{R}_{120})\cdot\theta_1 - \left[4D_{12}\cdot\bar{R}_{E20}+4D_{23}\cdot(\bar{R}_{E30}+\bar{R}_{230})\right]\cdot\omega_2$$
$$-\left[4K_{12}\cdot\bar{R}_{E20}+4K_{23}\cdot(\bar{R}_{230}+\bar{R}_{E30})\right]\cdot\theta_2+4D_{23}\cdot\bar{R}_{E30}\cdot\omega_3+4K_{23}\cdot\bar{R}_{E30}\cdot\theta_3$$
$$+\frac{m_2}{M}(m_5+m_6)\bar{r}_1\cdot\dot{\omega}_4+{}_4T_5\cdot\frac{m_2}{M}\left[(m_5+m_6)\bar{r}_2-m_6\bar{r}_3\right]\cdot\dot{\omega}_5-\frac{m_2m_6}{M}\,{}_4T_5\cdot\bar{r}_4\cdot\dot{\omega}_6$$
$$+\frac{m_1m_2}{M}\ddot{\varepsilon}_{12}+4D_{12}\cdot\dot{\varepsilon}_{12}+4K_{12}\cdot\varepsilon_{12}-\left[\frac{m_2(m_3+m_4+m_5+m_6)}{M}\ddot{\varepsilon}_{23}+4D_{23}\cdot\dot{\varepsilon}_{23}+4K_{23}\cdot\varepsilon_{23}\right]$$
$$-\frac{m_2}{M}(m_4+m_5+m_6)\ddot{\varepsilon}_{34} \qquad (92)$$

$$\frac{m_1+m_2+m_4+m_5+m_6}{M} F_{3e} - \frac{m_3}{M}\left[F_{1e}+F_{2e}+F_{4e}+{}_4T_5\cdot(F_{5e}+F_{6e})\right] = 4D_{23}\cdot(\bar{R}_{230}+\bar{R}_{E30})\cdot\omega_2$$
$$+4K_{23}\cdot(\bar{R}_{230}+\bar{R}_{E30})\cdot\theta_2-\left[4D_{23}\cdot\bar{R}_{E30}+4D_{34}\cdot(\bar{R}_{340}+\bar{R}_{E40})\right]\cdot\omega_3-\left[4K_{23}\cdot\bar{R}_{E30}\right.$$
$$\left.+4K_{34}\cdot(\bar{R}_{340}+\bar{R}_{E40})\right]\cdot\theta_3+\frac{m_3}{M}(m_5+m_6)\bar{r}_1\cdot\dot{\omega}_4+4D_{34}\cdot\bar{R}_{E40}\cdot\omega_4+4K_{34}\cdot\bar{R}_{E40}\cdot\theta_4$$
$$+{}_4T_5\cdot\frac{m_3}{M}\left[(m_5+m_6)\bar{r}_2-m_6\bar{r}_3\right]\cdot\dot{\omega}_5-\frac{m_3m_6}{M}\,{}_4T_5\cdot\bar{r}_4\cdot\dot{\omega}_6+\frac{m_1m_3}{M}\ddot{\varepsilon}_{12}+\frac{m_3(m_1+m_2)}{M}\ddot{\varepsilon}_{23}$$
$$+4D_{23}\cdot\dot{\varepsilon}_{23}+4K_{23}\cdot\varepsilon_{23}-\left[\frac{m_3(m_4+m_5+m_6)}{M}\ddot{\varepsilon}_{34}+4D_{34}\cdot\dot{\varepsilon}_{34}+4K_{34}\cdot\varepsilon_{34}\right] \qquad (93)$$

The following definitions are used in equations (85) thru (93)

$$J_4^* = \mathrm{diag}\left[J_{4x};J_{4y};J_{4z}\right]$$

$$+\frac{(m_1+m_2+m_3+m_4)(m_5+m_6)}{M}\begin{bmatrix}(r_{1y}^2+r_{1z}^2) & -r_{1x}r_{1y} & -r_{1x}r_{1z}\\ -r_{1x}r_{1y} & (r_{1x}^2+r_{1z}^2) & -r_{1y}r_{1z}\\ -r_{1x}r_{1z} & -r_{1y}r_{1z} & (r_{1x}^2+r_{1y}^2)\end{bmatrix} \qquad (94)$$

$$J_5^* = \text{diag}\left[J_{5x}; J_{5y}; J_{5z}\right]$$

$$+ \frac{(m_1+m_2+m_3+m_4)(m_5+m_6)}{M} \begin{bmatrix} (r_{2y}^2+r_{2z}^2) & -r_{2x}r_{2y} & -r_{2x}r_{2z} \\ -r_{2x}r_{2y} & (r_{2x}^2+r_{2z}^2) & -r_{2y}r_{2z} \\ -r_{2x}r_{2z} & -r_{2y}r_{2z} & (r_{2x}^2+r_{2y}^2) \end{bmatrix}$$

$$+ \frac{m_6(m_1+m_2+m_3+m_4+m_5)}{M} \begin{bmatrix} (r_{3y}^2+r_{3z}^2) & -r_{3x}r_{3y} & -r_{3x}r_{3z} \\ -r_{3x}r_{3y} & (r_{3x}^2+r_{3z}^2) & -r_{3y}r_{3z} \\ -r_{3x}r_{3z} & -r_{3y}r_{3z} & (r_{3x}^2+r_{3y}^2) \end{bmatrix}$$

$$+ \frac{m_6(m_1+m_2+m_3+m_4)}{M} \begin{bmatrix} (r_{2y}r_{3y}+r_{2z}r_{3z}) & -r_{2x}r_{3y} & -r_{2x}r_{3z} \\ -r_{2y}r_{3x} & (r_{2x}r_{3x}+r_{2z}r_{3z}) & -r_{2y}r_{3z} \\ -r_{2z}r_{3x} & -r_{2z}r_{3y} & (r_{2x}r_{3x}+r_{2y}r_{3y}) \end{bmatrix}$$

$$+ \frac{m_6(m_1+m_2+m_3+m_4)}{M} \begin{bmatrix} (r_{2y}r_{3y}+r_{2z}r_{3z}) & -r_{2y}r_{3x} & -r_{2z}r_{3x} \\ -r_{2x}r_{3y} & (r_{2x}r_{3x}+r_{2z}r_{3z}) & -r_{2z}r_{3y} \\ -r_{2x}r_{3z} & -r_{2y}r_{3z} & (r_{2x}r_{3x}+r_{2y}r_{3y}) \end{bmatrix} \quad (95)$$

$$J_6^* = \text{diag}\left[J_{6x}; J_{6y}; J_{6z}\right]$$

$$+ \frac{m_6(m_1+m_2+m_3+m_4+m_5)}{M} \begin{bmatrix} (r_{4y}^2+r_{4z}^2) & -r_{4x}r_{4y} & -r_{4x}r_{4z} \\ -r_{4x}r_{4y} & (r_{4x}^2+r_{4z}^2) & -r_{4y}r_{4z} \\ -r_{4x}r_{4z} & -r_{4y}r_{4z} & (r_{4x}^2+r_{4y}^2) \end{bmatrix} \quad (96)$$

$$J_{56} = \frac{m_6}{M}\left\{(m_1+m_2+m_3+m_4)\begin{bmatrix}(r_{2y}r_{4y}+r_{2z}r_{4z}) & -r_{2y}r_{4x} & -r_{2z}r_{4x}\\ -r_{2x}r_{4y} & (r_{2z}r_{4z}+r_{2x}r_{4x}) & -r_{2z}r_{4y}\\ -r_{2x}r_{4z} & -r_{2y}r_{4z} & (r_{2x}r_{4x}+r_{2y}r_{4y})\end{bmatrix}\right.$$

$$\left.+(m_1+m_2+m_3+m_4+m_5)\begin{bmatrix}(r_{3y}r_{4y}+r_{3z}r_{4z}) & -r_{3y}r_{4x} & -r_{3z}r_{4x}\\ -r_{3x}r_{4y} & (r_{3z}r_{4z}+r_{3x}r_{4x}) & -r_{3z}r_{4y}\\ -r_{3x}r_{4z} & -r_{3y}r_{4z} & (r_{3x}r_{4x}+r_{3y}r_{4y})\end{bmatrix}\right\} \quad (97)$$

$$J_{65} = \frac{m_6(m_1+m_2+m_3+m_4)}{M}\begin{bmatrix}(r_{2y}r_{4y}+r_{2z}r_{4z}) & -r_{4y}r_{2x} & -r_{4z}r_{2x}\\ -r_{4x}r_{2y} & (r_{4x}r_{2x}+r_{4z}r_{2z}) & -r_{4z}r_{2y}\\ -r_{4x}r_{2z} & -r_{4y}r_{2z} & (r_{4x}r_{2x}+r_{4y}r_{2y})\end{bmatrix}$$

$$+\frac{m_6(m_1+m_2+m_3+m_4+m_5)}{M}\begin{bmatrix}(r_{4y}r_{3y}+r_{4z}r_{3z}) & -r_{4y}r_{3x} & -r_{4z}r_{3x}\\ -r_{4x}r_{3y} & (r_{4x}r_{3x}+r_{4z}r_{3z}) & -r_{4z}r_{3y}\\ -r_{4x}r_{3z} & -r_{4y}r_{3z} & (r_{4x}{}_{3x}+r_{4y}r_{3y})\end{bmatrix} \quad (98)$$

$$\bar{R}_{120} = \begin{bmatrix}0 & -R_{120z} & R_{120y}\\ R_{120z} & 0 & -R_{120x}\\ -R_{120y} & R_{120x} & 0\end{bmatrix} \quad (99)$$

$$\bar{R}_{230} = \begin{bmatrix}0 & -R_{230z} & R_{230y}\\ R_{230z} & 0 & -R_{230x}\\ -R_{230y} & R_{230x} & 0\end{bmatrix} \quad (100)$$

$$\bar{\bar{R}}_{340} = \begin{bmatrix} 0 & -R_{340z} & R_{340y} \\ R_{340z} & 0 & -R_{340x} \\ -R_{340y} & R_{340x} & 0 \end{bmatrix} \tag{101}$$

$$\bar{\bar{R}}_{E20} = \begin{bmatrix} 0 & -R_{E20z} & R_{E20y} \\ R_{E20z} & 0 & -R_{E20x} \\ -R_{E20y} & R_{E20x} & 0 \end{bmatrix} \tag{102}$$

$$\bar{\bar{R}}_{E30} = \begin{bmatrix} 0 & -R_{E30z} & R_{E30y} \\ R_{E30z} & 0 & -R_{E30x} \\ -R_{E30y} & R_{E30x} & 0 \end{bmatrix} \tag{103}$$

$$\bar{\bar{R}}_{E40} = \begin{bmatrix} 0 & -R_{E40z} & R_{E40y} \\ R_{E40z} & 0 & -R_{E40x} \\ -R_{E40y} & R_{E40x} & 0 \end{bmatrix} \tag{104}$$

$$\bar{r}_1 = \begin{bmatrix} 0 & -r_{1z} & r_{1y} \\ r_{1z} & 0 & -r_{1x} \\ -r_{1y} & r_{1x} & 0 \end{bmatrix} \tag{105}$$

$$\bar{r}_2 = \begin{bmatrix} 0 & -r_{2z} & r_{2y} \\ r_{2z} & 0 & -r_{2x} \\ -r_{2y} & r_{2x} & 0 \end{bmatrix} \tag{106}$$

$$\bar{r}_3 = \begin{bmatrix} 0 & -r_{3z} & r_{3y} \\ r_{3z} & 0 & -r_{3x} \\ -r_{3y} & r_{3x} & 0 \end{bmatrix} \tag{107}$$

$$\bar{r}_4 = \begin{bmatrix} 0 & -r_{4z} & r_{4y} \\ r_{4z} & 0 & -r_{4x} \\ -r_{4y} & r_{4x} & 0 \end{bmatrix} \tag{108}$$

$$\varepsilon_{12} = \begin{bmatrix} \varepsilon_{12x} \\ \varepsilon_{12y} \\ \varepsilon_{12z} \end{bmatrix} \tag{109}$$

$$\varepsilon_{23} = \begin{bmatrix} \varepsilon_{23x} \\ \varepsilon_{23y} \\ \varepsilon_{23z} \end{bmatrix} \tag{110}$$

$$\varepsilon_{34} = \begin{bmatrix} \varepsilon_{34x} \\ \varepsilon_{34y} \\ \varepsilon_{34z} \end{bmatrix} \tag{111}$$

$$\theta_j = \begin{bmatrix} \theta_{jx} \\ \theta_{jy} \\ \theta_{jz} \end{bmatrix} \qquad j=1,\ldots,6 \tag{112}$$

$$\omega_j = \begin{bmatrix} \omega_{jx} \\ \omega_{jy} \\ \omega_{jz} \end{bmatrix} \qquad j=1,\ldots,6 \tag{113}$$

$$F_{je} = \begin{bmatrix} F_{jex} \\ F_{jey} \\ F_{jez} \end{bmatrix} \qquad j=1,\ldots,6 \tag{114}$$

$$T_{je} = \begin{bmatrix} T_{jex} \\ T_{jey} \\ T_{jez} \end{bmatrix} \qquad j=1,\ldots,6 \tag{115}$$

$$\bar{\bar{R}}_{jj} = \begin{bmatrix} 0 & -R_{jjz} & R_{jjy} \\ R_{jjz} & 0 & -R_{jjx} \\ -R_{jjy} & R_{jjx} & 0 \end{bmatrix} \qquad j=1,\ldots,6 \tag{116}$$

$${}_4T_5^{-1} = {}_5T_4 = \begin{bmatrix} a_{11} & a_{21} & a_{31} \\ a_{12} & a_{22} & a_{32} \\ a_{13} & a_{23} & a_{33} \end{bmatrix} \tag{117}$$

Equations (85) thru (93) form the complete set of linear equations of motion for the six body system being considered. The one additional thing required to specify the complete mathematical model of the six body system is the definition of all the possible control torque equations that can act on the system. For the three IPS options (i.e., IOG, SEPB, and Floated Pallet) being considered in this study the control on body 1 (i.e., T_{1c}) which represents the orbiter is zero for the following reason.

When considering the operation of the IOG or SEPB the orbiter vernier RCS is controlling the orbiter vehicle which operates essentially independently from the SEPB or the IOG. The disturbances applied to the system due to RCS firings are negligible when compared to the manned motion disturbance and hence can be neglected. When considering the Floated Pallet, the orbiter vernier RCS is inhibited and the complete system including the orbiter is controlled via a cluster of pallet mounted double gimbal control moment gyros.

The control torque structure is assumed to be in all cases a linear combination of rate, position, and the integral of position. Throughout it is assumed that system rate is measured by a set of rate gyros whose output is integrated twice to obtain system position and the integral of position thus enabling the formation of the command control torque vector. The control torque T_{2c} can be formed by information derived from a set of rate gyros mounted either on body 2 or 3. Assuming the gyros to be mounted on body 2 the control torque command vector can be expressed as

$$T_{2c_{comm}} = -\left[K_{Rp} \cdot \omega_{2m} + K_{Pp} \cdot \frac{\omega_{2m}}{s} + K_{Ip} \cdot \frac{\omega_{2m}}{s^2}\right] \tag{118}$$

where:

ω_{2m} = measured rate of body 2

K_{Rp} = floated pallet rate gain

K_{Pp} = floated pallet position gain

K_{Ip} = floated pallet integral gain

and

$$K_{Rp} = \text{diag}\left[K_{Rpx}; K_{Rpy}; K_{Rpz}\right] \tag{119}$$

$$K_{Pp} = \text{diag}\left[K_{Ppx}; K_{Ppy}; K_{Ppz}\right] \tag{120}$$

$$K_{Ip} = \text{diag}\left[K_{Ipx}; K_{Ipy}; K_{Ipz}\right] \tag{121}$$

The relationship between the actual and measured system rate assuming second order sensor dynamics can be written as

$$\omega_{m2}=\left[\frac{\omega_{ns}^2}{s^2+2\zeta_s\omega_{ns}s+\omega_{ns}^2}\right]\omega_2 \tag{122}$$

where:

ω_{ns} = gyro natural frequency

ζ_s = gyro damping ratio

The relationship between the command torque vector and the actual torque vector applied to the vehicle assuming second order control moment gyro dynamics is given by

$$T_{2c}=\left[\frac{\omega_{na}^2}{s^2+2\zeta_a\omega_{na}s+\omega_{na}^2}\right]T_{2c_{comm}} \tag{123}$$

where:

ω_{na} = actuator (CMG) natural frequency

ζ_a = actuator (CMG) damping ratio

Substituting equation (122) into equation (118) and in turn substituting the results into equation (123) gives

$$T_{2c}=-\left[\frac{\omega_{na}^2}{s^2+2\zeta_a\omega_{na}s+\omega_{na}^2}\right]\left[\frac{\omega_{ns}^2}{s^2+2\zeta_s\omega_{ns}s+\omega_{ns}^2}\right]\left[K_{Rp}\cdot\omega_2+K_{Pp}\cdot\theta_2+K_{Ip}\cdot\frac{\theta_2}{s}\right] \tag{124}$$

If the rate gyros were mounted on body 3 the control torque is given by

$$T_{2c}=-\left[\frac{\omega_{na}^2}{s^2+2\zeta_a\omega_{na}s+\omega_{na}^2}\right]\left[\frac{\omega_{ns}^2}{s^2+2\zeta_s\omega_{ns}s+\omega_{ns}^2}\right]\left[K_{Rp}\cdot\omega_3+K_{Pp}\cdot\theta_3+K_{Ip}\cdot\frac{\theta_3}{s}\right] \tag{125}$$

Using the same approach as above the control torques on body 3 can be written as

$$T_{3c}=-\left[\frac{\omega_{na}^2}{s^2+2\zeta_a\omega_{na}s+\omega_{na}^2}\right]\left[\frac{\omega_{ns}^2}{s^2+2\zeta_s\omega_{ns}s+\omega_{ns}^2}\right]\left[K_{Rp}\cdot\omega_3+K_{Pp}\cdot\theta_3+K_{Ip}\cdot\frac{\theta_3}{s}\right] \quad (126)$$

$$T_{3c}=-\left[\frac{\omega_{na}^2}{s^2+2\zeta_a\omega_{na}s+\omega_{na}^2}\right]\left[\frac{\omega_{ns}^2}{s^2+2\zeta_s\omega_{ns}s+\omega_{ns}^2}\right]\left[K_{Rp}\cdot\omega_2+K_{Pp}\cdot\theta_2+K_{Ip}\cdot\frac{\theta_2}{s}\right] \quad (127)$$

Using the same approach as above for determination of the hinge torques T_H realizing that the hinge cannot be moved hence it always applies torques to bodies 4 and 5 but that the rate gyros can be mounted on body 5 or 6 the following results

$$T_H=-\left[\frac{\omega_{nT}}{s+\omega_{nT}}\right]\left[\frac{\omega_{ns}^2}{s^2+2\zeta_s\omega_{ns}s+\omega_{ns}^2}\right]\left[K_{R6}\cdot\omega_6+K_{P6}\cdot\theta_6+K_{I6}\cdot\frac{\theta_6}{s}\right] \quad (128)$$

$$T_H=-\left[\frac{\omega_{nT}}{s+\omega_{nT}}\right]\left[\frac{\omega_{ns}^2}{s^2+2\zeta_s\omega_{ns}s+\omega_{ns}^2}\right]\left[K_{R6}\cdot\omega_5+K_{P6}\cdot\theta_5+K_{I6}\cdot\frac{\theta_5}{s}\right] \quad (129)$$

where:

$\frac{1}{\omega_{nT}}$ = gimbal torquer time constant

K_{R6} = telescope rate gain

K_{P6} = telescope position gain

K_{I6} = telescope integral gain

Additionally

$$K_{R6}=\text{diag}\left[K_{R6x};K_{R6y};K_{R6z}\right] \quad (130)$$

$$K_{P6}=\text{diag}\left[K_{P6x};K_{P6y};K_{P6z}\right] \quad (131)$$

$$K_{I6}=\text{diag}\left[K_{I6x};K_{I6y};K_{I6z}\right] \quad (132)$$

In the derivation of the hinge torques it is assumed that the gimbal torquer has first order dynamics. It should be noted that at no time can more than one of the control torques defined in equations (124), (125), (126), (127), (128) and (129) be acting on the six body system.

Equations (85) thru (93) in conjunction with equations (124) thru (129) constitute the linear mathematical model of the IPS. This model was programmed on a digital computer and used in the evaluation of the three IPS options, the IOG, SEPB and Floated Pallet. Each of these systems can be obtained from the IPS model defined above by proper initialization in the following manner. To obtain the IOG, the suspension parameters between bodies 1 and 2, i.e., d_{12}, k_{12}, D_{12} and K_{12} are set to reflect a structural interface while the suspension parameters between bodies 3 and 4, i.e., d_{34}, k_{34}, D_{34} and K_{34} are set to reflect the IOG suspension characteristics. The control torques T_{2c} and T_{3c} are identically set to zero. To obtain the SEPB the suspension parameters between bodies 1 and 2 and 3 and 4 are set to reflect a structural interface while the control torques T_{2c} and T_{3c} are set identically to zero. In addition $r_2+r_3+r_4<<1$ which means that the gimbal suspension is close to the telescope center of mass. To obtain the Floated Pallet d_{34}, k_{34}, D_{34}, K_{34} and T_H are identically set to zero while the suspension parameters between bodies 1 and 2 are set to reflect the floated pallet suspension characteristics.

2.1.3 Parameters for IPS Pointing Performance Evaluation - Tables 2-1, 2-2 and 2-3 list the nominal parameters that were used to evaluate the pointing performance of the IOG, SEPB and Floated Pallet, respectively. Table 2-4 lists a set of general control gain functions from which the gains for any loop bandwidth for arbitrary inertia can be computed assuming a control law structure of rate, position, plus integral of position.

2.2 Slewing Model - The sections that follow will outline the derivation of the mathematical model employed for slewing.

2.2.1 Translational Equations of Motion - Referring to figure 2-4 and using the same nomenclature as defined above the following translational equations of motion can be written for the system depicted.

$$F_{1e}+F_{c12}=m_1\ddot{\rho}_1 \tag{133}$$

$$F_{2e}-F_{c12}+F_H=m_2\ddot{\rho}_2 \tag{134}$$

$$F_{3e}-F_H=m_3\ddot{\rho}_3 \tag{135}$$

$$\sum_{j=1}^{3} F_{je}=M\ddot{\rho}_o;\ M=(m_1+m_2+m_3) \tag{136}$$

Additionally from the geometry shown in figure 2-4 we have

$$\rho_1=\rho_o+R_1 \tag{137}$$

$$\rho_2=\rho_o+R_2 \tag{138}$$

$$\rho_3=\rho_o+R_3 \tag{139}$$

From the definition of the composite system center of mass

$$m_1R_1+m_2R_2+m_3R_3=0 \tag{140}$$

Also from geometrical considerations

$$R_2=R_1+R_{120}+\varepsilon_{12} \tag{141}$$

$$R_3=R_1+R_{120}+\varepsilon_{12}+r_1+r_2 \tag{142}$$

Substituting equations (141) and (142) into equation (140) and solving for R_1 yields

$$R_1=-\frac{1}{M}\left[(m_2+m_3)(R_{120}+\varepsilon_{12})+m_3(r_1+r_2)\right] \tag{143}$$

Substituting equations (139), (143) and (136) into equation (135) and solving for the hinge force yields

$$F_H=\frac{1}{M}\left[(m_1+m_2)F_{3e}-m_3(F_{1e}+F_{2e})-m_1m_3\ddot{\varepsilon}_{12}-m_3(m_1+m_2)(\ddot{r}_1+\ddot{r}_2)\right] \tag{144}$$

The compliance force between bodies 1 and 2 of the k^{th} isolator can be written as

$$F_{c12k}=K_{12}\cdot\varepsilon_{12}+D_{12}\cdot\dot{\varepsilon}_{12}+K_{12}\cdot\left[(\beta_{k2}^{12}-\beta_{k20}^{12})-(\beta_{k1}^{12}-\beta_{k10}^{12})\right]+D_{12}\cdot\left[\dot{\beta}_{k2}^{12}-\dot{\beta}_{k1}^{12}\right] \quad (145)$$

Substituting equations (29) thru (34) into equation (144) results in

$$F_{c12k}=K_{12}\cdot\left[\varepsilon_{12}+(\theta_2-\theta_1)xR_{E20}-\theta_1xR_{120}+(\theta_2-\theta_1)x\alpha_{k20}^{12}\right]$$
$$+D_{12}\cdot\left[\dot{\varepsilon}_{12}+(\omega_2-\omega_1)xR_{E20}+(\omega_2-\omega_1)x\alpha_{k20}^{12}-\omega_1xR_{120}\right] \quad (146)$$

However

$$F_{c12}=\sum_{k=1}^{4}F_{c12k} \quad (147)$$

which yields

$$F_{c12}=4K_{12}\cdot\left[\varepsilon_{12}+(\theta_2-\theta_1)xR_{E20}-\theta_1xR_{120}\right]+4D_{12}\cdot\left[\dot{\varepsilon}_{12}+(\omega_2-\omega_1)xR_{E20}-\omega_1xR_{120}\right] \quad (148)$$

A force equation will be required in order to solve for ε_{12}. This equation is obtained by substituting equations (148), (143) and (137) into equation (133) which results in

$$\frac{m_2+m_3}{M}F_{1e}-\frac{m_1}{M}(F_{2e}+F_{3e})=-\left[\frac{m_1}{M}(m_2+m_3)\ddot{\varepsilon}_{12}+4D\cdot\dot{\varepsilon}_{12}+4K_{12}\cdot\varepsilon_{12}\right]$$
$$+4D_{12}\cdot\left[(\omega_1-\omega_2)xR_{E20}+\omega_1xR_{120}\right]+4K_{12}\cdot\left[(\theta_1-\theta_2)xR_{E20}+\theta_1xR_{120}\right]$$
$$-\frac{m_1m_3}{M}(\ddot{r}_1+\ddot{r}_2) \quad (149)$$

2.2.2 Rotational Equations of Motion - The following paragraphs will develop the rotational equations of motion of the system depicted in figure 2-4. In this development it will be assumed that the coordinate frames of bodies 1 and 2 are aligned. However, the coordinate frame of body 3 can be at an arbitrary orientation with respect to bodies 1 and 2.

Body 1 - The rotational equation of motion for body 1 can be written as

$$T_{1e}+R_{11}xF_{1e}+\sum_{k=1}^{4}\beta_{k1}^{12}xF_{c12k}=\frac{d}{dt}(J_1\cdot\omega_1) \qquad (150)$$

Substituting equations (29), (33) and (146) into equation (150) and doing the indicated summation eliminating second order terms yields

$$T_{1e}+R_{11}xF_{1e}=\frac{d}{dt}(J_1\cdot\omega_1)+d_{12}\cdot(\omega_1-\omega_2)+k_{12}\cdot(\theta_1-\theta_2)$$

$$+4(R_{120}+R_{E20})x\left\{D_{12}\cdot\left[(\omega_1-\omega_2)xR_{E20}+\omega_1xR_{120}\right]\right.$$

$$\left.+K_{12}\cdot\left[(\theta_1-\theta_2)xR_{E20}+\theta_1xR_{120}\right]\right\}-4(R_{120}+R_{E20})x\left[D_{12}\cdot\dot{\varepsilon}_{12}+K_{12}\cdot\varepsilon_{12}\right] \qquad (151)$$

Body 2 - The rotational equation of motion for body 2 can be written as

$$T_{2e}-T_H^2+R_{22}xF_{2e}-\sum_{k=1}^{4}\beta_{k2}^{12}xF_{c12k}+r_1xF_H=\frac{d}{dt}(J_2\cdot\omega_2) \qquad (152)$$

Substituting equations (30), (34), (144) and (146) into equation (152) and eliminating second order terms gives

$$T_{2e}+R_{22}xF_{2e}+\frac{(m_1+m_2)}{M}r_1xF_{3e}^2-\frac{m_3}{M}r_1x(F_{1e}+F_{2e})=\frac{d}{dt}(J_2\cdot\omega_2)+d_{12}\cdot(\omega_2-\omega_1)$$

$$+k_{12}\cdot(\theta_2-\theta_1)+4R_{E20}x\left\{D_{12}\cdot\left[(\omega_2-\omega_1)xR_{E20}-\omega_1xR_{120}\right]+K_{12}\cdot\left[(\theta_2-\theta_1)xR_{E20}-\theta_1xR_{120}\right]\right\}$$

$$+\frac{m_1m_3}{M}r_1x\ddot{\varepsilon}_{12}+4R_{E20}x\left[D_{12}\cdot\dot{\varepsilon}_{12}+K_{12}\cdot\varepsilon_{12}\right]+\frac{m_3(m_1+m_2)}{M}r_1(\ddot{r}_1x\ddot{r}_2^2)+T_H^2 \qquad (153)$$

where:

F_{3e}^2 = external force acting on body 3 written in body 2 coordinates

T_H^2 = hinge torque acting on bodies 2 and 3 written in body 2 coordinates

r_2^2 = distance from hinge point to CM of body 3 written in body 2 coordinates

Body 3 - The rotational equation of motion for body 3 can be expressed as

$$T_H+T_{3e}+R_{33}xF_{3e}+r_2xF_H=\frac{d}{dt}(J_3\cdot\omega_3) \tag{154}$$

Substituting equation (144) into equation (154) yields

$$T_{3e}+R_{33}xF_{3e}+\frac{(m_1+m_2)}{M}r_2xF_{3e}-\frac{m_3}{M}r_2x(F_{1e}^3+F_{2e}^3)=\frac{d}{dt}(J_3\cdot\omega_3)$$
$$-T_H+\frac{m_1m_3}{M}r_2x\ddot{\varepsilon}_{12}^3+\frac{m_3(m_1+m_2)}{M}r_2x(\ddot{r}_1^3+\ddot{r}_2) \tag{155}$$

where:

F_{1e}^3, F_{2e}^3 = external force acting on bodies 1 and 2, respectively, written in body 3 coordinates

r_1^3 = distance from CM of body 2 to hinge point, written in body 3 coordinates

Rewriting equations (149), (151), (153) and (155) in matrix form yields

$$\begin{aligned}
&T_{1e}+\bar{R}_{11}\cdot F_{1e}=J_1\cdot\dot{\omega}_1+d_{12}\cdot(\omega_1-\omega_2)+k_{12}\cdot(\theta_1-\theta_2)\\
&-4(\bar{R}_{120}+\bar{R}_{E20})\cdot\left\{D_{12}\cdot\left[\bar{R}_{E20}\cdot(\omega_1-\omega_2)+\bar{R}_{120}\cdot\omega_1\right]\right.\\
&\left.+K_{12}\cdot\left[\bar{R}_{E20}\cdot(\theta_1-\theta_2)+\bar{R}_{120}\cdot\theta_1\right]\right\}\\
&-4(\bar{R}_{120}+\bar{R}_{E20})\cdot\left[D_{12}\cdot\dot{\varepsilon}_{12}+K_{12}\cdot\varepsilon_{12}\right]
\end{aligned} \tag{156}$$

$$T_{2e}+\bar{R}_{22}\cdot F_{2e}+\frac{m_1+m_2}{M}\bar{r}_1\cdot {}_2T_3\cdot F_{3e}-\frac{m_3}{M}\bar{r}_1\cdot(F_{1e}+F_{2e})=J_2^*\cdot\dot{\omega}_2+d_{12}\cdot(\omega_2-\omega_1)$$
$$+k_{12}\cdot(\theta_2-\theta_1)-4\bar{R}_{E20}\cdot\left\{D_{12}\cdot\left[\bar{R}_{E20}\cdot(\omega_2-\omega_1)-\bar{R}_{120}\cdot\omega_1\right]+K_{12}\cdot\left[\bar{R}_{E20}\cdot(\theta_2-\theta_1)-R_{120}\cdot\theta_1\right]\right\}$$
$$+\frac{m_1m_3}{M}\bar{r}_1\cdot\ddot{\varepsilon}_{12}+4\bar{R}_{E20}\cdot\left[D_{12}\cdot\dot{\varepsilon}_{12}+K_{12}\cdot\varepsilon_{12}\right]-\frac{m_3(m_1+m_2)}{M}\bar{r}_1\cdot\left\{{}_2T_3\cdot\left[\bar{r}_2\cdot\dot{\omega}_3+\bar{\omega}_3\cdot(\bar{r}_2\cdot\omega_3)\right]\right\}$$
$$+{}_2T_3\cdot T_H \qquad (157)$$

$$T_{3e}+R_{33}\cdot F_{3e}+\frac{m_1+m_2}{M}\bar{r}_2\cdot F_{3e}-\frac{m_3}{M}\bar{r}_2\cdot {}_2T_3^{-1}\cdot(F_{1e}+F_{2e})=J_3^*\cdot\dot{\omega}_3+\bar{\omega}_3\cdot\left[J_3^*\cdot\omega_3\right]$$
$$+\frac{m_1m_3}{M}\bar{r}_2\cdot\left[{}_2T_3^{-1}\cdot\ddot{\varepsilon}_{12}\right]-\frac{m_3(m_1+m_2)}{M}\bar{r}_2\cdot\left[{}_2T_3^{-1}\cdot\bar{r}_1\cdot\dot{\omega}_2\right]-T_H \qquad (158)$$

$$\frac{m_2+m_3}{M}F_{1e}-\frac{m_1}{M}(F_{2e}+{}_2T_3\cdot F_{3e})=-\left[\frac{m_1}{M}(m_2+m_3)\ddot{\varepsilon}_{12}+4D_{12}\cdot\dot{\varepsilon}_{12}+4K_{12}\cdot\varepsilon_{12}\right]$$
$$-4D_{12}\cdot\left[\bar{R}_{E20}\cdot(\omega_1-\omega_2)+\bar{R}_{120}\cdot\omega_1\right]-4K_{12}\cdot\left[\bar{R}_{E20}\cdot(\theta_1-\theta_2)+\bar{R}_{120}\cdot\theta_1\right]+\frac{m_1m_3}{M}(\bar{r}_1\cdot\dot{\omega}_2)$$
$$+\frac{m_1m_3}{M}\left\{{}_2T_3\cdot\left[\bar{r}_2\cdot\dot{\omega}_3+\bar{\omega}_3\cdot(\bar{r}_2\cdot\omega_3)\right]\right\} \qquad (159)$$

where:

$$J_2^*=\mathrm{diag}\left[J_{2x};J_{2y};J_{2z}\right]+\frac{m_3(m_1+m_2)}{M}\begin{bmatrix}(r_{1y}^2+R_{1z}^2) & -r_{1x}r_{1y} & -r_{1x}r_{1z}\\ -r_{1x}r_{1y} & (r_{1x}^2+R_{1z}^2) & -r_{1y}r_{1z}\\ -r_{1x}r_{1z} & -r_{1y}r_{1z} & (r_{1x}^2+r_{1y}^2)\end{bmatrix} \qquad (160)$$

$$J_3^*=\mathrm{diag}\left[J_{3x};J_{3y};J_{3z}\right]+\frac{m_3(m_1+m_2)}{M}\begin{bmatrix}(r_{2y}^2+r_{2z}^2) & -r_{2x}r_{2y} & -r_{2x}r_{2z}\\ -r_{2x}r_{2y} & (r_{2x}^2+r_{2z}^2) & -r_{2y}r_{2z}\\ -r_{2x}r_{2z} & -r_{2y}r_{2z} & (r_{2x}^2+r_{2y}^2)\end{bmatrix} \qquad (161)$$

$$\bar{\omega}_3=\begin{bmatrix}0 & -\omega_{3z} & \omega_{3y}\\ \omega_{3z} & 0 & -\omega_{3x}\\ -\omega_{3y} & \omega_{3x} & 0\end{bmatrix} \qquad (162)$$

and ${}_2T_3$ is the transformation from body 3 to body 2 coordinates and is equal to

$$ {}_2T_3 = \begin{bmatrix} a_{11} & a_{12} & a_{13} \\ a_{21} & a_{22} & a_{23} \\ a_{31} & a_{32} & a_{33} \end{bmatrix} \tag{163} $$

$$ {}_2T_3^{-1} = {}_3T_2 = \begin{bmatrix} a_{11} & a_{21} & a_{31} \\ a_{12} & a_{22} & a_{32} \\ a_{13} & a_{23} & a_{33} \end{bmatrix} \tag{164} $$

An assumption inherent in equations (156) thru (159) is that the nonlinear Euler, centrifugal and Coriolis terms are negligible for bodies 1 and 2. Equations (156) thru (159) form the complete set of equations of motion of the system shown in figure 2-4.

It now becomes necessary to define the control torques T_H and the computation scheme for updating ${}_2T_3$. The control torques are given by

$$ T_H = -\left[\frac{\omega_{nT}}{s+\omega_{nT}}\right]\left[\frac{\omega_{ns}^2}{s^2+2\zeta_s\omega_{ns}s+\omega_{ns}^2}\right]\left[K_{R3}\cdot\omega_3^* + K_{P3}\cdot\theta_3^* + K_{I3}\cdot\frac{\theta_3^*}{s}\right] \tag{165} $$

and

$$ \omega_3^* = (\omega_3 - \omega_{3c}) \tag{166} $$

$$ \theta_3^* = (\theta_3 - \theta_{3c}) \tag{167} $$

$$ \theta_{3c} = \int_0^t \omega_{3c}\,dt \tag{168} $$

where:

$$ K_{R3} = \text{diag}\left[K_{R3x}; K_{R3y}; K_{R3z}\right] \tag{169} $$

$$ K_{P3} = \text{diag}\left[K_{P3x}; K_{P3y}; K_{P3z}\right] \tag{170} $$

$$K_{I3}=\text{diag}\left[K_{I3x};K_{I3y};K_{I3z}\right] \tag{171}$$

$\vec{\omega}_{3c}$ = rate command vector

$\vec{\theta}_{3c}$ = angular position command

The computational scheme for updating ${}_2T_3$ is given by the following equation

$$\dot{{}_2T_3}={}_2T_3\cdot\bar{\omega}_3 \tag{172}$$

Equations (156) thru (159), (163) and (172) form the slewing model used to evaluate IOG slewing performance.

Table 2-5 lists the parameters that were used in the IOG slewing simulation.

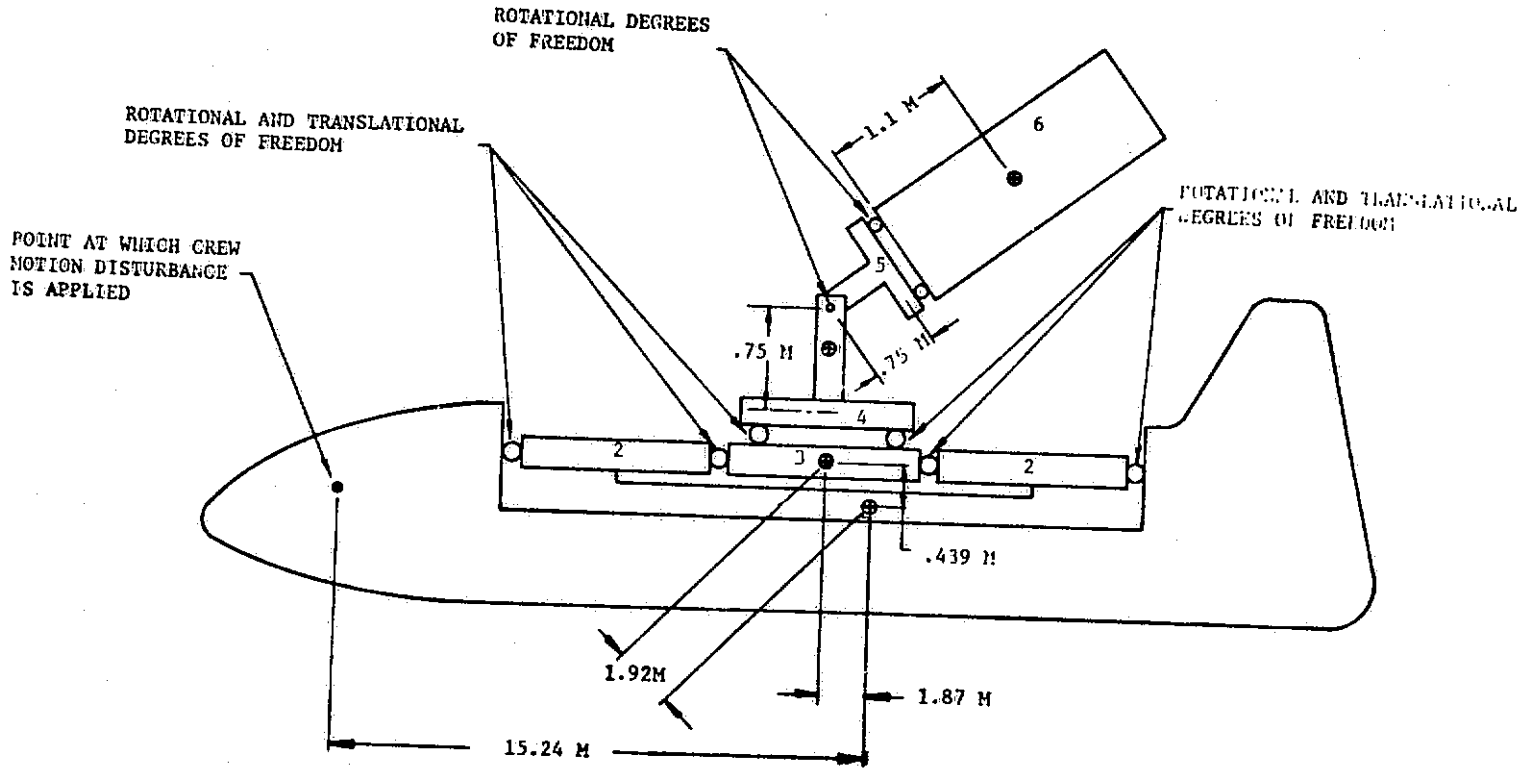

Figure 2-1. Schematic Diagram of Model Used for Evaluation of Performance of the Floated Pallet and IOG Systems

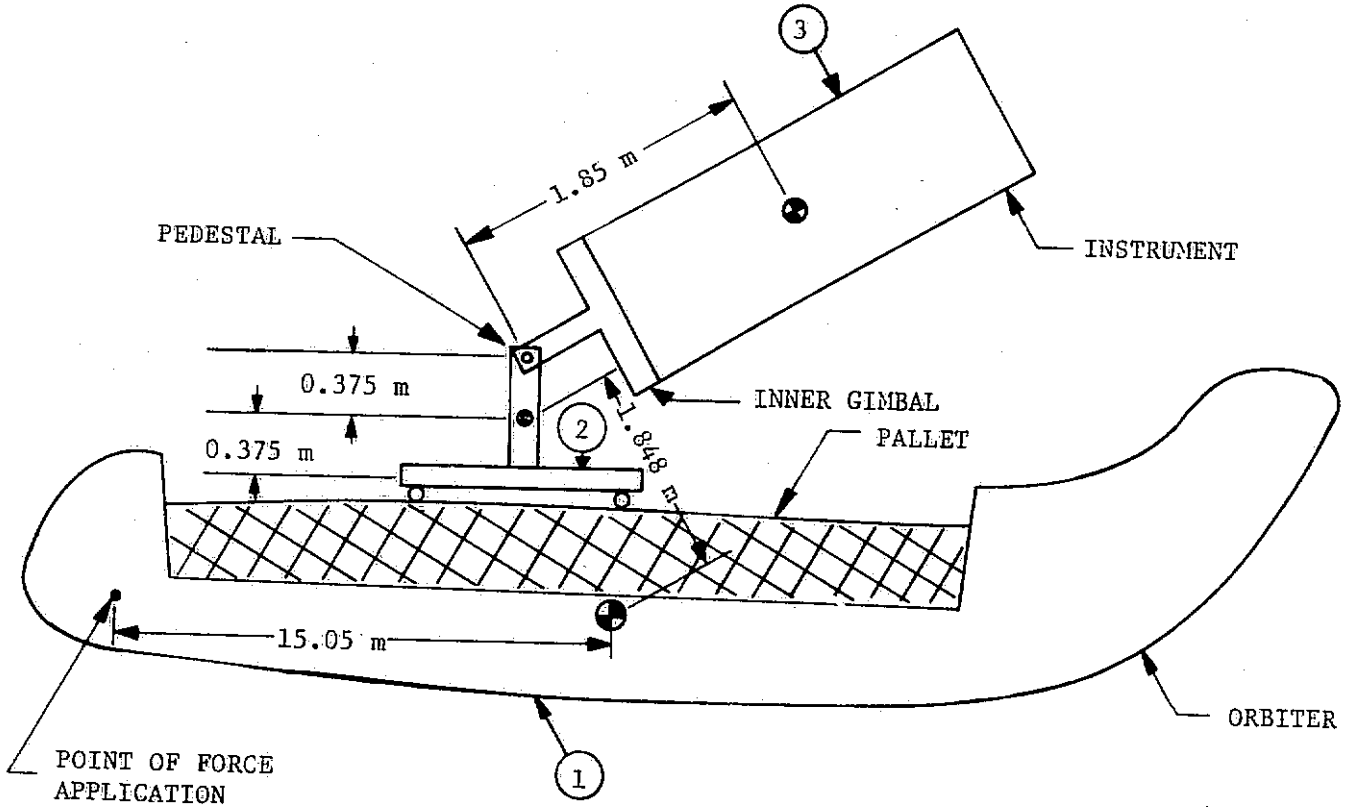

Figure 2-2. Schematic Diagram of Slewing Simulation

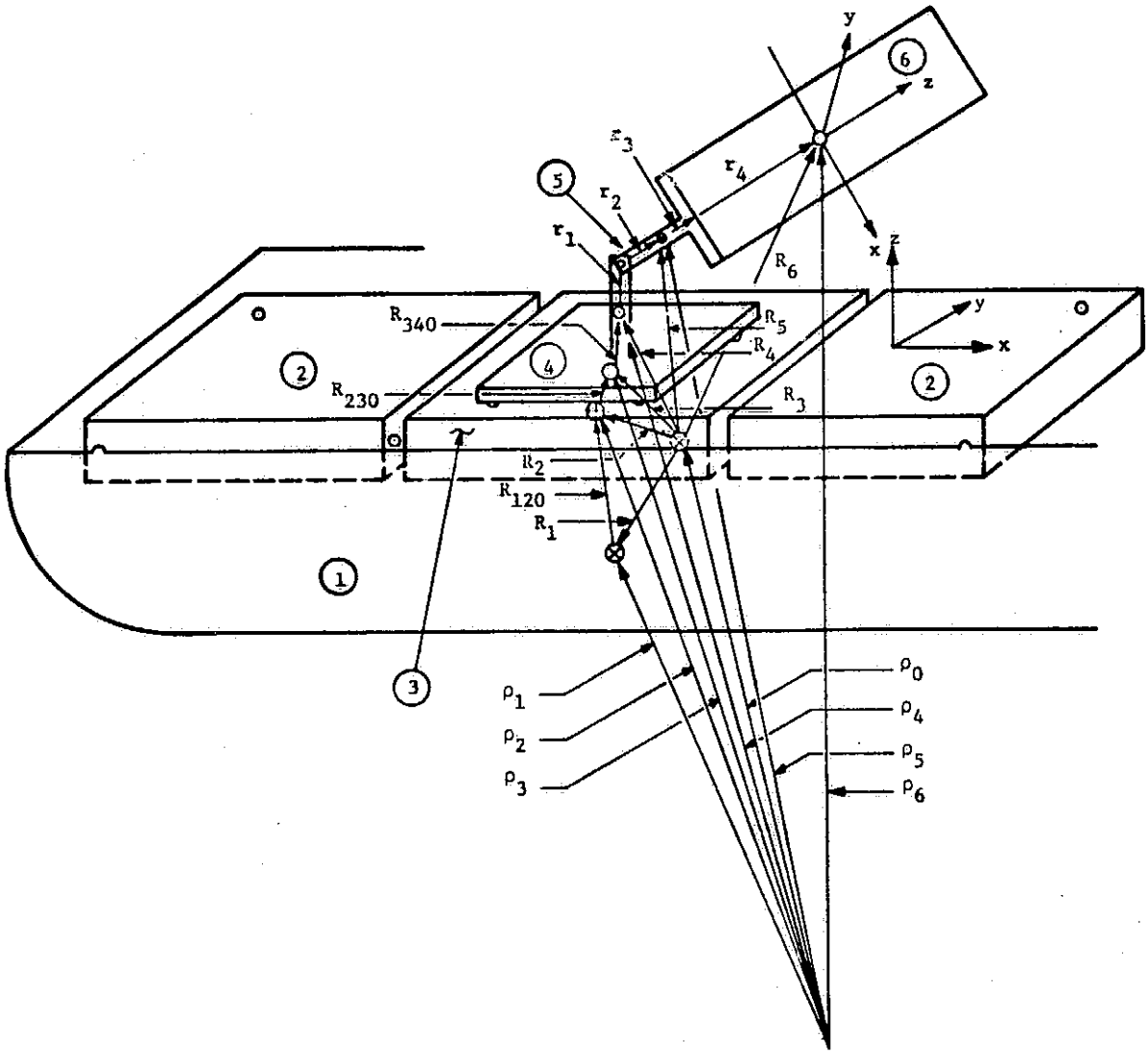

Figure 2-3. Schematic Diagram for Six Body Linear Model

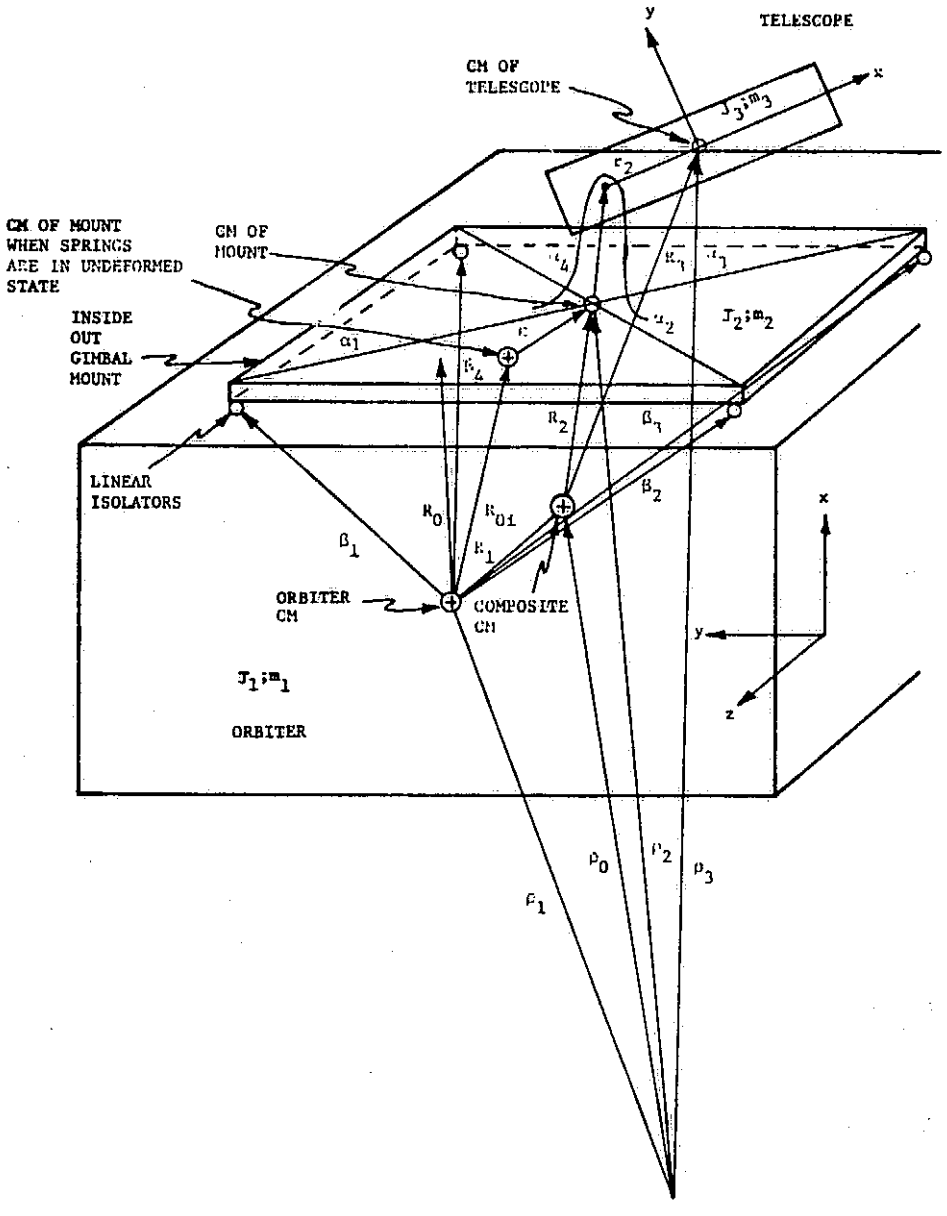

Figure 2-4. IPS Schematic Diagram

Table 2-1. IOG System Parameters

m_1=72,496 kg	J_{4z}=50.21 kg-m^2
m_2=5,398 kg	J_{5x}=74.63 kg-m^2
m_3=2,699 kg	J_{5y}=100.4 kg-m^2
m_4=195 kg	J_{5z}=74.63 kg-m^2
m_5=293 kg	J_{6x}=2.26x10^3 kg-m^2
m_6=2.39x10^3 kg	J_{6y}=1.98x10^3 kg-m^2
M=8.35x10^4 kg	J_{6z}=2.53x10^3 kg-m^2
J_{1x}=1.00x10^6 kg-m^2	R_{11}=-15.24 $\hat{1}_x$ m
J_{1y}=7.44x10^6 kg-m^2	R_{120}=-1.87 $\hat{1}_x$ +0.439 $\hat{1}_z$ m
J_{1z}=7.65x10^6 kg-m^2	R_{230}=0
J_{2x}=7.25x10^3 kg-m^2	R_{340}=0.375 $\hat{1}_z$ m
J_{2y}=8.58x10^4 kg-m^2	R_{E20}=0
J_{2z}=8.84x10^4 kg-m^2	R_{E30}=0
J_{3x}=3.63x10^3 kg-m^2	R_{E40}=-0.375 $\hat{1}_z$ m
J_{3y}=4.29x10^4 kg-m^2	r_1=0.375 $\hat{1}_z$ m
J_{3z}=4.42x10^4 kg-m^2	r_2=0.375 $\hat{1}_z$ m
J_{4x}=50.21 kg-m^2	r_3=0.375 $\hat{1}_z$ m
J_{4y}=50.21 kg-m^2	r_4=1.1 $\hat{1}_z$ m

Table 2-1. IOG System Parameters (Continued)

$D_{12x}=D_{12y}=D_{12z}=\frac{2(.01)}{4}(m_2+m_3)2\pi f_{n12T}=2.54\times10^{2}$	$f_{n12T}=254$ n-sec/rad (nominal)
$K_{12x}=K_{12y}=K_{12z}=\frac{m_2+m_3}{4}(2\pi f_{n12T})^2=7.99\times10^{4}$	$f^2_{n12T}=7.99\times10^{4}$ n-sec/rad (nominal)
$d_{12x}=2(.01)(J_{2x}+J_{3x})2\pi f_{n12Rx}=1.367\times10^{3}$	$f_{n12Rx}=1.367\times10^{3}$ (n-m-sec)/rad (nominal)
$d_{12y}=2(.01)(J_{2y}+J_{3y})2\pi f_{n12Ry}=1.617\times10^{4}$	$f_{n12Ry}=1.617\times10^{4}$ (n-m-sec)/rad (nominal)
$d_{12z}=2(.01)(J_{2z}+J_{3z})2\pi f_{n12Rz}=1.666\times10^{4}$	$f_{n12Rz}=1.666\times10^{4}$ (n-m-sec)/rad (nominal)
$k_{12x}=(J_{2x}+J_{3x})(2\pi f_{n12Rx})^2=4.295\times10^{5}$	$f^2_{n12Rx}=4.295\times10^{5}$ n-m/rad (nominal)
$k_{12y}=(J_{2y}+J_{3y})(2\pi f_{n12Ry})^2=5.081\times10^{6}$	$f^2_{n12Ry}=5.081\times10^{6}$ n-m/rad (nominal)
$k_{12z}=(J_{2z}+J_{3z})(2\pi f_{n12Rz})^2=5.235\times10^{6}$	$f^2_{n12Rz}=5.235\times10^{6}$ n-m/rad (nominal)
$D_{23x}=D_{23y}=D_{23z}=\frac{2(.01)}{4}m_3(2\pi f_{n23T})=84.8$	$f_{n23T}=84.8$ n-sec/rad (nominal)
$K_{23x}=K_{23y}=K_{23z}=\frac{m_3}{4}(2\pi f_{n23T})^2=2.66\times10^{4}$	$f^2_{n23T}=2.66\times10^{4}$ n/rad (nominal)
$d_{23x}=2(.01)J_{3x}2\pi f_{n23Rx}=4.562\times10^{2}$	$f_{n23Rx}=4.562\times10^{2}$ (n-m-sec)/rad (nominal)
$d_{23y}=2(.01)J_{3y}2\pi f_{n23Ry}=5.39\times10^{3}$	$f_{n23Ry}=5.39\times10^{3}$ (n-m-sec)/rad (nominal)
$d_{23z}=2(.01)J_{3z}2\pi f_{n23Rz}=5.554\times10^{3}$	$f_{n23Rz}=5.554\times10^{3}$ (n-m-sec)/rad (nominal)
$k_{23x}=J_{3x}(2\pi f_{n23Rx})^2=1.433\times10^{5}$	$f^2_{n23Rx}=1.433\times10^{5}$ n-m/rad (nominal)
$k_{23y}=J_{3y}(2\pi f_{n23Ry})^2=1.694\times10^{6}$	$f^2_{n23Ry}=1.694\times10^{6}$ n-m/rad (nominal)
$k_{23z}=J_{3z}(2\pi f_{n23Rz})^2=1.745\times10^{6}$	$f^2_{n23Rz}=1.745\times10^{6}$ n-m/rad (nominal)
$K_{34x}=K_{34y}=K_{34z}=2.5\times10^{3}$ n/m (nominal)	
$D_{34x}=D_{34y}=D_{34z}=2.68\times10^{2}$ n-sec/m (nominal)	This value of damping yields a damping ratio of 0.1 when the mass considered is $m_4+m_5+m_6$.

Table 2-1. IOG System Parameters (Concluded)

$d_{34x}=4D_{34z}(\alpha^{34}_{140y})^2=66.9$ (n-m-sec)/rad (nominal)
$d_{34y}=4D_{34z}(\alpha^{34}_{140x})^2=66.9$ (n-m-sec)/rad (nominal)
$d_{34z}=4D_{34y}(\alpha^{34}_{140x})^2+4D_{34x}(\alpha^{34}_{140y})^2=133.8$ (n-m-sec)/rad (nominal)
$k_{34x}=4K_{34z}(\alpha^{34}_{140y})^2=625$ n-m/rad (nominal)
$k_{34y}=4K_{34z}(\alpha^{34}_{140x})^2=625$ n-m/rad (nominal)
$k_{34z}=4K_{34y}(\alpha^{34}_{140x})^2+4K_{34x}(\alpha^{34}_{140y})^2=1.25\times10^3$ n-m/rad (nominal)
$\alpha^{34}_{140x}=\alpha^{34}_{140y}=\alpha^{34}_{140z}=0.25$ m
$d_{56x}=2(.01)J_{6x}2\pi f_{n56Rx}=2.84\times10^2\ f_{n56Rx}$
$d_{56y}=2(.01)J_{6y}2\pi f_{n56Ry}=2.488\times10^2\ f_{n56Ry}$
$d_{56z}=2(.01)J_{6z}2\pi f_{n56Rz}=3.179\times10^2\ f_{n56Rz}$
$k_{56x}=J_{6x}(2\pi f_{n56Rx})^2=8.922\times10^4\ f^2_{n56Rx}$
$k_{56y}=J_{6y}(2\pi f_{n56Ry})^2=7.817\times10^4\ f^2_{n56Ry}$
$k_{56z}=J_{6z}(2\pi f_{n56Rz})^2=9.988\times10^4\ f_{n56Rz}$

Table 2-2. Parameters for SEPB

$R_{11}=-15.24\ \hat{1}_x$ m ($-50\ \hat{1}_x$ ft)	$J_{4x}=2.402\text{x}10^3$ kg-m^2
$R_{120}=-1.87\ \hat{1}_x+.429\ \hat{1}_z$ m ($-6.125\ \hat{1}_x+1.408\ \hat{1}_z$ ft)	$J_{4y}=2.102\text{x}10^3$ kg-m^2
$m_1=72{,}496$ kg	$J_{4z}=2.603\text{x}10^3$ kg-m^2
$m_2=5{,}081$ kg	$J_{5x}=4.437\text{x}10^2$ kg-m^2
$m_3=2{,}541$ kg	$J_{5y}=1.224\text{x}10^3$ kg-m^2
$m_4=675$ kg	$J_{5z}=1.541\text{x}10^3$ kg-m^2
$m_5=287$ kg	$J_{6x}=2.265\text{x}10^3$ kg-m^2
$m_6=2{,}390$ kg	$J_{6y}=1.981\text{x}10^3$ kg-m^2
$J_{1x}=1.00\text{x}10^6$ kg-m^2	$J_{6z}=2.532\text{x}10^3$ kg-m^2
$J_{1y}=7.44\text{x}10^6$ kg-m^2	$R_{230}=0$
$J_{1z}=7.65\text{x}10^6$ kg-m^2	$R_{340}=.9332\ \hat{1}_z$ m
$J_{2x}=7.237\text{x}10^3$ kg-m^2	$r_1=2\ \hat{1}_z$ m
$J_{2y}=8.576\text{x}10^4$ kg-m^2	$r_2=0$
$J_{2z}=8.838\text{x}10^4$ kg-m^2	$r_3=0$
$J_{3x}=3.618\text{x}10^3$ kg-m^2	$r_4=0$
$J_{3y}=4.288\text{x}10^4$ kg-m^2	$R_{E440}=-2\ \hat{1}_z$ m
$J_{3z}=4.419\text{x}10^4$ kg-m^2	$R_{E220}=R_{E330}=0$

Table 2-2. Parameters for SEPB (Continued)

$D_{12x}=D_{12y}=D_{12z}=\frac{2(.01)}{4}(m_2+m_3)(2\pi)f_{n12T}=2.395\times10^{2}$ $f_{n12T}=2.395\times10^{2}$ n-sec/m (nominal)
$K_{12x}=K_{12y}=K_{12z}=(m_2+m_3)\frac{(2\pi)^2}{4}$ $f^2_{n12T}=7.523\times10^{4}$ $f^2_{n12T}=7.523\times10^{4}$ n/m (nominal)
$D_{23x}=D_{23y}=D_{23z}=\frac{2(.01)}{4}m_3(2\pi)f_{n23T}=79.83$ $f_{n23T}=79.83$ n-sec/m (nominal)
$K_{23x}=K_{23y}=K_{23z}=\frac{m_3}{4}(2\pi)^2$ $f^2_{n23T}=2.508\times10^{4}$ $f^2_{n23T}=2.508\times10^{4}$ n/m (nominal)
$D_{34x}=D_{34y}=D_{34z}=\frac{1}{4}(2)(.01)(m_4+m_5+m_6)(2\pi)f_{n34T}=1.053\times10^{2}$ $f_{n34T}=1.053\times10^{2}$ n-sec/m (nominal)
$K_{34x}=K_{34y}=K_{34z}=\frac{1}{4}(m_4+m_5+m_6)(2\pi)^2$ $f^2_{n34T}=3.308\times10^{4}$ $f^2_{n34T}=3.308\times10^{4}$ n/m (nominal)
$d_{12x}=2(.01)(J_{2x}+J_{3x})(2\pi)f_{n12Rx}=1.364\times10^{3}$ $f_{n12Rx}=1.364\times10^{3}$ (n-m-sec)/rad (nominal)
$d_{12y}=2(.01)(J_{2y}+J_{3y})(2\pi)f_{n12Ry}=1.617\times10^{4}$ $f_{n12Ry}=1.617\times10^{4}$ (n-m-sec)/rad (nominal)
$d_{12z}=2(.01)(J_{2z}+J_{3z})(2\pi)f_{n12Rz}=1.666\times10^{4}$ $f_{n12Rz}=1.666\times10^{4}$ (n-m-sec)/rad (nominal)
$k_{12x}=(J_{2x}+J_{3x})(2\pi)^2$ $f^2_{n12Rx}=4.285\times10^{5}$ $f^2_{n12Rx}=4.285\times10^{5}$ n-m/rad (nominal)
$k_{12y}=(J_{2y}+J_{3y})(2\pi)^2$ $f^2_{n12Ry}=5.079\times10^{6}$ $f^2_{n12Ry}=5.079\times10^{6}$ n-m/rad (nominal)
$k_{12z}=(J_{2z}+J_{3z})(2\pi)^2$ $f^2_{n12Rz}=5.234\times10^{6}$ $f^2_{n12Rz}=5.234\times10^{6}$ n-m/rad (nominal)
$d_{23x}=2(.01)J_{3x}(2\pi)f_{n23Rx}=4.547\times10^{2}$ $f_{n23Rx}=4.547\times10^{2}$ (n-m-sec)/rad (nominal)
$d_{23y}=2(.01)J_{3y}(2\pi)f_{n23Ry}=5.388\times10^{3}$ $f_{n23Ry}=5.388\times10^{3}$ (n-m-sec)/rad (nominal)
$d_{23z}=2(.01)J_{3z}(2\pi)f_{n23Rz}=5.553\times10^{3}$ $f_{n23Rz}=5.553\times10^{3}$ (n-m-sec)/rad (nominal)
$k_{23x}=J_{3x}(2\pi)^2$ $f^2_{n23Rx}=1.428\times10^{5}$ $f^2_{n23Rx}=1.428\times10^{5}$ n-m/rad (nominal)
$k_{23y}=J_{3y}(2\pi)^2$ $f^2_{n23Ry}=1.693\times10^{6}$ $f^2_{n23Ry}=1.693\times10^{6}$ n-m/rad (nominal)
$k_{23z}=J_{3z}(2\pi)^2$ $f^2_{n23Rz}=1.745\times10^{6}$ $f^2_{n23Rz}=1.745\times10^{6}$ n-m/rad (nominal)

Table 2-2. Parameters for SEPB (Concluded)

$d_{34x}=4D_{34z}(\alpha^{34}_{140y})^2$ $f_{n34T}=26.33$ $f_{n34T}=26.33$ (n-m-sec)/rad (nominal)
$d_{34y}=4D_{34z}(\alpha^{34}_{140x})^2$ $f_{n34T}=26.33$ $f_{n34T}=26.33$ (n-m-sec)/rad (nominal)
$d_{34z}=4D_{34z}(\alpha^{34}_{140x})^2+4D_{34x}(\alpha^{34}_{140y})^2=52.65$ $f_{n34T}=52.65$ (n-m-sec)/rad (nominal)
$k_{34x}=4K_{34z}(\alpha^{34}_{140y})^2=4(3.308\times10^4)(.25)^2$ $f^2_{n34T}=8.27\times10^3$ $f^2_{n34T}=8.27\times10^3$ n-m/rad (nominal)
$k_{34y}=4K_{34z}(\alpha^{34}_{140x})^2=4(3.308\times10^4)(.25)^2$ $f^2_{n34T}=8.27\times10^3$ $f^2_{n34T}=8.27\times10^3$ n-m/rad (nominal)
$k_{34z}=4K_{34z}(\alpha^{34}_{140x})^2+4K_{34x}(\alpha^{34}_{140y})^2=1.654\times10^4$ $f^2_{n34T}=1.654\times10^4$ n-m/rad (nominal)
$d_{56x}=2(.01)(2\pi)J_{6x}f_{n56Rx}=2.846\times10^2$ f_{n56Rx} (n-m-sec)/rad
$d_{56y}=2(.01)(2\pi)J_{6y}f_{n56Ry}=2.489\times10^2$ f_{n56Ry} (n-m-sec)/rad
$d_{56z}=2(.01)(2\pi)J_{6z}f_{n56Rz}=3.182\times10^2$ f_{n56Rz} (n-m-sec)/rad
$k_{56x}=J_{6x}(2\pi)^2$ $f^2_{n56Rx}=8.942\times10^4$ f^2_{n56Rx} n-m/rad
$k_{56y}=J_{6y}(2\pi)^2$ $f^2_{n56Ry}=7.821\times10^4$ f^2_{n56Ry} n-m/rad
$k_{56z}=J_{6z}(2\pi)^2$ $f^2_{n56Rz}=9.996\times10^4$ f^2_{n56Rz} n-m/rad

Table 2-3. Parameters for Floated Pallet

m_1=72,496 kg m_2=7,338 kg m_3=3,662 kg
$J_{1x}=1.00\times10^6$ kg-m^2 $J_{1y}=7.47\times10^6$ kg-m^2 $J_{1z}=7.67\times10^6$ kg-m^2 J_{2x}=14,247 kg-m^2 J_{2y}=92,881 kg-m^2 J_{2z}=90,610 kg-m^2 J_{3x}=7,123 kg-m^2 J_{3y}=46,441 kg-m^2 J_{3z}=45,305 kg-m^2
$K_{12x}=\frac{m_2+m_3}{4}(2\pi f_{n12Tx})^2$=719 n/m (nominal) $K_{12y}=\frac{m_2+m_3}{4}(2\pi f_{n12Ty})^2$=719 n/m (nominal) $K_{12z}=\frac{m_2+m_3}{4}(2\pi f_{n12Tz})^2$=404 n/m (nominal) $D_{12x}=\frac{m_2+m_3}{4}2(.1)(2\pi f_{n12Tx})$=229 n-sec/m (nominal) $D_{12y}=\frac{m_2+m_3}{4}2(.1)(2\pi f_{n12Ty})$=229 n-sec/m (nominal) $D_{12z}=\frac{m_2+m_3}{4}2(.1)(2\pi f_{n12Tz})$=129 n-sec/m (nominal)
$k_{12x}=4K_{12z}(\alpha^{12}_{120y})^2$=8,401 n-m/rad (nominal)

Table 2-3. Parameters for Floated Pallet (Continued)

$k_{12y}=4K_{12z}(\alpha^{12}_{120x})^2=21{,}650$ n-m/rad (nominal)
$k_{12z}=4\left[K_{12y}(\alpha^{12}_{120x})^2+K_{12x}(\alpha^{12}_{120y})^2\right]=5.340\times10^4$ n-m/rad (nominal)
$d_{12x}=4(D_{12z})(\alpha^{12}_{120y})^2=2{,}682$ (n-m-sec)/rad (nominal)
$d_{12y}=4D_{12z}(\alpha^{12}_{120x})^2=6{,}912$ (n-m-sec)/rad (nominal)
$d_{12z}=4\left[D_{12y}(\alpha^{12}_{120x})^2+D_{12x}(\alpha^{12}_{120y})^2\right]=17{,}030$ (n-m-sec)/rad (nominal)
$k_{23x}=J_{3x}(2\pi f_{n23Rx})^2$
$k_{23y}=J_{3y}(2\pi f_{n23Ry})^2$
$k_{23z}=J_{3z}(2\pi f_{n23Rz})^2$
$d_{23x}=2(.01)J_{3x}(2\pi f_{n23Rx})$
$d_{23y}=2(.01)J_{3y}(2\pi f_{n23Ry})$
$d_{23z}=2(.01)J_{3z}(2\pi f_{n23Rz})$
$K_{23x}=K_{23y}=K_{23z}=\frac{m_3}{4}(2\pi f_{n23T})^2$
$D_{23x}=D_{23y}=D_{23z}=\frac{m_3}{4}(2)(.01)(2\pi f_{n23T})$
$K_{34x}=K_{34y}=K_{34z}=0$
$D_{34x}=D_{34y}=D_{34z}=0$
$k_{34x}=k_{34y}=k_{34z}=0$
$d_{34x}=d_{34y}=d_{34z}=0$

Table 2-3. Parameters for Floated Pallet (Concluded)

$\alpha^{12}_{120x}=3.66$ m

$\alpha^{12}_{120y}=2.28$ m

$R_{11}=-15.24\ \hat{1}_x$ m

$R_{120}=-1.87\ \hat{1}_x+.528\ \hat{1}_z$ m

$R_{230}=0$

$R_{E220}=0$

$R_{E330}=0$

Table 2-4. Generalized Control Gains

$$K_{Rj}=4.736\ J_j f_n \text{ (n-m-sec)/rad}$$

$$K_{Pj}=8.41\ J_j f_n^2 \text{ n-m/rad}$$

$$K_{Ij}=6.64\ J_j f_n^3 \text{ n-m/sec}$$

where

J_j = inertia of the j^{th} vehicle axis ($kg\text{-}m^2$)

f_n = loop bandwidth defined as the -3 db point of the output torque to command torque transfer function (Hz)

Table 2-5. IOG Parameters for Slewing

$m_1=8.0593\times10^4$ kg	$D_{12x}=D_{12y}=D_{12z}=59.93$ n-sec/m
$m_2=1.95\times10^2$ kg	$K_{12x}=K_{12y}=K_{12z}=125$ n/m
$m_3=2.683\times10^3$ kg	$d_{12x}=14.96$ (n-m-sec)/rad
$J_{1x}=1.011\times10^6$ kg-m^2	$d_{12y}=14.96$ (n-m-sec)/rad
$J_{1y}=7.569\times10^6$ kg-m^2	$d_{12z}=29.92$ (n-m-sec)/rad
$J_{1z}=7.783\times10^6$ kg-m^2	$k_{12x}=31.25$ n-m/rad
$J_{2x}=50.21$ kg-m^2	$k_{12y}=31.25$ n-m/rad
$J_{2y}=50.21$ kg-m^2	$k_{12z}=62.5$ n-m/rad
$J_{2z}=50.21$ kg-m^2	$K_{R3x}=2.214\times10^4$; 3.674×10^3 (n-m-sec)/rad
$J_{3x}=2.335\times10^3$; 591.8 kg-m^2	$K_{R3y}=1.972\times10^4$; 3.674×10^3 (n-m-sec)/rad
$J_{3y}=2.08\times10^3$; 617.6 kg-m^2	$K_{R3z}=2.47\times10^4$; 1.628×10^4 (n-m-sec)/rad
$J_{3z}=2.605\times10^3$; 1.794×10^3 kg-m^2	$K_{P3x}=7.856\times10^4$; 1.306×10^4 n-m/rad
$R_{11}=-15.05\ \hat{1}_x\ -4.411\times10^{-2}\ 1_z$ m	$K_{P3y}=7.00\times10^4$; 1.306×10^4 n-m/rad
$R_{E20}=-0.375\ \hat{1}_z$ m	$K_{P3z}=8.764\times10^4$; 5.784×10^4 n-m/rad
$r_1=0.375\ \hat{1}_z$ m	$K_{I3x}=1.24\times10^5$; 2.061×10^4 n-m/sec
$r_2=1.85\ \hat{1}_z$; $1.039\ \hat{1}_z$ m	$K_{I3y}=1.105\times10^5$; 2.061×10^4 n-m/sec
$R_{120}=-1.68\ \hat{1}_x\ +.7699\ \hat{1}_z$ m	$K_{I3z}=1.384\times10^5$; 9.131×10^4 n-m/sec

3. DESCRIPTION AND OVERALL OPERATING CHARACTERISTICS OF THE IPS

This section describes the manner of operation and the operational characteristics of the IOG, SEPB, and the Floated Pallet. The control loop bandwidths and suspension frequencies where applicable will be defined in order to achieve ± 1 sec peak pointing stability in the presence of crew motion disturbances.

3.1 Inside-Out Gimbal System (IOG) - The IOG system is unique in that it is configured for exclusive operation in a zero gravity environment. Examination of figure 2-1 indicates that a rather large moment arm (approximately 1.85 meters) exists between the telescope CM and the gimbal intersection/suspension points. This would give rise to moments in the area of 4×10^3 n-m for the class of telescopes being considered in order to maintain telescope orientation in a 1 "g" environment. In a zero "g" field this is not felt and the large telescope CM offset will cause considerable torque coupling into the telescope as the IOG gimbal pedestal is linearly accelerated. (It should be noted that the primary coupling into the telescope is due to translation. Rotational coupling is small by comparison.) In order to overcome the effects of this large CM offset the IOG base (pedestal) is isolated from pallet motion through a six degree of freedom suspension. This suspension must be soft enough such that the disturbances introduced into the telescope will not result in pointing error in excess of ± 1 sec peak for both realistic pointing loop bandwidths and control torque levels. The suspension must ultimately provide torques equal and opposite to the applied telescope control torques in order to keep the IOG pedestal from rotating and hence acts as a momentum desaturator for the IOG base. The IOG system can therefore be grossly viewed as a momentum exchange system where the momentum exchange device is the IOG base or pedestal. The suspension system then desaturates the IOG base and prevents it from continuous rotation. Therefore the suspension characteristics have "little" effect on the bandwidth and damping that can be achieved by the telescope pointing control loop. Control torque as in the case of a reaction wheel system is quickly available (the only delay being the gimbal torquer time constant) via the gimbal torquers resulting in a subsequent acceleration and momentum transfer of the IOG base which is in turn desaturated by the suspension system. However, the above description only partially describes IOG operation as will be shown in the paragraphs that follow.

3.1.1 Determination of IOG Loop Bandwidth - In order to determine the IOG pointing control loop required to meet 1 sec pointing stability in the presence of crew motion disturbances, the telescope optical axis was pointed straight up out of the orbiter cargo bay

and the crew motion disturbances were applied along the orbiter y axis. Nominal IOG suspension parameters were initially used and are tabulated in table 2-1. The crew motion disturbance profile used for this evaluation is shown in figure 3-1. The profile shown in figure 3-1 was used in the performance evaluation of the SEPB and Floated Pallet as well.

For the conditions described above the IOG pointing control loop bandwidth required to maintain pointing stability within ± 1 $\widehat{\text{sec}}$ peak was 2 Hz. It was initially thought that the loop bandwidth required to meet 1 $\widehat{\text{sec}}$ pointing stability performance would be independent of telescope look angle, i.e., angle of telescope optical axis with the orbiter z axis. The only requirement necessary to make the zero and 90 degree telescope look angles equivalent was to apply the crew motion disturbance along the y and z orbiter axes, respectively. However, further investigation showed this notion to be fallacious and the curve shown in figure 3-2 was obtained as the telescope look angle was varied for a 2 Hz IOG control loop bandwidth for the suspension parameters listed in table 2-1. From the curve shown in figure 3-2 it is clearly apparent that IOG system operation is grossly different at zero look angle regardless of direction of crew motion force application than at a 90 degree look angle. In fact the pointing error incurred is a strong function of look angle as figure 3-2 indicates. Upon reevaluating the manner in which the IOG operates the following became apparent. When the telescope is either in the zero or 90 degree look angle positions and the crew motion force is applied along the orbiter y and z axes respectively, the suspension does not isolate the telescope from this disturbance very effectively. The reason for this is the following. Since the primary coupling into the telescope is translational in nature via the translation of the hinge point, the initial equivalent suspension translational natural frequency is important in order to determine the amount of hinge motion. Since the hinge is completely frictionless the telescope is free to rotate initially about its center of mass in order to track the translational motion of the hinge point. Hence the initial translational natural frequency of the suspension is approximated by

$$f_{Ti}\Big|_{max} = \frac{1}{2\pi}\left[\frac{4K_{34}}{m_4}\right]^{1/2} \qquad (1)$$

Substitution of the values given in table 2-1 into equation (1) results in

$$f_{Ti} = \frac{1}{2\pi}\left[\frac{4(2.5\times10^{3})}{195}\right]^{1/2} = 1.14 \text{ Hz} \qquad (2)$$

The suspension natural frequency calculated above is the highest value that it can possibly have. This would be the initial translational suspension natural frequency if the telescope pointing control loop bandwidth were zero or the telescope were uncontrolled. It is clearly seen that as the telescope control loop bandwidth increases the equivalent mass that the suspension interacts with increases hence the initial suspension natural frequency decreases. In the limit for an infinite pointing control loop bandwidth the mass that the suspension interacts with is the sum of m_4, m_5, and m_6. Using the values given in table 2-1 results in a suspension translational natural frequency of

$$f_{Ti}|_{min} = \frac{1}{2\pi}\left[\frac{4K_{34}}{m_4+m_5+m_6}\right]^{1/2} = 0.2967 \text{ Hz} \qquad (3)$$

Hence the translational suspension natural frequency initially or for that matter at any time is bracketed between 1.14 and 0.3 Hz for the nominal suspension parameters. The Fourier transform of the disturbance profile shown in figure 3-1 is given by

$$F(j\omega) = j\left\{\int_{-\infty}^{+\infty} f(t)\sin\omega t\,dt\right\} = j\left\{\int_{-\infty}^{+\infty} \frac{B}{a}(t+2a)\sin\omega t\,dt + \int_{a}^{2a}\left[-B+\frac{B}{a}(t-a)\right]\sin\omega t\,dt\right\} \qquad (4)$$

where:

a = time interval of one of the applied triangular force disturbance

B = maximum amplitude of the force disturbance

Evaluation of the integrals shown in equation (4) yields

$$F(j\omega) = j\left\{\frac{2B}{a\omega^2}[\sin 2a\omega - \sin a\omega] - \frac{2B}{\omega}\cos 2a\omega\right\} \qquad (5)$$

A plot of equation (5) is shown in figure 3-3 for a=0.8 seconds.

Examination of figure 3-3 shows that the spectrum of the disturbance signal peaks at approximately 0.16 Hz which is nearly a factor of two below the lowest possible suspension translational

natural frequency. Hence it is apparent that the suspension with the nominal parameters given does not isolate the telescope from this disturbance very effectively.

The reason for the sensitivity of pointing error with respect to look angle can be explained in the following manner. When the telescope look angle is zero and a disturbance is applied along the orbiter y axis, or for that matter in the xy plane, the control torques applied to the telescope in order to maintain pointing also translates the IOG base and hinge points. This translation is due to rotational translational coupling in the IOG base due to distances between the IOG center of mass and the telescope hinge point (r_1) and the center of elasticity (R_{E40}) of the IOG suspension. It can be shown that the hinge point translation subtracts from the translation due to the crew motion disturbance, hence greatly reducing the translational coupling into the telescope. This action can be viewed as a juggling phenomenon where the hinge point tends to remain directly under the telescope center of mass when the telescope look angle is zero. However, when the telescope has a look angle of 90 degrees and the crew motion disturbance is applied along the orbiter z axis, no hinge translation can take place that would reduce the translational coupling into the telescope. This is apparent since the translational coupling into the telescope occurs along the z axis and, for the given geometrical arrangement, initial hinge point translation due to telescope control torque along the z axis is not possible.

If the explanation given above were valid then it would directly follow that nearly equivalent operation as that exhibited when the telescope look angle is 90 degrees would be achieved with a zero telescope look angle when the distances between the IOG center of mass, the hinge point, and the suspension center of elasticity are zero. This was done and the results are shown in figure 3-4. Examination of this figure indicates that essentially equivalent pointing performance was obtained for zero look angle as that achieved for a 90 degree look angle once the hinge point, center of elasticity of the IOG suspension, and the pedestal center of mass coincide. This result substantiates the explanation given above.

To even further substantiate the explanation of IOG operation given above, the translational stiffness of the IOG suspension was increased by an order of magnitude without increasing the suspension rotational stiffness. (This is possible mathematically, however, it is not possible physically without changing the distance between the isolators.) If the above contentions were true, then the pointing errors incurred for zero telescope look angle should

be independent of this variation. This was verified on the computer simulation thus supporting the above contentions.

It is therefore apparent that in choosing an IOG loop bandwidth the telescope should be positioned at the worst possible look angle consistent with its operational range. For the orbiter/IOG/telescope system being considered the telescope maximum look angle is ±65 degrees. Examination of figure 3-2 indicates that a pointing error of approximately 9 $\widehat{\text{sec}}$ results at a telescope look angle of 65 degrees for a 2 Hz control loop bandwidth in the presence of a crew motion disturbance. Increasing the loop bandwidth much beyond 2 Hz is not desirable from structural and noise (i.e., sensor and actuator) viewpoints. Hence the only way to achieve the desired pointing stability of ±1 $\widehat{\text{sec}}$ peak is to soften the suspension as described in the next paragraph.

3.1.2 Selection of IOG Suspension Stiffness - Figure 3-4 shows pointing error as a function of suspension stiffness for various telescope look angles for a 2 Hz pointing control loop bandwidth. Examination of the curve for a 65 degree telescope look angle (the maximum look angle projected for IOG operation) shows that a reduction in suspension stiffness by approximately a factor of 20 would result in a peak pointing error of 0.5 $\widehat{\text{sec}}$ for a 2 Hz control loop bandwidth. This then is the recommended reduction in suspension stiffness in order to meet the pointing performance of 1 $\widehat{\text{sec}}$ peak without increasing the pointing control loop bandwidth beyond 2 Hz.

3.1.3 IOG Pointing Performance as a Function of Moment Arm and Control Loop Bandwidth - Figure 3-5 shows IOG pointing performance as a function of distance from the hinge point to the telescope center of mass (i.e., moment arm) for several pointing control loop bandwidths for 1/20 nominal suspension stiffness and a telescope look angle of 65 degrees. Examination of this figure shows that pointing error increases as the telescope moment arm increases. However, it is apparent that the pointing error is approaching a maximum value as the telescope moment arm is increasing. In fact if the moment arm were to keep on increasing, the telescope incurred pointing error would begin to decrease. The reason for this phenomenon is that the telescope rotation about its center of mass required to track the translation of the hinge point due to crew motion disturbances, decreases as the moment arm is increased. This is apparent since the linear translation of the hinge point must be equal to "rθ", where "r" is the telescope moment arm and θ is the telescope angular rotation. Figure 3-6 shows telescope pointing error as a function of pointing control loop bandwidth for various values of telescope moment

arm, for 1/20 nominal suspension stiffness, and a telescope look angle of 65 degrees. As expected, telescope pointing error decreases as the pointing control loop bandwidth increases.

3.1.4 Observed IOG System Instability - In the course of investigating IOG pointing performance, an instability was observed at a telescope look angle of 90 degrees for nominal suspension stiffness parameters. The roots associated with the instability had small positive real parts making their presence felt only after 10 to 15 seconds. In order to verify that the observed instability was real and not a computer simulation problem, a two body model of the IOG system was defined and the equations of motion for this model developed. The characteristic equation of this two body system was derived and a Routh stability array was run. In the paragraphs that follow the two body model will be defined, the equations of motion derived, and the results of the stability analysis performed are presented.

3.1.4.1 Equations of Motion For the Two Body Stability Model - Figure 3-7 is a schematic representation of the two body model used for the investigation and the substantiation of the IOG instability observed on the six body computer simulation. As figure 3-7 indicates the two body stability model assumes that the IOG pedestal is suspended from an inertial base which represents the orbiter/pallet combination. This should approximate the actual system with respect to stability characteristics because of the large difference in mass and inertia characteristics between the orbiter/pallet and the IOG/telescope combinations.

Using the same techniques described in section 2, the linear equations of motion of the system shown in figure 3-7 are given by

$$F_{1e}-F_c+F_H=m_1\ddot{\varepsilon} \tag{6}$$

$$-F_H=m_2\ddot{\rho}_2 \tag{7}$$

$$\ddot{\rho}_2=\ddot{\varepsilon}+\ddot{r}_1+\ddot{r}_2 \tag{8}$$

Substituting equation (8) into equation (7) gives

$$-F_H=m_2\ddot{\varepsilon}+m_2(\ddot{r}_1+\ddot{r}_2) \tag{9}$$

where:

ε = distance from origin of inertial coordinate frame to IOG pedestal CM (body 1)

ρ_c = distance from origin of inertial coordinate frame to CM of telescope plus inertial gimbal of IOG (body 2)

F_H = hinge force

m_1 = mass of body 1

m_2 = mass of body 2

r_1 = distance from CM of body 1 to hinge point

r_2 = distance from hinge point to CM of body 2

F_{1e} = external force on body 1

F_c = IOG suspension compliance force

The compliance force F_c can be written as

$$F_c = 4D \cdot \dot{\varepsilon} + 4K \cdot \varepsilon + 4D \cdot (\omega_1 \times R_{E1}) + 4K \cdot (\theta_1 \times R_{E1}) \qquad (10)$$

where:

ω_1 = inertial rate of body 1

θ_1 = inertial angular position of body 1

R_{E1} = distance from CM of body 1 to center of elasticity of the IOG suspension

D = viscous damping of IOG mount

K = spring constant of IOG suspension

$$D = \mathrm{diag}[D_x; D_y; D_z]$$

$$K = \mathrm{diag}[K_x; K_y; K_z] \qquad (11)$$

Substituting equation (10) and (9) into equation (6) results in

$$\boxed{F_{1e}=(m_1+m_2)\ddot{\varepsilon}+4D\cdot\dot{\varepsilon}+4K\cdot\varepsilon+4D\cdot(\omega_1 x R_{E1})+4K\cdot(\theta_1 x R_{E1})+m_2(\ddot{r}_1+\ddot{r}_2)} \quad (12)$$

The rotational equations of motion for bodies 1 and 2 can be written as

$$T_c-T_H+R_{11}xF_{1e}+r_1xF_H=\frac{d}{dt}(J_1\cdot\omega_1) \quad (13)$$

$$T_H+r_2xF_H=\frac{d}{dt}(J_2\cdot\omega_2) \quad (14)$$

where:

T_c = suspension compliance torque

T_H = hinge control torque

J_1 = inertia of body 1

J_2 = inertia of body 2

R_{11} = distance from CM of body 1 to point of external force application on body 1

and

$$J_1=\text{diag}[J_{1x};J_{1y};J_{1z}] \quad (15)$$

$$J_2=\text{diag}[J_{2x};J_{2y};J_{2z}] \quad (16)$$

The suspension compliance torques can be written as (see section 2)

$$T_c=-\left\{d\cdot\omega_1+k\cdot\theta_1+4R_{E1}x\left[D\cdot(\omega_1 xR_{E1})\right]+4R_{E1}x\left[K\cdot(\theta_1 xR_{E1})\right]+4R_{E1}x(D\cdot\dot{\varepsilon})+4R_{E1}x(K\cdot\varepsilon)\right\} \quad (17)$$

where:

d = suspension rotational damping matrix

k = suspension rotational spring constant matrix

and

$$d=\text{diag}[d_x;d_y;d_z] \tag{18}$$

$$k=\text{diag}[k_x;k_y;k_z] \tag{19}$$

The hinge control torque T_H can be written as

$$T_H=-\left[K_R\cdot\omega_2+K_P\cdot\theta_2+K_I\cdot\frac{\theta_2}{s}\right] \tag{20}$$

where:

K_R = rate gain matrix

K_P = position gain matrix

K_I = integral gain matrix

and

$$K_R=\text{diag}[K_{Rx};K_{Ry};K_{Rz}] \tag{21}$$

$$K_P=\text{diag}[K_{Px};K_{Py};K_{Pz}] \tag{22}$$

$$K_I=\text{diag}[K_{Ix};K_{Iy};K_{Iz}] \tag{23}$$

Substituting equation (20), (17), and (9) into equations (13) and (14) results in

$$R_{11}xF_{1e}=\frac{d}{dt}(J_1\cdot\omega_1)+d\cdot\omega_1+k\cdot\theta_1+4R_{E1}x\left[D\cdot(\omega_1xR_{E1})\right]+4R_{E1}x\left[K\cdot(\theta_1xR_{E1})\right]$$
$$+m_2r_1x(\ddot{r}_1+\ddot{r}_2)+m_2r_1x\ddot{\varepsilon}+4R_{E1}x(D\cdot\dot{\varepsilon})+4R_{E1}x(K\cdot\varepsilon)-\left[K_R\cdot\omega_2+K_P\cdot\theta_2+K_I\cdot\frac{\theta_2}{s}\right] \tag{24}$$

$$0=\frac{d}{dt}(J_2\cdot\omega_2)+K_R\cdot\omega_2+K_P\cdot\theta_2+K_I\cdot\frac{2}{s}+r_2x(m_2\ddot{\varepsilon})+m_2r_2x(\ddot{r}_1+\ddot{r}_2) \tag{25}$$

Equations (12), (24), and (25) form a complete set of equations of motion for the two body stability model defined.

Assuming that the telescope look angle is 90 degrees, equations (12), (24), and (25) can be linearized and written in component form in the following manner

$$R_{11}{}^{x}F_{1e}\big|_x=(J_{1x}+m_2r_{1z}^2)\dot{\omega}_{1x}+(d_x+4D_yR_{E1z})\omega_{1x}+(k_x+4K_yR_{E1z}^2)\theta_{1x}$$
$$-\left[K_{Rx}\omega_{2x}+K_{Px}\theta_{2x}+K_{Ix}\frac{\theta_{2x}}{s}\right]-m_2r_{1z}r_{2x}\dot{\omega}_{2z}-(m_2r_{1z}\ddot{\varepsilon}_y+4R_{E1z}D_y\dot{\varepsilon}_y+4R_{E1z}K_y\varepsilon_y) \quad (26)$$

$$R_{11}{}^{x}F_{1e}\big|_y=(J_{1y}+m_2r_{1z}^2)\dot{\omega}_{1y}+(d_y+4D_xR_{E1z}^2)\omega_{1y}+(k_y+4K_xR_{E1z}^2)\theta_{1y}$$
$$-\left[K_{Ry}\omega_{2y}+K_{Py}\theta_{2y}+K_{Iy}\frac{\theta_{2y}}{s}\right]+m_2r_{1z}\ddot{\varepsilon}_x+4R_{E1z}D_x\dot{\varepsilon}_x+4R_{E1z}K_x\varepsilon_x \quad (27)$$

$$R_{11}{}^{x}F_{1e}\big|_z=J_{1z}\dot{\omega}_{1z}+d_z\omega_{1z}+k_z\theta_{1z}-\left[K_{Rz}\omega_{2z}+K_{Pz}\theta_{2z}+K_{Iz}\frac{\theta_{2z}}{s}\right] \quad (28)$$

$$0=J_{2x}\dot{\omega}_{2x}+K_{Rx}\omega_{2x}+K_{Px}\theta_{2x}+K_{Ix}\frac{\theta_{2x}}{s} \quad (29)$$

$$0=(J_{2y}+m_2r_{2x}^2)\dot{\omega}_{2y}+K_{Ry}\omega_{2y}+K_{py}\theta_{2y}+K_{Iy}\frac{\theta_{2y}}{s}-m_2r_{2x}\ddot{\varepsilon}_z \quad (30)$$

$$0=(J_{2z}+m_2r_{2x}^2)\dot{\omega}_{2z}+K_{Rz}\omega_{2z}+K_{Pz}\theta_{2z}+K_{Iz}\frac{\theta_{2z}}{s}-m_2r_{1z}r_{2x}\dot{\omega}_{1x}+m_2r_{2x}\ddot{\varepsilon}_y \quad (31)$$

$$F_{1e}\big|_x=(m_1+m_2)\ddot{\varepsilon}_x+4D_x\dot{\varepsilon}_x+4K_x\varepsilon_x+4D_xR_{E1z}\omega_{1y}+4K_xR_{E1z}\theta_{1y}+m_2r_{1z}\dot{\omega}_{1y} \quad (32)$$

$$F_{1e}\big|_y=(m_1+m_2)\ddot{\varepsilon}_y+4D_y\dot{\varepsilon}_y+4K_y\varepsilon_y-4D_yR_{E1z}\omega_{1x}-4K_yR_{E1z}\theta_{1x}-m_2r_{1z}\dot{\omega}_{1x}+m_2r_{2x}\dot{\omega}_{2z} \quad (33)$$

$$F_{1e}\big|_z=(m_1+m_2)\ddot{\varepsilon}_z+4D_z\dot{\varepsilon}_z+4K_z\varepsilon_z-m_2r_2\dot{\omega}_{2y} \quad (34)$$

Examination of equations (26) through (33) reveals that they break into three distinct sets. Set 1 is formed by equations (27), (30), (32), and (34) corresponding to degrees of freedom θ_{1y}, θ_{2y}, ε_x, and ε_z. Set 2 is formed by equations (26), (29), (31), and (33) corresponding to degrees of freedom θ_{1x}, θ_{2x}, θ_{2z}, and ε_y. Set 3 is formed by equation (28) which concerns the degree of freedom θ_{1z}.

The characteristic equation for set 1 can be written as

$$\Delta_1=(a_1a_7-a_3a_6)(a_4a_9-a_5a_8) \quad (35)$$

where:

$$a_1=(J_{1y}+m_2r_{1z}^2)s^2+(d_y+4D_xR_{Elz}^2)s+(k_y+4K_xR_{Elz}^2) \quad (36)$$

$$a_3=m_2r_{1z}s^2+4R_{Elz}D_xs+4R_{Elz}K_x \quad (37)$$

$$a_4=(J_{2y}+m_2r_{2x}^2)s^2+K_{Ry}s+K_{Py}+\frac{K_{Iy}}{s} \quad (38)$$

$$a_5=-m_2r_{2x}s^2 \quad (39)$$

$$a_6=m_2r_{1z}s^2+4D_xR_{Elz}s+4K_xR_{Elz} \quad (40)$$

$$a_7=(m_1+m_2)s^2+4D_xs+4K_x \quad (41)$$

$$a_8=-m_2r_{2x}s^2 \quad (42)$$

$$a_9=(m_1+m_2)s^2+4D_zs+4K_z \quad (43)$$

The values for the parameters shown in equations (36) thru (43) are derived from table 2-1 for nominal suspension parameters and are given in table 3-1.

Using the values given in table 3-1 and substituting them into equation (35) results in

$$\Delta_1=\left[2.18\times10^5s^4+1.894\times10^6s^3+1.774\times10^7s^2+1.338\times10^6s+6.25\times10^6\right]$$
$$\left[7.77\times10^6s^5+6.882\times10^7s^3+3.352\times10^8s^2+5.902\times10^8s+8.185\times10^8+\frac{1.105\times10^9}{s}\right] \quad (44)$$

Running a Routh stability array on the two bracketed expressions given in equation (44) shows that the first bracket is stable and the second bracket is unstable. The roots associated with the first bracket are given by

$$s_{1,2}=-.0189\pm j.596 \quad (45)$$

$$s_{3,4}=-4.325\pm j7.874 \quad (46)$$

The roots associated with the second bracket are given by

$$s_1=0 \quad (47)$$

$$s_2 = -2 \tag{48}$$

$$s_{3,4} = 0.0184 \pm j1.621 \quad \text{(unstable root)} \tag{49}$$

$$s_{5,6} = -3.452 \pm j3.893 \tag{50}$$

It is seen that the instability is associated with telescope rotational motion about the y axis and translational motion of the IOG pedestal along the z axis. In addition the positive real part of the unstable root is small which substantiates the fact that the computer simulation had to run 10 to 15 seconds before the effect of the instability was noticed.

In order to further verify that the stability model used to determine the unstable root shown above was valid, and that the root shown was indeed the only unstable root in the system, Routh stability arrays on the open loop system given by set 1 and the closed loop system given by set 2 were performed. Both were shown to be stable. In addition the open loop poles associated with equation set 1 are given by

$$s_{1,2} = 0 \tag{51}$$

$$s_{3,4} = -.0189 \pm j.596 \tag{52}$$

$$s_{5,6} = -4.325 \pm j7.874 \tag{53}$$

$$s_{7,8} = -.7768 \pm j3.728 \tag{54}$$

In order to better understand the reason for the instability, the IOG suspension parameters were parameterized in the two body stability model described above. It was found that with a slight decrease in suspension stiffness from the nominal values the system was stable. However, the suspension stiffness had to be increased by approximately a factor of 15 before IOG system stability was reestablished. For these parameterizations, IOG damping ratio was held constant. Additionally a slight increase in suspension damping by approximately a factor of 1.5 gave stable system roots.

The values of R_{Elz} and r_{iz} were parameterized and were shown to have little effect on the system instability. However, when the control law integral gain was set to zero all roots were stable regardless of IOG suspension stiffness.

Most of the results described above have been verified on the six body pointing performance model for a telescope look angle of 90 degrees. The one exception was that increasing shockmount damping did not stabilize the six body IOG computer simulation as it did the two body stability model. The result of this investigation indicates that more effort is required in order to understand the overall stability characteristics of the IOG and the interrelationships between the various system parameter (i.e., control law structure and suspension parameters) and their effect on IOG stability.

3.2 Standard Experiment Pointing Base (SEPB) - The SEPB is a conventional gimballing system in which the telescope center of mass is located in the vicinity of the gimbal intersection point. The base of the SEPB is hard mounted to the pallet. Isolation from crew motion is achieved by maintaining the telescope CM close to the gimbal intersection points in order to keep translational coupling into the telescope small without the use of a suspension. It is clearly seen that if the telescope CM were located exactly at the gimbal intersection point and in the absence of gimbal friction telescope isolation from crew motion would be achieved without the need for a pointing control loop. However, it is not possible to keep the telescope CM precisely at the gimbal intersection points, hence a pointing control loop is required to control the disturbances that couple into the telescope due to crew motions. The required pointing control loop bandwidth is a direct function of the telescope CM offset from the gimbal intersection or hinge point. This dependence is shown in figure 3-8 for a 1 and 2 Hz pointing control loop bandwidth.

Examination of figure 3-8 shows that a telescope CM offset of 3.2 and 8.9 centimeters (1.26 and 3.5 inches) for control loop bandwidths of 1 and 2 Hz, respectively, will result in peak pointing errors of ± 1 $\widehat{\text{sec}}$ in the presence of crew motion disturbances. Both of these allowable mass offsets require telescope mass balancing. Since it is not anticipated that balancing the telescope to 3 centimeters is no more difficult than balancing it to 9 centimeters, the smaller telescope mass offset is recommended, thus allowing the use of a 1 Hz pointing control loop for the SEPB. This would result in advantages when considering the effects of structural flexibility and system noise over a 2 Hz pointing control loop bandwidth.

3.3 Floated Pallet - In the floated pallet concept for the spacelab, the total pallet is isolated with respect to the orbiter through a passive spring damper suspension. (Details of the design and characteristics of this suspension are given in volume III of this report.) Four Skylab double gimbal CMGs are mounted on the pallet in order to control the total pallet to ± 1 $\widehat{\text{sec}}$ peak pointing

error in the presence of crew motion disturbances. The isolation system not only acts to isolate the pallet from crew motion disturbances but also allows the gross attitude control of the orbiter through the pallet suspension system via the control moment gyros mounted on the pallet. Hence the orbiter reaction control system is not required to maintain orbiter attitude and are inoperative. Therefore the floated pallet concept eliminates the contaminants from the orbiter hypergolic RCS that are present in both the IOG and SEPB concepts.

The recommended suspension design sets the suspension natural frequency both in rotation and translation in the vicinity of 0.1 Hz with a damping ratio of approximately 0.1. This is accomplished by the use of gas filled bellows springs which have appropriate linear stiffness and damping coefficients, and which are placed appropriately to achieve the desired rotational characteristics. This is explained fully in volume III of this report. It was anticipated and subsequently verified that a suspension natural frequency in the area of 0.1 Hz both in rotation and translation not only yields satisfactory isolation from crew motion disturbances, but will also allow the maintenance of orbiter attitude through the suspension system without large elongations of the pallet suspension system. Figure 3-9 shows a plot of peak pointing error as a function of floated pallet control loop bandwidth for the recommended suspension configuration in the presence of crew motion disturbances. From this figure it is seen that a pallet control loop bandwidth of approximately 1 Hz will limit the peak pointing error due to crew motion disturbance within ± 1 sec.

Figure 3-10 shows a plot of pallet pointing error vs suspension damping for nominal suspension stiffness and a 1 Hz pallet pointing control loop bandwidth. As the plot shows, pallet pointing error is only affected slightly as the damping ratio is varied by an order of magnitude. In fact, pointing error increases slightly as the damping ratio is increased from its nominal value of 0.1. Therefore suspension damping, the most uncertain quantity of the suspension parameters, does not require precise control in order to meet satisfactory pallet pointing stability performance.

Figure 3-11 shows a plot of pointing error vs pallet suspension natural frequency for a constant damping ratio of 0.1 for a 1 Hz pointing control loop bandwidth. As expected, the pointing error incurred is a fairly sensitive function of suspension natural frequency increasing appreciably as the suspension natural frequency is increased.

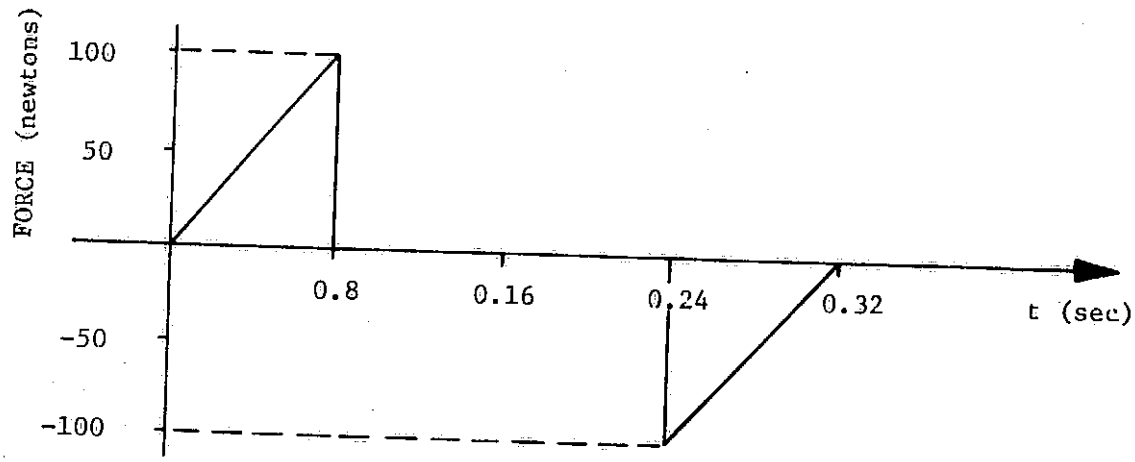

Figure 3-1. Crew Motion Disturbance Profile

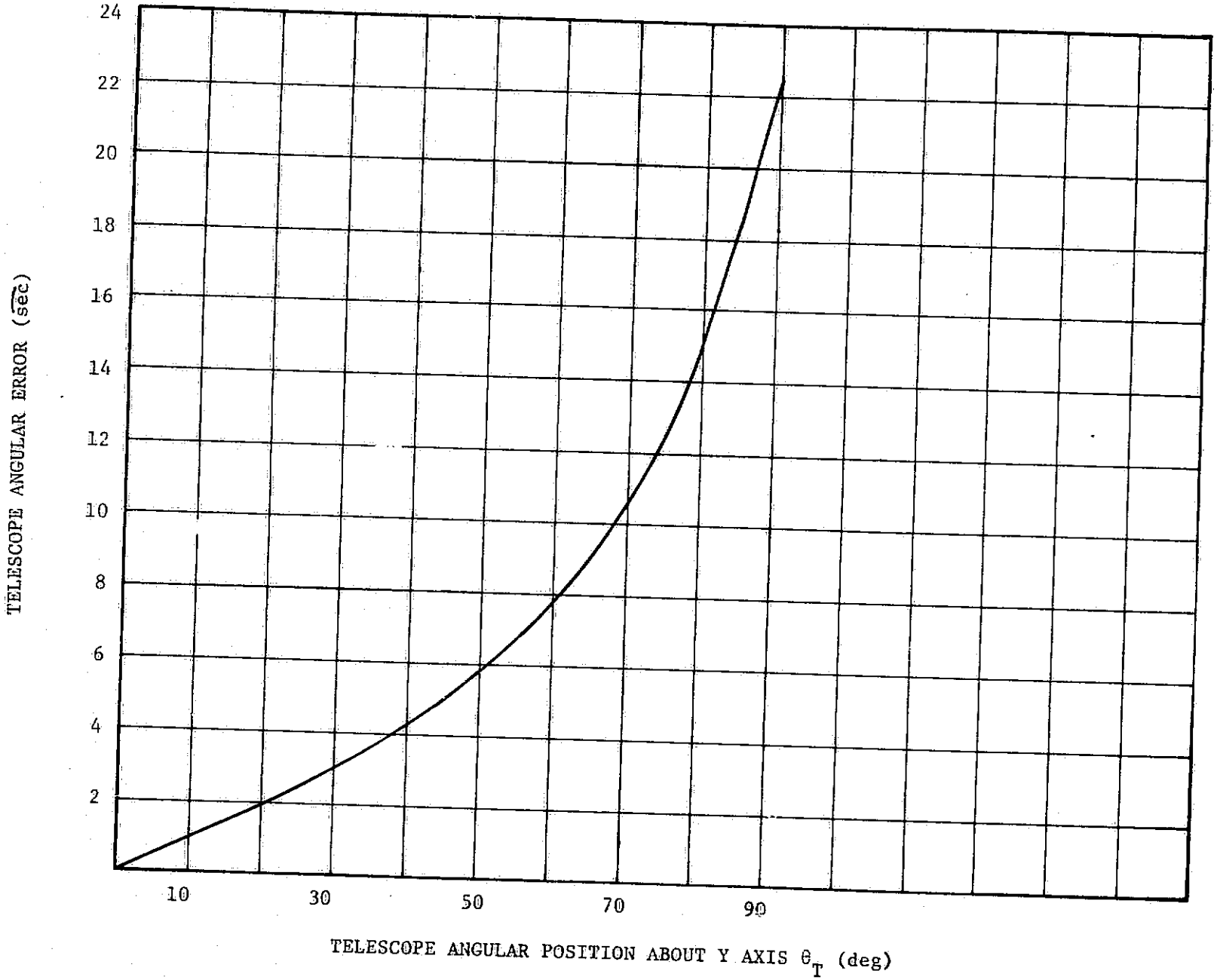

Figure 3-2. Telescope Error Vs Telescope Angular Position For Nominal Suspension Stiffness Force Applied Along z Axis and 2 Hz Pointing Control Loop Bandwidth

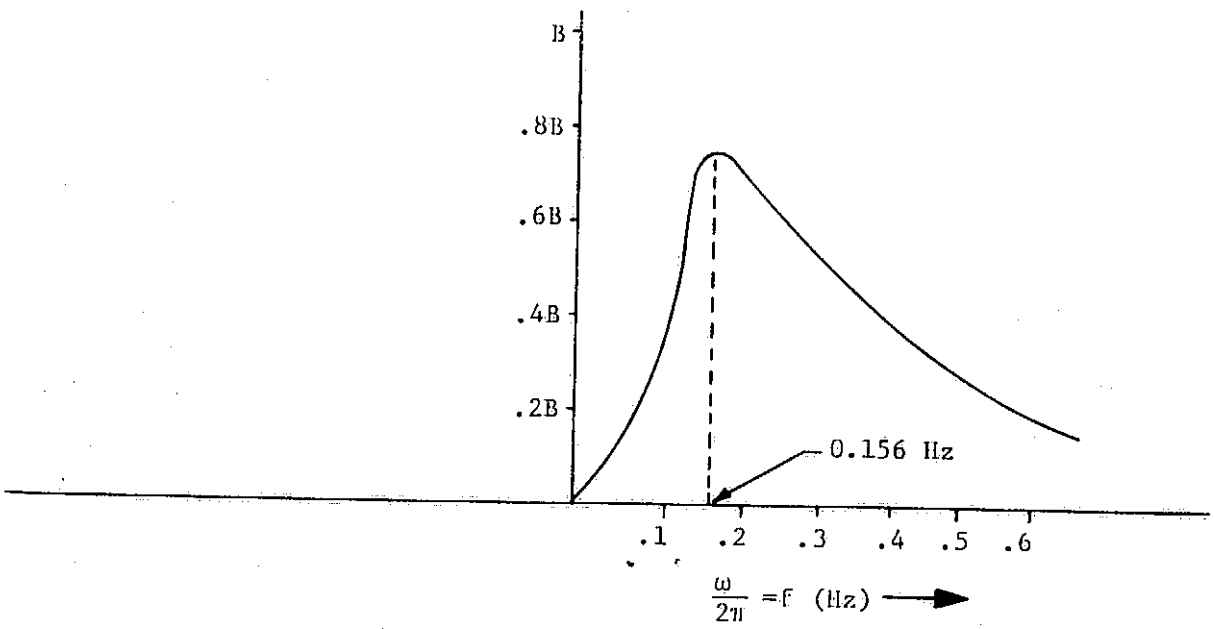

Figure 3-3. Fourier Spectrum of Disturbance Force

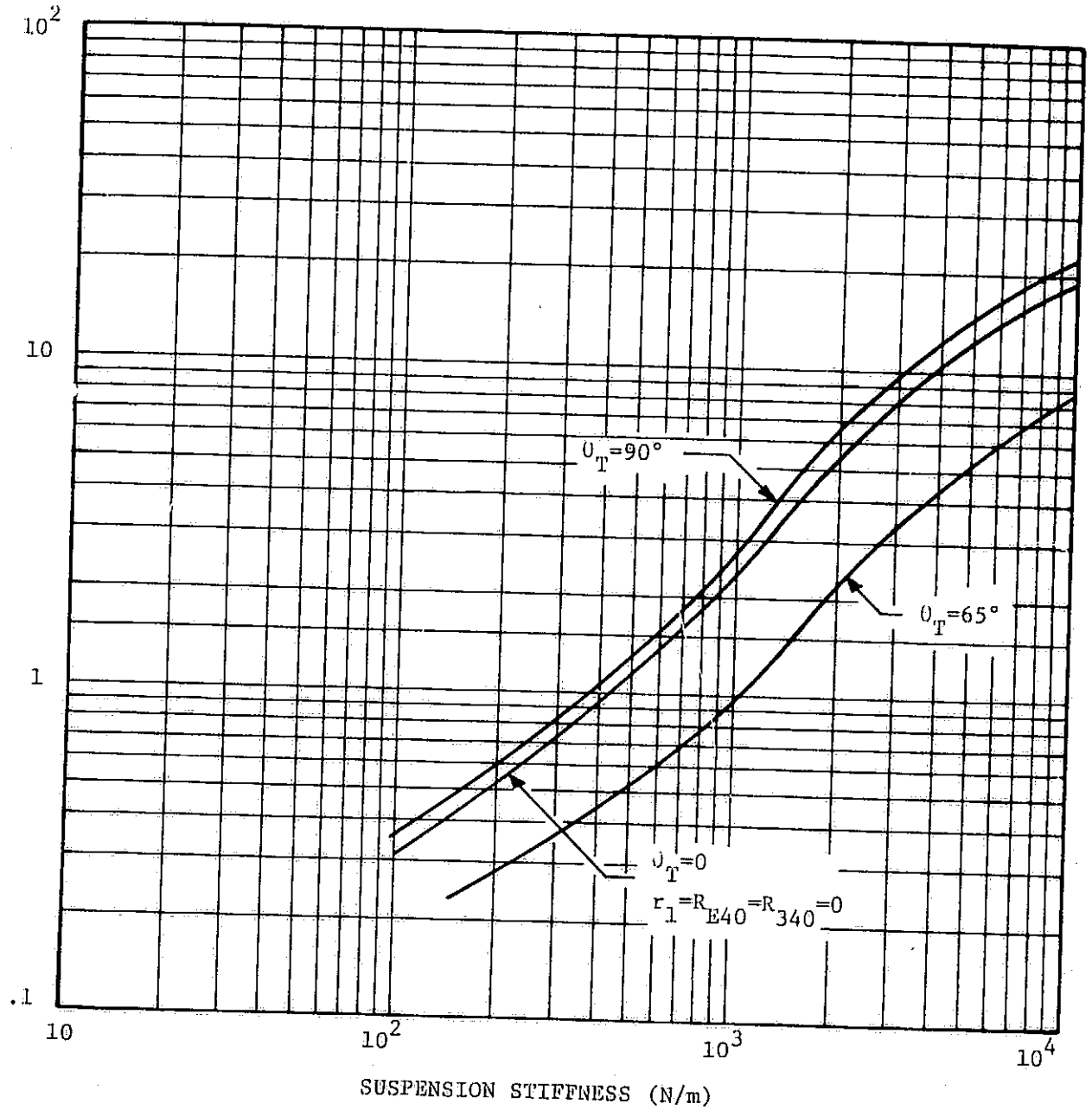

Figure 3-4. Telescope Pointing Error Vs Suspension Stiffness For 2 Hz Pointing Control Loop Bandwidth

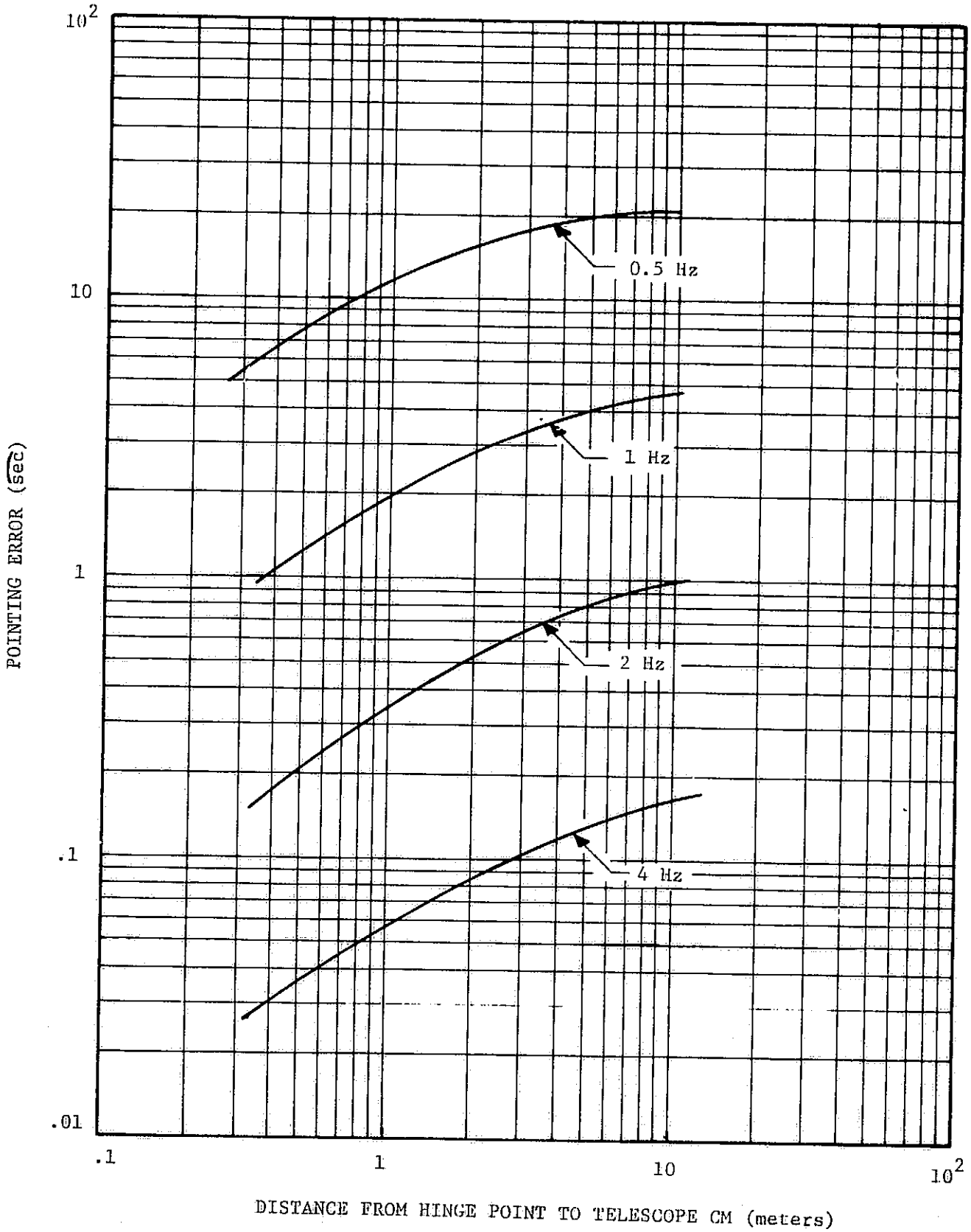

Figure 3-5. Pointing Error Vs Telescope Moment Arm For 1/20 Nominal Suspension Stiffness and 65 Degree Telescope Look Angle

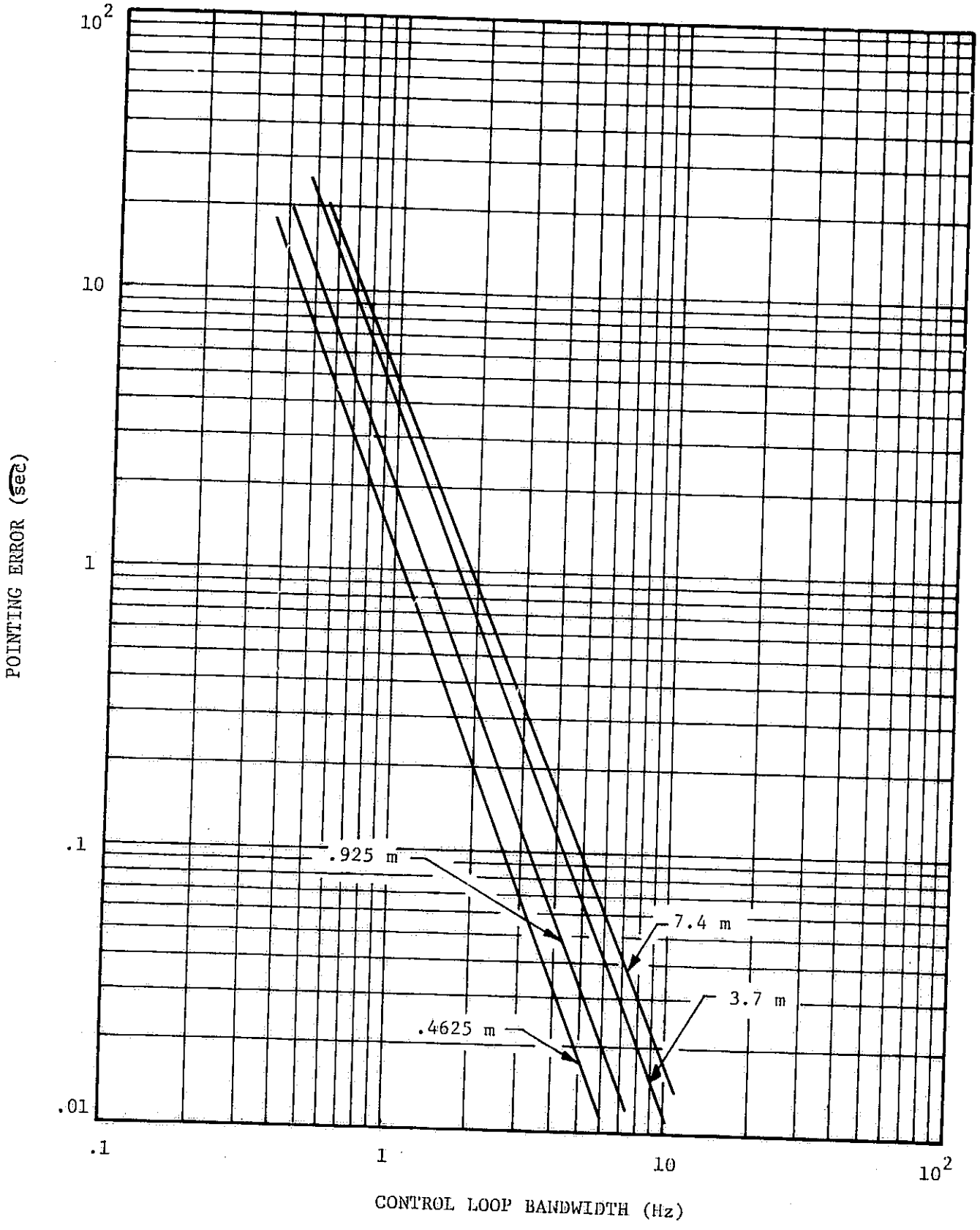

Figure 3-6. Pointing Error Vs Pointing Control Loop Bandwidth For 1/20 Nominal Suspension Stiffness and 65 Degree Telescope Look Angle

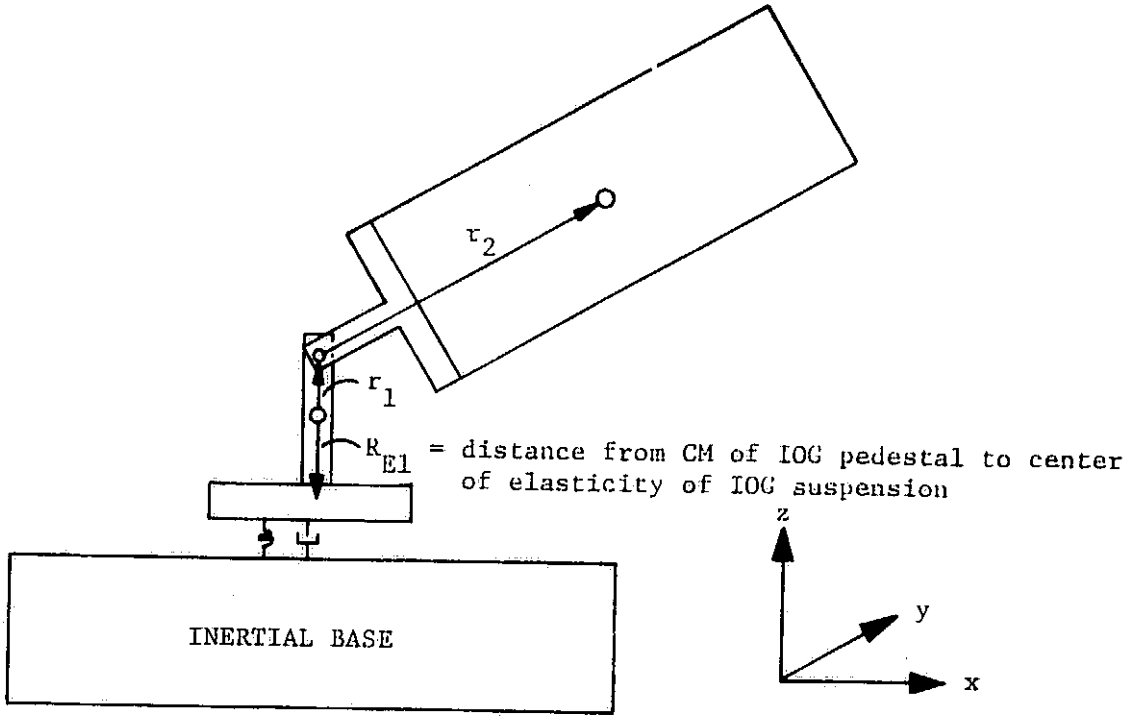

Figure 3-7. Two Body Stability Model

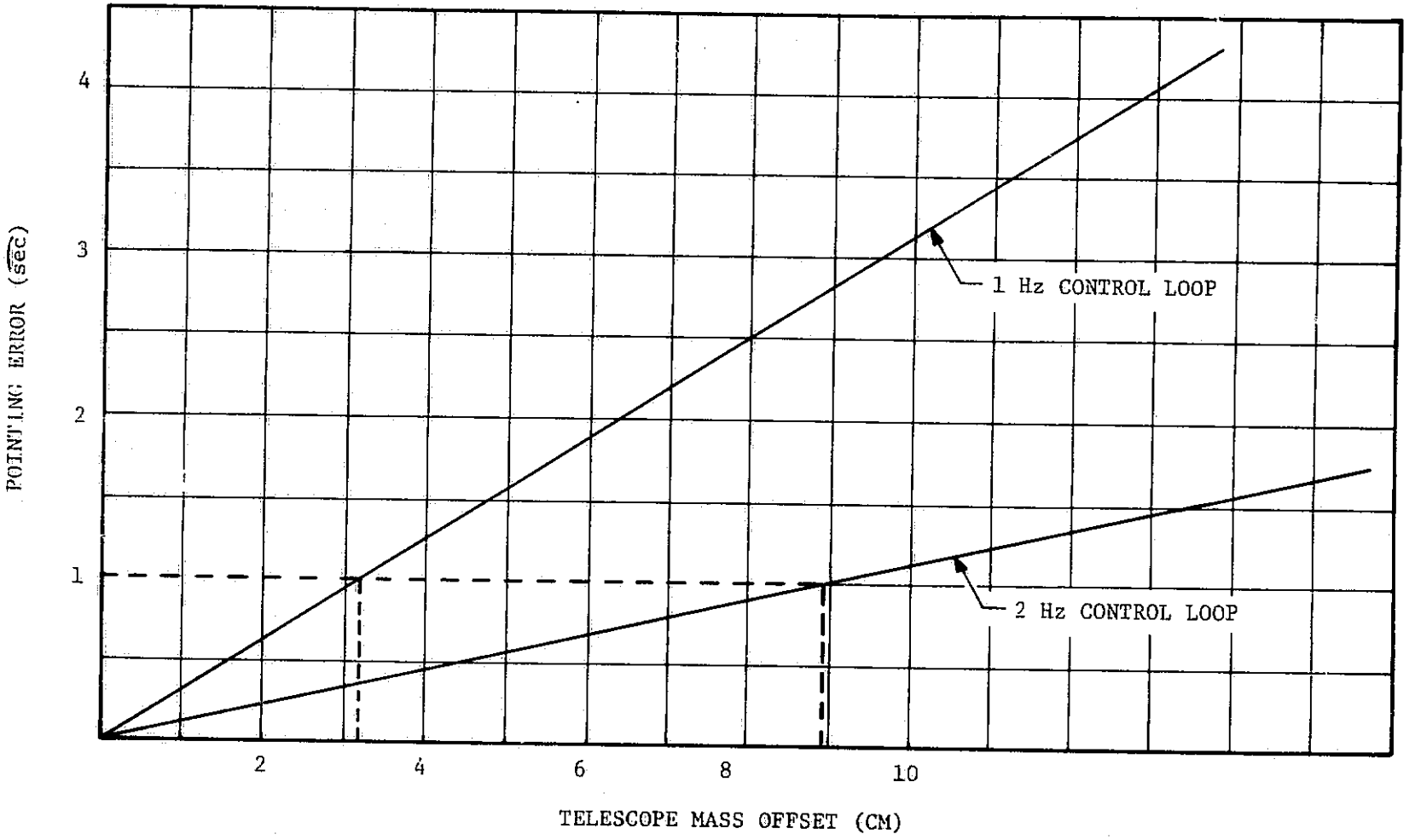

Figure 3-8. Pointing Error Vs Telescope Mass Offset For SEPB

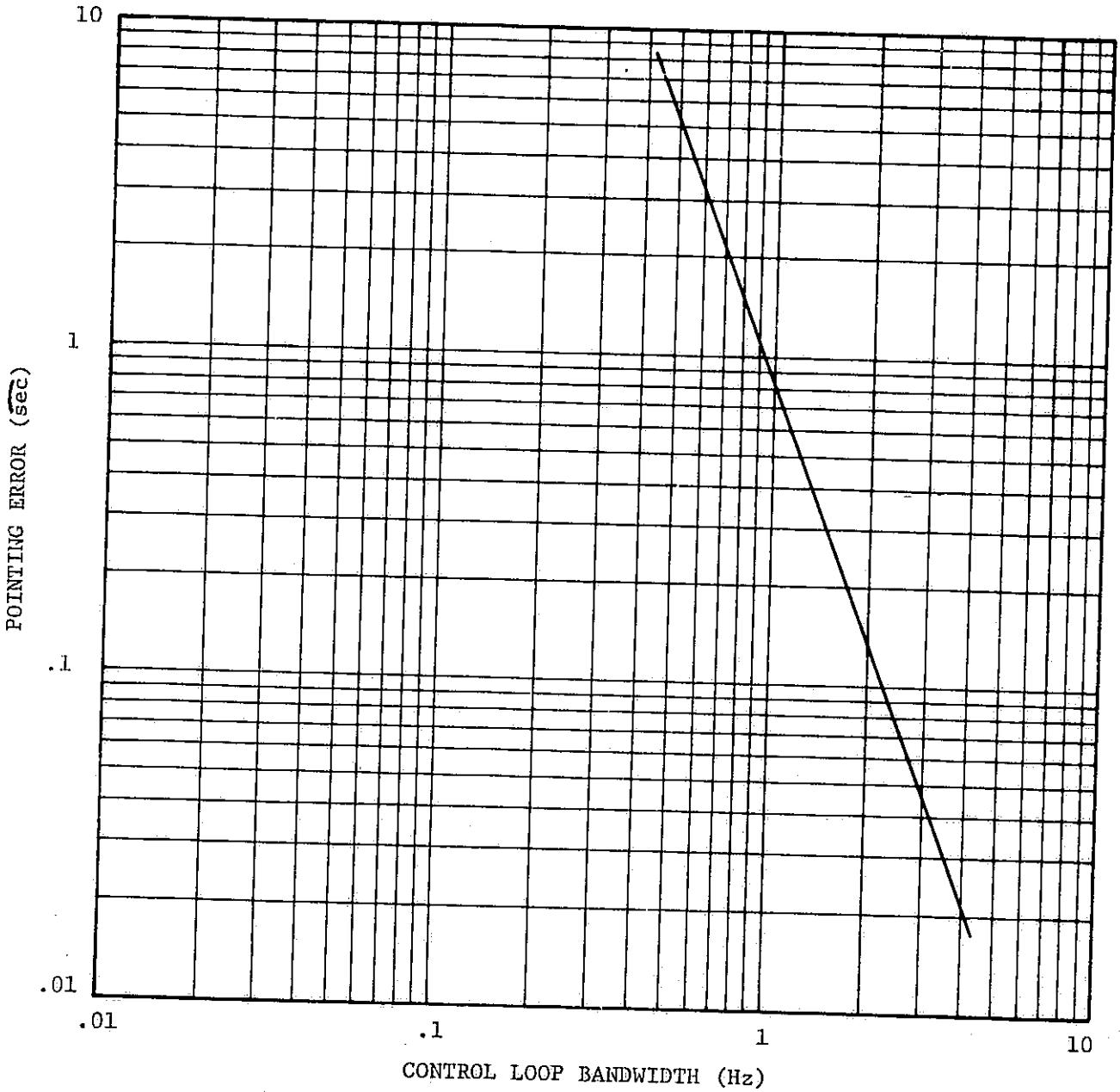

Figure 3-9. Pointing Error Vs Control Loop Bandwidth For 0.1 Hz Suspension Natural Frequency

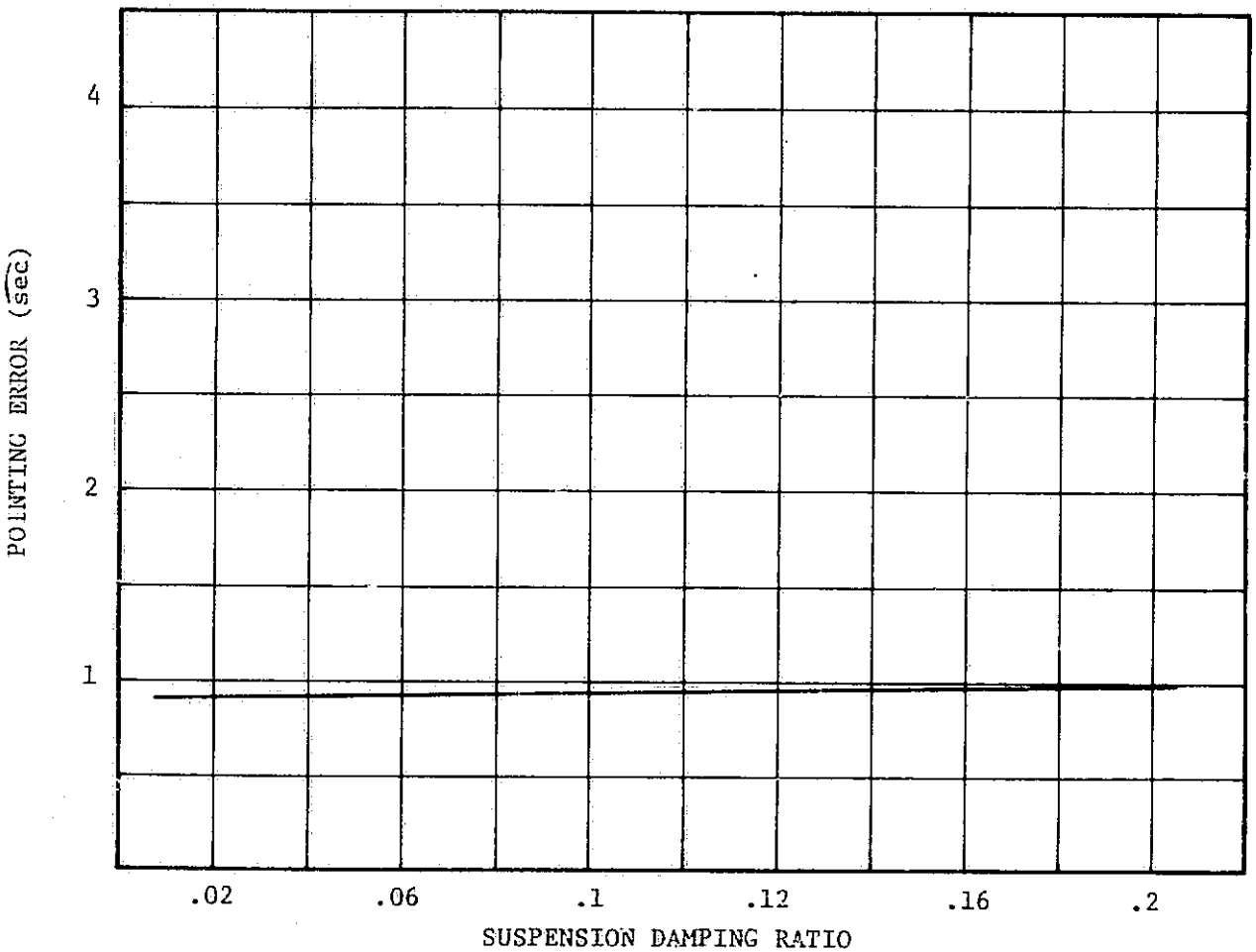

Figure 3-10. Pointing Error Vs Suspension Damping Ratio For 1 Hz Loop Bandwidth and 0.1 Hz Suspension Natural Frequency

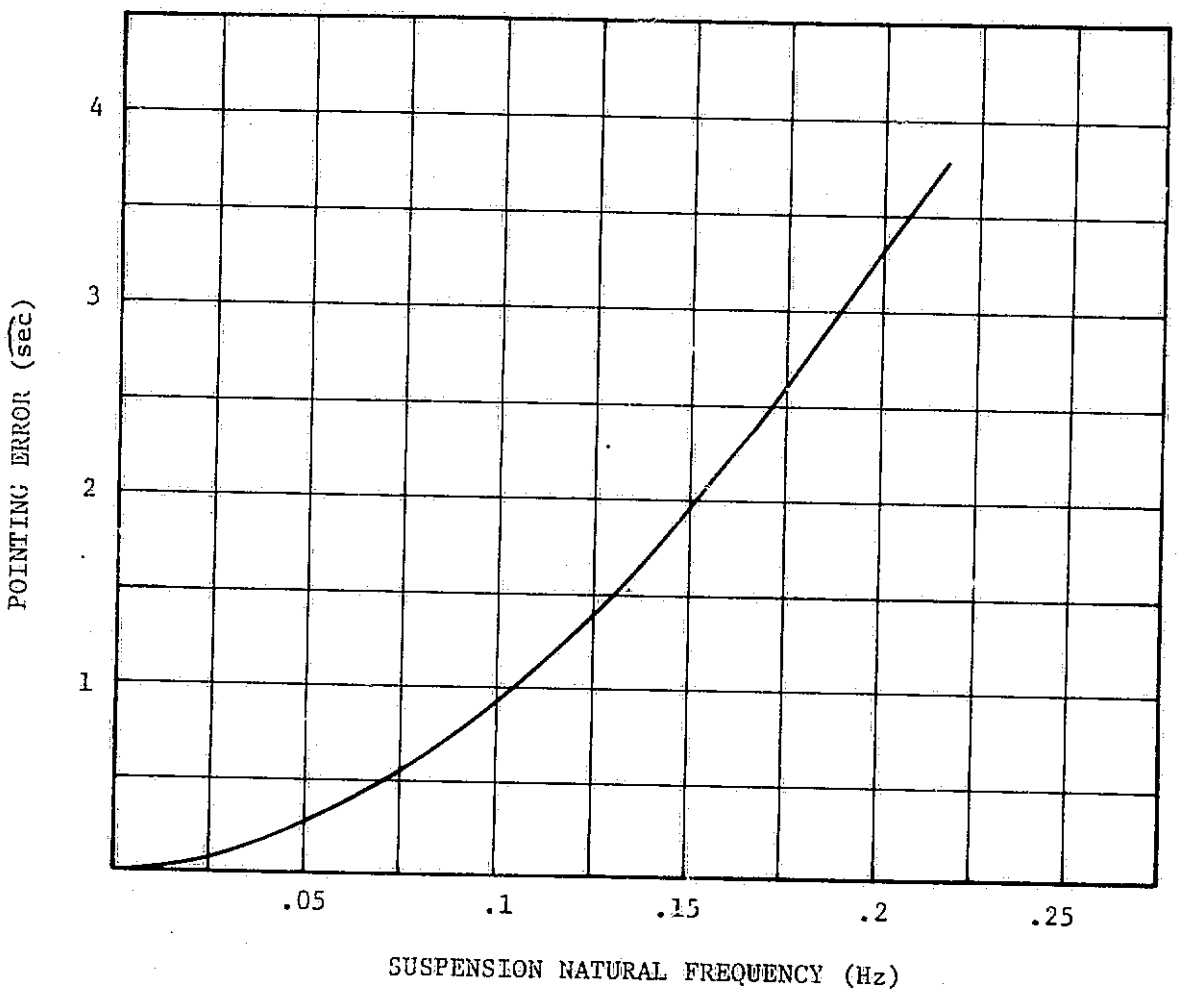

Figure 3-11. Pointing Error Vs Suspension Natural Frequency For 1 Hz Control Loop and 0.1 Suspension Damping Ratio

Table 3-1. Parameters For Two Body Stability Model

$J_{1x}=50.21$ kg-m^2	$R_{E1z}=-.375$ m
$J_{1y}=50.21$ kg-m^2	$r_{1z}=.375$ m
$J_{1z}=50.21$ kg-m^2	$r_{2x}=1.85$ m
$J_{2x}=2.605\times10^3$ kg-m^2	$K_{Rx}=2.47\times10^4$ n-m-sec
$J_{2y}=2.08\times10^3$ kg-m^2	$K_{Ry}=1.472\times10^4$ n-m-sec
$J_{2z}=2.335\times10^3$ kg-m^2	$K_{Rz}=2.214\times10^4$ n-m-sec
$m_1=1.95\times10^2$ kg	$K_{Px}=8.764\times10^4$ n-m
$m_2=2.683\times10^2$ kg	$K_{Py}=7\times10^4$ n-m
$D_x=D_y=D_z=2.68\times10^2$ n-sec/m	$K_{Pz}=7.856\times10^4$ n-m
$K_x=K_y=K_z=2.5\times10^3$ n/m	$K_{Ix}=1.384\times10^5$ n-m/sec
$d_x=d_y=66.9$ n-m-sec	$K_{Iy}=1.105\times10^5$ n-m/sec
$k_x=k_y=625$ n-m	$K_{Iz}=1.24\times10^5$ n-m/sec

4. EFFECTS OF FLEXIBILITY ON POINTING CONTROL LOOP

The following section presents a general discussion of the effects of flexibility on the pointing control loop which applies to all of the IPS options being considered in this study. Data on the effects of flexibility will then be presented for the three (i.e., IOG, SEPB, and Floated Pallet) IPS options being investigated. Finally analytical verification of an instability first observed on the linear pointing performance simulation for nominal IOG suspension parameters will be presented.

4.1 General Discussion on the Effects of Flexibility on Pointing Control Loop - The problem of flexibility can be divided into two broad classes:

a. Flexibility between sensors and actuators as exemplified by the classical booster problem.

b. Sensors and actuators mounted on a relatively rigid structural portion which is in turn connected through a flexible interface to the remaining structure. Skylab was an example of this type of problem.

Both of these effects cause stability problems, however, they are different in nature. When flexibility exists between sensors and actuators the flexibility acts as a lag in the control system which can be grossly viewed as the equivalent of having low bandwidth actuators thus causing instability. When sensors and actuators are mounted on a relatively rigid portion of structure which is connected through a flexible interface to the remaining structure, the effect of the flexibility is to cause an apparent decrease in the controllable vehicle inertia when the natural frequency of the flexible interface is exceeded. This decrease in inertia can be viewed as an increase in loop gain which can cause instability if the inertia reduction is appreciable, and the stiffness of the interface does not yield a sufficiently high structural natural frequency. Both of these effects can be illustrated by the simplified single axis system shown in figures 4-1 and 4-2.

The transfer function for the vehicle dynamics assuming that sensors and actuators are mounted on body 1 can be derived from the following set of equations:

$$(T_D - T_C) - D(\omega_1 - \omega_2) - K(\theta_1 - \theta_2) = J_1 \dot{\omega}_1 \qquad (1)$$

$$D(\omega_1 - \omega_2) + K(\theta_1 - \theta_2) = J_2 \dot{\omega}_2 \qquad (2)$$

Rearranging terms and taking the Laplace transform gives:

$$(T_D - T_C) = (J_1 s^2 + Ds + K)\theta_1 - (Ds + K)\theta_2 \tag{3}$$

$$0 = -(Ds + K)\theta_1 + (J_2 s^2 + Ds + K)\theta_2 \tag{4}$$

Solving equations (3) and (4) for θ_1 and θ_2 gives

$$\theta_1 = \frac{(T_D - T_C)(J_2 s^2 + Ds + K}{s^2\left[J_1 J_2 s^2 + (J_1 + J_2)(Ds + K)\right]} \tag{5}$$

$$\theta_2 = \frac{(T_D - T_C)(Ds + K)}{s^2\left[J_1 J_2 s^2 + (J_1 + J_2)(Ds + K)\right]} \tag{6}$$

Rewriting equations (5) and (6) using $\omega = s\theta$

$$\omega_1 = \frac{(T_D - T_C)}{(J_1 + J_2)s}\left[\frac{\frac{J_2}{K} s^2 + \frac{D}{K} s + 1}{\frac{J_1 J_2}{K(J_1 + J_2)} s^2 + \frac{D}{K} s + 1}\right] \tag{7}$$

$$\omega_2 = \frac{T_D - T_C}{(J_1 + J_2)s}\left[\frac{\frac{D}{K} s + 1}{\frac{J_1 J_2}{K(J_1 + J_2)} s^2 + \frac{D}{K} s + 1}\right] \tag{8}$$

Examination of equation (7) shows that at low frequencies the vehicle inertia is represented by $(J_1 + J_2)$, however, at high frequencies the vehicle inertia is just equal to J_1. With the use of equation (7) and the expressions shown in figure 4-1 the loop gain of the simplified single axis system can be written as

$$HG(s)=\frac{1}{(J_1+J_2)s}\left[\frac{\frac{J_2}{K}s^2+\frac{D}{K}s+1}{\frac{J_1J_2}{K(J_1+J_2)}s^2+\frac{D}{K}s+1}\right]\left[\frac{1}{(\frac{s}{\omega_s})^2+\frac{2\zeta}{\omega_s}s+1}\right]\left[K_R+\frac{K_P}{s}+\frac{K_I}{s^2}\right]\left[\frac{1}{\frac{s}{\omega_a}+1}\right] \quad (9)$$

(STRUCTURAL DYNAMICS; SENSOR DYNAMICS; VEHICLE CONTROL LAW; ACTUATOR DYNAMICS)

Since the total body (i.e., body 1 plus body 2) is to be controlled, the vehicle control gains are normally chosen to give satisfactory stability and system performance assuming an inertia of J_1+J_2. However, if the natural frequency of the flexible interface is not sufficiently high, particularly in the case where $J_2>>J_1$, examination of equation (9) shows that a large increase in loop gain occurs once the natural frequency of the flexible interface [i.e., $\omega>(\frac{K}{J_2})^{1/2}$] is exceeded. This increase in loop gain, approximately equal to $(\frac{J_2}{J_1})$, causes an actuator or sensor pole to cross into the right half plane causing an instability.

Examination of equation (8) indicates that the vehicle dynamics acts as a second order lag for radian frequencies $\frac{K(J_1+J_2)}{J_1J_2}<\omega<\frac{K}{D}$ and then acts as a first order lag for $\omega>\frac{K}{D}$. Writing the loop gain for the simplified single axis system shown in figure 4-1 using equation (8) as the representation of vehicle dynamics results in

$$HG(s)=\frac{1}{(J_1+J_2)s}\left[\frac{\frac{D}{K}s+1}{\frac{J_1J_2}{K(J_1+J_2)}s^2+\frac{D}{K}s+1}\right]\left[\frac{1}{(\frac{s}{\omega_s})^2+\frac{2\zeta}{\omega_s}s+1}\right]\left[K_R+\frac{K_P}{s}+\frac{K_I}{s^2}\right]\left[\frac{1}{\frac{s}{\omega_a}+1}\right] \quad (10)$$

(STRUCTURAL DYNAMICS; SENSOR DYNAMICS; VEHICLE CONTROL LAW; ACTUATOR DYNAMICS)

Examination of equation (10) shows that if the interface stiffness is not sufficient to keep the second order lag break frequency [i.e., $\omega_B=\left[\frac{K(J_1+J_2)}{J_1J_2}\right]^{1/2}$] appreciably greater than the desired pointing control loop bandwidth excessive lags will occur causing an instability where a vehicle pole crosses over into the right half plane. Additionally it is seen that as J_1 decreases with respect to J_2 the second order

lag break frequency ω_B increases thus improving system stability exactly the reverse of the effect observed when the sensors and actuators are mounted on body 1. The increase in stability as J_1 decreases with respect to J_2 can be argued from a physical standpoint. Since the torque applied to body 2 must be applied through the flexible interface between bodies 1 and 2, the faster body 1 can be deflected the faster the control torques are applied to body 2. Hence as the inertia of body 1 decreases it can be deflected more rapidly by the torque applied by the actuators on body 1 thus reducing the overall system lag and increasing overall system stability margins.

The instabilities caused by flexure in both classes of the problem can be compensated for by two general techniques:

a. Design the bandwidth of the control loop below the natural frequencies of the vehicle flexibilities (i.e., gain stabilization). This type of design results in a low control loop bandwidth and hence pointing performance will not be met under the influence of disturbances, particularly those due to crew motion.

b. Use phase stabilization techniques which would yield adequate control loop bandwidth thus enabling high accuracy system pointing performance. However, this technique requires the accurate knowledge of the vehicle bending characteristics which are not readily available and can necessitate on-board measurement of vehicle flexibility characteristics.

Therefore, the approach taken in this study is to evaluate the loop bandwidth that is required to meet 1 $\widehat{\text{sec}}$ system pointing performance assuming a rigid structure as described in section 3. Flexibility is then inserted and the structural stiffness (i.e., structural natural frequencies) required to yield satisfactory system stability and performance determined without the use of bending mode filters. This determination was conducted for both classes of the flexibility problem outlined above.

The model that was used for these determinations was the linear pointing performance model as outlined in section 2.1 of this report.

4.2 Effects of Flexibility on the IOG Pointing Control Loop - Using an IOG loop bandwidth of 2 Hz determined in section 3.1.1 with sensors and actuators mounted on body 5, the inertial gimbal of the IOG, the flexible interface between bodies 5 and 6 was varied in order to determine the interface frequency required for system stability. The result of this investigation showed that an interface

frequency of approximately 8 Hz corresponding to an interface stiffness of 1.291×10^7 n-m/rad was required to achieve neutral stability. The interface frequency is defined by the following relationship

$$k_I = (J_{CM} + mr^2)(2\pi f_I)^2 \qquad (11)$$

where:

J_{CM} = inertia of the telescope about principal axes

m = mass of telescope

r = distance from flexible interface to telescope center of mass

When the sensors are mounted on the telescope the interface frequency required for system neutral stability was approximately 2.8 Hz corresponding to an interface stiffness of 1.647×10^6 n-m/rad. This is approximately a factor of 2.8 less than the interface frequency required when sensors and actuators are mounted on body 5, the IOG intertial gimbal. These results support the general discussion given in section 4.1. Figure 4-3 shows the interface frequency required for neutral stability as a function of loop bandwidth for sensors mounted on the telescope (i.e., body 6).

Variations in the flexibility characteristics of the pallet (i.e., bodies 2 and 3) and the interface between pallet and orbiter (i.e., bodies 1 and 2) over wide ranges had little effect on overall IOG system stability and performance.

In summary the conclusions that are drawn from the investigation of the effects of flexibility on the IOG system performance and configuration are the following:

a. In order to minimize the interface and telescope frequency and stiffness required for stability sensors should be mounted on the telescope rather than the inertial gimbal of the IOG. This would necessitate both a mechanical and electrical interface with the various telescopes that are to be mounted on the IOG.

b. The interface frequency and corresponding stiffness required for neutral stability is approximately 2.8 Hz and 1.647×10^6 n-m/rad, respectively. It should be noted that these values are required for neutral stability. In order to achieve adequate stability margins the interface frequency should be increased between a factor of 1.5 to 2 corresponding to an increase

in stiffness of 2.25 to 4. It should be noted that the interface stiffness represents the gimbal stiffness, telescope mounting interface stiffness, and the stiffness of the telescope support module as a lumped parameter. The reason for this is that the sensors will be mounted on the optical bench in order to control the telescope line of sight while the attach point to the IOG will be on the back end of the telescope. Therefore, the IOG gimbal compliance, interface compliance, and telescope support module compliance can be roughly viewed as springs in series. Hence it is seen that severe stiffness requirements will be placed on the telescope support module in order to achieve system stability which traditionally has no such requirement thus complicating its structural design. If bending mode filters are to be employed to alleviate the telescope stiffness requirements accurate knowledge of system bending modes would be required and each telescope would require its own bending mode filter design making the IOG very payload sensitive.

4.3 Effects of Flexibility on the SEPB - Using the 1 Hz pointing control loop as outlined in section 3.2 the interface frequency and stiffness requirements were determined when sensors were mounted on the inertial gimbal of the SEPB and when they were mounted on the telescope.

When the sensors (i.e., rate gyros) were mounted on the inertial gimbal of the SEPB (i.e., body 5) the interface frequency and stiffness required for neutral stability was 0.5 and 2.5×10^4 n-m/rad, respectively. When the sensors were mounted on the telescope the interface frequency and stiffness required for neutral stability was 6 Hz and 3.6×10^6 n-m/rad, respectively. For the SEPB the relationship between interface frequency and stiffness is given by

$$k_I = J_{CM}(2\pi f_I)^2 \tag{12}$$

These results are the reverse of those obtained for the IOG and further points up the effects of structural flexibility discussed in section 4.1. Examination of the inertias of the SEPB inner gimbal and the telescope (table 2-2) indicate that they are of the same order for the y and z axes and differ by a factor of 5 for the x axis. This is much smaller than the factors of 34 or 70 encountered for the IOG depending on whether telescope inertia about the principal axes or a coordinate frame centered at the telescope to IOG gimbal attach point is employed. Hence when sensors are mounted on the inertial gimbal of the SEPB an apparent loop gain increase of a factor

of 5 occurs for the x axis and only requires a structural interface frequency of 0.5 Hz to achieve neutral stability. In fact the x axis is the only axis for which a minimum interface stiffness is required for stability. For the y and z axes there is no interface stiffness required for absolute stability about these axes. However, if pointing stability is to be maintained to within ± 1 $\widehat{\text{sec}}$ peak the interface frequency and stiffness required is 3 Hz and 9.0×10^5 n-m/rad, respectively. However, it should be noted that this interface frequency and stiffness requirement is only required to meet pointing performance but not for stability. Hence it is not required that margins of 1.5 or 2 be applied to these numbers in order to assure satisfactory system performance which would be the case as pointed out above when structural interface frequency and stiffness requirements are necessary from a stability viewpoint.

When the sensors are mounted on the telescope (body 6) the interface frequency and stiffness requirement for neutral stability is 6 Hz and 3.6×10^6 n-m/rad, respectively. Again this result supports the discussion given in section 3.1. Since the inertias about the y and z axes for the SEPB inertial gimbal and the telescope differ by only a factor of 1.6 a large system lag results as indicated by equation (10); therefore, the interface frequency and stiffness has to be relatively high in order to set the second order break frequency high enough with respect to the control loop bandwidth in order to achieve stability. In fact the axes which govern the interface frequency and stiffness requirements are the y and z axes. The value of interface frequency and stiffness required for the x axis is appreciably below that which is required for the y and z axes.

In summary the following are the conclusions that are drawn from the investigations performed on the effects of flexibility on SEPB pointing control loop performance:

a. Sensors should be mounted on the SEPB inertial gimbal in order to minimize the structural frequency and interface requirements for stability. The interface frequency and stiffness required for stability is 0.5 Hz and 2.5×10^4 n-m/rad and is governed by the x axis.

b. The interface frequency and stiffness required to maintain ± 1 $\widehat{\text{sec}}$ peak pointing stability in the presence of crew motion disturbances is 3 Hz and 9.0×10^5 n-m/rad, respectively. This value of interface stiffness is approximately 0.5 that required

for the IOG thus alleviating the structural requirements for the telescope. In addition it should be noted that the SEPB would attach to the telescope metering truss which is traditionally quite stiff due to thermal and dimensional stability requirements. Hence a 3 Hz interface frequency with its corresponding interface stiffness should be easier to achieve than a similar interface stiffness for the IOG.

c. The interface frequency and stiffness required for neutral stability if sensors are mounted on the telescope is 6 Hz and 3.6×10^6 n-m/rad, respectively. This is an increase of a factor of 2 in interface frequency and a factor of 4 in interface stiffness over that which is required when sensors are mounted on the inertial gimbal of the SEPB.

4.4 Effects of Flexibility on the Floated Pallet - Using the 1 Hz control loop bandwidth established in section 3.3, the interface frequency and stiffness requirements for stability and pointing performance were determined for the following cases:

1. Sensors and actuators mounted on body 3 which corresponds to one-third of the pallet inertia.

2. Actuators mounted on body 2 and sensors mounted on body 3.

3. Sensors and actuators mounted on body 2.

For case 1 where sensors and actuators were mounted on body 3 there was no interface frequency or stiffness requirement between bodies 2 and 3 from an absolute stability viewpoint. However, if ± 1 $\widehat{\text{sec}}$ peak pointing stability is to be met in the presence of crew motion disturbances over the total pallet structure the rotational and translational interface frequency, rotational stiffness, and translational stiffness had to be 4 Hz, 2.93×10^7 n-m/rad, and 5.78×10^5 n/m, respectively.

For case 2 where sensors were mounted on body 3 and actuators on body 2 the rotational and translational interface frequency, rotational stiffness, and translational stiffness had to be 8 Hz, 1.44×10^8 n-m/rad, and 2.313×10^6 n/m, to achieve neutral stability. It should be noted that the same results would be obtained if the actuators were mounted on body 3 and the sensors were mounted on body 2 since the system is reciprocal and the system characteristic equation does not change.

For case 3 where both sensors and actuators were mounted on body 2 there was no interface frequency or stiffness requirement between bodies 2 and 3 required from the standpoint of absolute stability. However, approximately a 0.5 Hz interface frequency corresponding to linear interface stiffness of 3.6×10^4 n/m and a rotational stiffness of 4.58×10^5 n/m was required in order to meet ± 1 $\widehat{\text{sec}}$ pointing stability over the total pallet. The significance of this result is that it gives an estimate as to the interface frequency and stiffness required by instruments that are mounted to the pallet. Since body 3 gets perturbed only through the flexible interface between bodies 2 and 3, body 3 can be considered as an experiment bolted to the pallet which can be considered as body 2. It is therefore seen that the interface frequency between experiments and pallet which is being stabilized to ± 1 $\widehat{\text{sec}}$ peak is only required to be in the vicinity of 0.5 Hz. Therefore, the floated pallet places the least restriction on telescope and positioning gimballing structural design. It should also be noted that the pallet pointing control system is least sensitive to payload characteristics and hence truly acts as an experiment base which can accommodate a wide variety of payloads requiring precise pointing accuracies.

In summary the following are the conclusions derived from the investigations on the effect of flexibility on the floated pallet:

a. In order to minimize the floated pallet stiffness requirements sensors and actuators should be mounted on a relatively stiff section of pallet corresponding to approximately 30 percent of the total pallet inertia having a first significant bending mode in excess of 8 Hz. The interface frequency between this section and the rest of the pallet should be 4 Hz if 1 $\widehat{\text{sec}}$ pointing stability is to be maintained over the total pallet.

b. The interface structural frequency between instruments mounted on a pallet stabilized to ± 1 $\widehat{\text{sec}}$ in order to meet ± 1 $\widehat{\text{sec}}$ pointing stability on the instrument is approximately 0.5 Hz. This poses the least restriction on telescope structural design of any of the systems investigated and can easily be met. This makes the pallet quite insensitive to payload characteristics and hence truly acts as an experiment base capable of accommodating a large variety of instruments requiring precise pointing.

Table 4-1 summarizes the results obtained for the LOG, SEPB, and Floated Pallet with respect to the effects of structural flexibility.

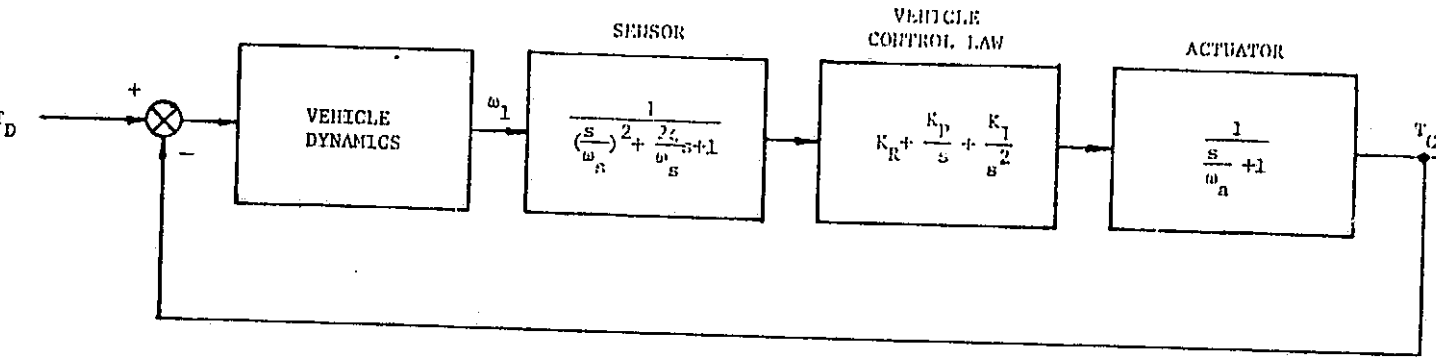

Figure 4-1. Simplified Single Axis System

where:

T_D = Disturbance torque

T_C = Control torque

ω_s = Sensor natural frequency (rate gyro was assumed)

ω_a = Actuator natural frequency

K_R = Vehicle rate gain (n-m/rad/sec)

K_P = Vehicle position gain (n-m/rad)

K_I = Vehicle integral gain (n-m-sec/rad)

The vehicle dynamics shown in figure 4-1 are schematically represented in figure 4-2.

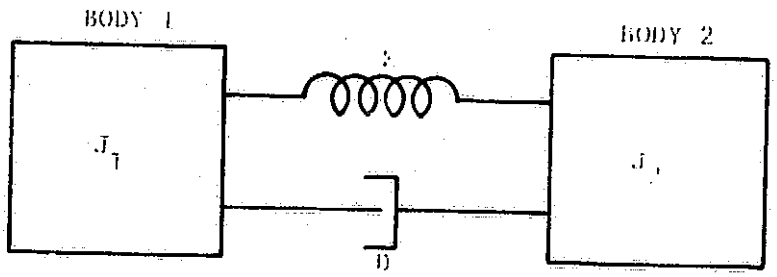

Figure 4-2. Vehicle Dynamics

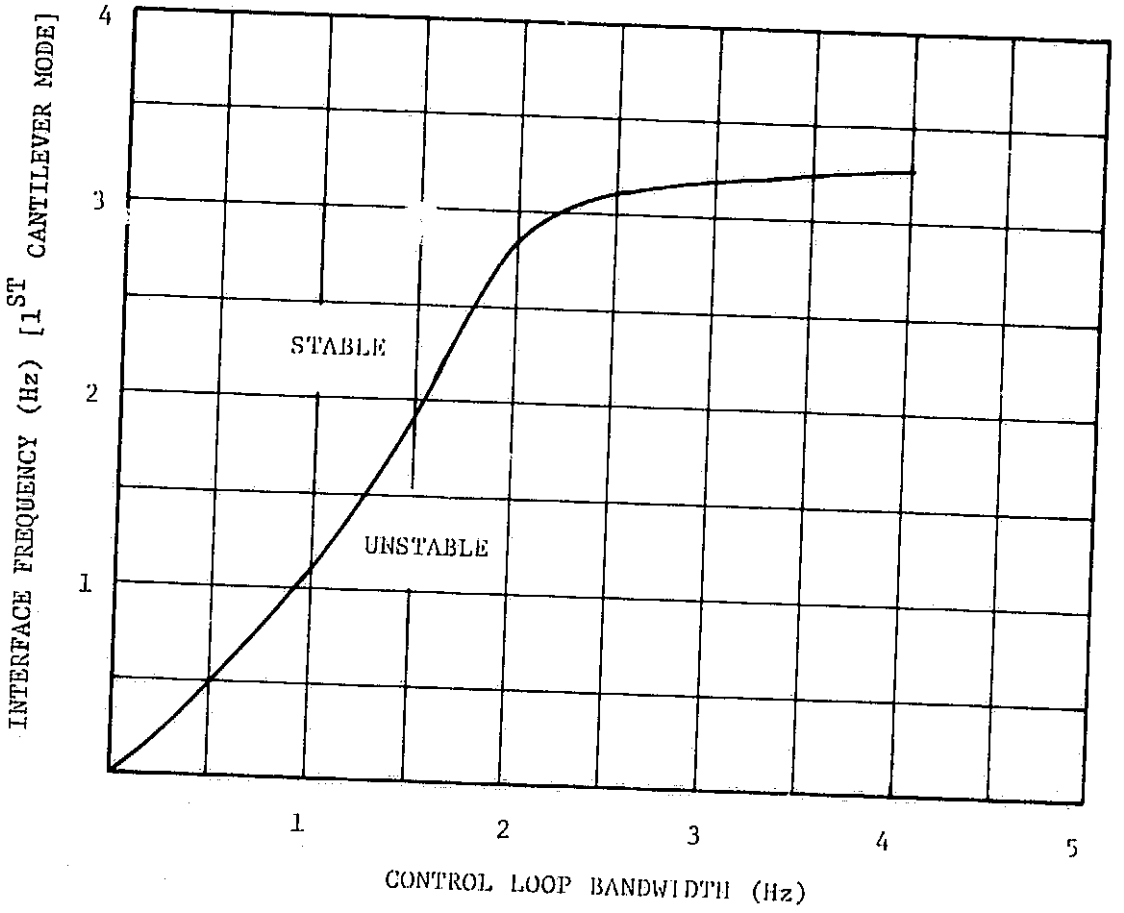

Figure 4-3. Gimbal Interface Frequency Vs LOG Control Loop Bandwidth (Sensors Mounted on the Telescope)

Table 4-1. Effects of Structural Flexibility for the IPS

SYSTEM	INTERFACE STIFFNESS FOR STABILITY WITH FLEXIBLE INTERFACE BETWEEN SENSORS AND ACTUATORS	INTERFACE STIFFNESS FOR STABILITY WITH SENSORS AND ACTUATORS MOUNTED ON RIGID STRUCTURE	INTERFACE STIFFNESS TO MEET POINTING STABILITY REQUIREMENT OF ±1 SEC PEAK
Inside-Out Gimbal System (IOG) 2 Hz Control Loop 2.5×10^3 kg-m^2 Instrument	1st Cantilever Mode f_n=2.846 Hz k=1.647×10^6 n-m/rad Should at least be increased by a factor of 2 (5.692 Hz) to achieve adequate system response	1st Cantilever Mode f_n=7.967 Hz k=1.291×10^7 n-m/rad	Not applicable
Standard Experiment Pointing Base (SEPB) 1 Hz Control Loop 2.5×10^3 kg-m^2 Instrument	f_n=6 Hz k=3.599×10^6 n-m/rad	f_n=0.5 Hz k=2.499×10^4 n-m/rad	f_n=3 Hz k=8.996×10^5 n-m/rad
Floated Pallet 1 Hz Control Loop	f_n=8 Hz k=1.73×10^8 n-m/rad K=2.313×10^6 n/m	None required as long as rigid (i.e., 8 Hz) section corresponds to approximately 30 percent of the total pallet inertia	f_n=4 Hz k=2.93×10^7 n-m/rad K=5.784×10^5 n/m

5. SLEWING PERFORMANCE OF THE INSIDE-OUT GIMBAL (IOG) SYSTEM

This section describes the performance of the IOG during telescope slewing. Two slew profiles were used in this evaluation. One profile represents the rate required to track an earth fixed point. The other profile was chosen to give 50 percent higher rates than that required for earth tracking. Both of these slewing profiles were supplied by NASA. Two telescopes were also used in the IOG slewing evaluation. One of the telescopes is the same as that used in the IOG pointing performance evaluations described in the preceding sections, the parameters of which are listed in table 2-5. The second telescope evaluated was considerably lighter than that used in the pointing performance studies. The geometric configuration and mass characteristics for this telescope are shown in figure 5-1 and listed in table 5-1, respectively. In all of the slewing studies the the suspension stiffness was set a 1/20 nominal as shown in section 3. For convenience, the telescope used above in the IOG pointing performance evaluations will be referred to as the "baseline telescope" while the second telescope will be called the "slewing telescope."

The two slew profiles that were used are given in the equations below.

Slew Profile 1 (earth tracking)

$$\theta(t)=1.136 \tanh\left[\frac{372-t}{65}\right] \tag{1}$$

$$\omega(t)=-1.748\times10^{-2} \operatorname{sech}^2\left[\frac{372-t}{65}\right] \tag{2}$$

Slew Profile 2 (50 percent higher rates than earth tracking)

$$\theta(t)=1.136 \tanh\left[\frac{246-t}{43}\right] \tag{3}$$

$$\omega(t)=-2.642\times10^{-2} \operatorname{sech}^2\left[\frac{246-t}{43}\right] \tag{4}$$

Both of the slew profiles described in equations (1) thru (4) were applied to the baseline and slewing telescopes. The telescopes were slewed about the -y axis for both profiles. In addition, both telescopes were slewed using profile 1 about an axis in the xy plane making an angle of $\pi/4$ (45 degrees) with both the -x and -y telescope axes, which results in maximum coupling between the x and y telescope axes and IOG pedestal axes.

A satisfactory slew about this axis would imply satisfactory slewing about any axis located in the x-y plane. Examination of the slew profiles defined above implies that at time equal to zero the telescope is rotated 1.136 rad (65 degrees) negatively with respect to the axis about which the telescope is to be slewed. The telescope maneuvers between $\pm$1.136 rad about the slew axis in 744 and 492 seconds for slew profiles 1 and 2, respectively. Due to the computer running times involved it was not feasible to run a complete slew profile for either of the profiles defined. In order to achieve realistic computer running times, 100 seconds of the slew profiles described were run. The system was initialized properly for $\pm$50 seconds about the point at which maximum rate occurs which is 372 and 246 seconds for profiles 1 and 2, respectively. This initialization runs through the maximum telescope rates and accelerations represented by both slewing profiles thus resulting in maximum telescope tracking errors, IOG pedestal rotations and translations, and IOG isolator elongations. Table 5-2 summarizes the results of the IOG slewing studies.

Examination of table 5-2 indicates that the IOG is capable of satisfactorily slewing the "slewing telescope" through both slew profiles about any axis in the xy plane. The maximum resulting pedestal rotation and isolator elongation is approximately 9.12×10^{-2} rad (5 degrees) and 2.65×10^{-2} m (1.04 inches), respectively. These values especially for the isolator elongation are within state-of-the-art isolator design. In addition, the maximum control torque required was 1.69 n-m when using profile 2 which is well within the capability of direct drive DC torquers of feasible size and volume. Direct drive DC torquers are desirable from a pointing control viewpoint since they eliminate the nonlinearities that usually accompany geared torquers. The largest tracking error incurred was 1.474 $\widehat{\text{sec}}$ when using slew profile 2. However, it is anticipated that this error could be reduced to less than an arc second by a slight increase in telescope control loop gains.

Examination of table 5-2 shows that slewing the baseline telescope evenly through slew profile 1 results in relatively large rotations and translations of the IOG pedestal accompanied by substantial elongations of the IOG isolators. The IOG pedestal rotated .176 rad (10 degrees) and 0.179 rad (10.3 degrees) about the x and y axes, respectively, and was accompanied by an isolator elongation of 9.161×10^{-2} m (3.61 inches) when the telescope was slewed about an axis in the xy plane making an angle of $\pi/4$ rad (45 degrees) with respect to the telescope -x and -y axes. It is difficult to design a suspension that will give satisfactory performance and have uniform characteristics for elongations in the

order of 10.16 cm (4 inches). When attempting to slew the baseline telescope through slew profile 2, pedestal rotations and isolator elongations are appreciably more severe than those incurred using slew profile 1, as table 5-2 indicates. It should be noted that when using slew profile 2, the rotations of the IOG pedestal are so severe that the assumptions of small angular rotation of the IOG pedestal, made in the derivation of the equations of motion for the slewing model, are no longer valid.

The results of the IOG slewing studies further indicate the sensitivity of IOG performance to payload characteristics. It is doubtful that the IOG will be able to satisfactorily track a point on earth with a telescope whose inertia is in excess of 10^3 kg-m^2 within acceptable pedestal rotations and translations, and isolator elongations. This sensitivity of IOG performance to payload characteristics, also shown in section 4, is the most significant shortcoming of the IOG system.

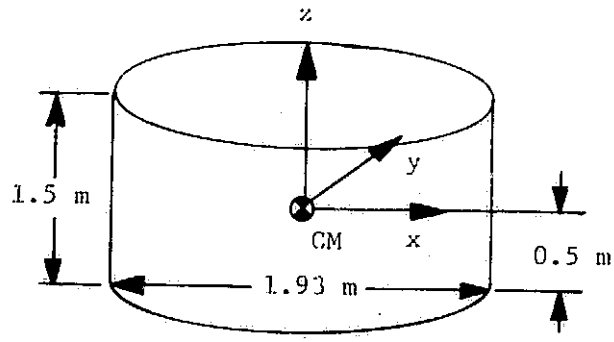

Figure 5-1. Slewing Telescope Geometric Configuration

Table 5-1. Slewing Telescope Mass Properties

$M=932$ kg
$J_x=388$ kg-m^2
$J_y=388$ kg-m^2
$J_z=1,719$ kg-m^2

Table 5-2. IOG Slewing Performance

	SLEW PROFILE	TELESCOPE SLEW AXIS	TRACKING ERROR (rad)	IOG PEDESTAL ROTATION (rad)	IOG PEDESTAL CM TRANSLATION (meters)	ISOLATOR ELONGATION (meters)	CONTROL TORQUE (n-m)
Slewing Telescope (932 kg)	1	-y axis	$\theta_{xE}=0$ $\theta_{yE}=4.89\times10^{-6}$ (1.008 sec) $\theta_{zE}=0$	$\theta_x=0$ $\theta_y=4.59\times10^{-2}$ (2.63 deg) $\theta_z=0$	$\epsilon_x=1.88\times10^{-2}$ (.7402 in) $\epsilon_y=0$ $\epsilon_z=1.26\times10^{-3}$ (.05 in)	$x=1.588\times10^{-3}$ (.0625 in) $y=0$ $z=1.182\times10^{-2}$ (.4652 in)	$T_{cx}=0$ $T_{cy}=0.836$ $T_{cz}=0$
	2	-y axis	$\theta_{xE}=0$ $\theta_{yE}=7.15\times10^{-6}$ (1.474 sec) $\theta_{zE}=0$	$\theta_x=0$ $\theta_y=9.12\times10^{-2}$ (5.225 deg) $\theta_z=0$	$\epsilon_x=3.72\times10^{-2}$ (1.465 in) $\epsilon_y=0$ $\epsilon_z=2.61\times10^{-3}$ (.103 in)	$x=3\times10^{-3}$ (.118 in) $y=0$ $z=2.29\times10^{-2}$ (.902 in)	$T_{cx}=0$ $T_{cy}=1.69$ $T_{cz}=0$
	1	In xy plane $\pi/4$ rad with respect to telescope -x and -y axes	$\theta_{xE}=4.53\times10^{-6}$ (.934 sec) $\theta_{yE}=4.59\times10^{-6}$ (.9464 sec) $\theta_{zE}\approx0$	$\theta_x=5.27\times10^{-2}$ (3.02 deg) $\theta_y=5.32\times10^{-2}$ (3.048 deg) $\theta_z\approx0$	$\epsilon_x=2.18\times10^{-2}$ (.858 in) $\epsilon_y=2.17\times10^{-2}$ (.854 in) $\epsilon_z=2.04\times10^{-3}$ (.08 in)	$x=1.85\times10^{-3}$ (.073 in) $y=1.938\times10^{-3}$ (.076 in) $z=2.653\times10^{-2}$ (1.044 in)	$T_{cx}=0.949$ $T_{cy}=0.963$ $T_{cz}\approx0$
Baseline Telescope (2.39×10^3 kg)	1	-y axis	$\theta_{xE}=0$ $\theta_{yE}=4.17\times10^{-6}$ (0.86 sec) $\theta_{zE}=0$	$\theta_x=0$ $\theta_y=0.249$ (14.27 deg) $\theta_z=0$	$\epsilon_x=9.92\times10^{-2}$ (3.906 in) $\epsilon_y=0$ $\epsilon_z=4.39\times10^{-3}$ (.1728 in)	$x=5.725\times10^{-3}$ (.2254 in) $y=0$ $z=6.592\times10^{-2}$ (2.595 in)	$T_{cx}=0$ $T_{cy}=5.33$ $T_{cz}=0$
	2	-y axis	$\theta_{xE}=0$ $\theta_{yE}=8.05\times10^{-6}$ (1.66 sec) $\theta_{zE}=0$	$\theta_x=0$ $\theta_y=0.674$ (38.6 deg) $\theta_z=0$	$\epsilon_x=0.270$ (10.6 in) $\epsilon_y=0$ $\epsilon_z=8.62\times10^{-3}$ (.339 in)	$x=1.725\times10^{-2}$ (.679 in) $y=0$ $z=0.1726$ (6.795 in)	$T_{cx}=0$ $T_{cy}=14.1$ $T_{cz}=0$
	1	In xy plane $\pi/4$ rad with respect to telescope -x and -y axes	$\theta_{xE}=2.09\times10^{-6}$ (.431 sec) $\theta_{yE}=2.26\times10^{-6}$ (.466 sec) $\theta_{zE}=0$	$\theta_x=0.176$ (10.08 deg) $\theta_y=0.179$ (10.26 deg) $\theta_z\approx0$	$\epsilon_x=7.15\times10^{-2}$ (2.815 in) $\epsilon_y=6.71\times10^{-2}$ (2.642 in) $\epsilon_z=3.93\times10^{-3}$ (.155 in)	$x=4.375\times10^{-3}$ (.172 in) $y=3.975\times10^{-3}$ (.157 in) $z=4.161\times10^{-2}$ (3.61 in)	$T_{cx}=3.89$ $T_{cy}=3.85$ $T_{cz}\approx0$

6. COMPARISON OF THE IOG, SEPB, AND FLOATED PALLET SYSTEMS

In this section the IOG, SEPB, and Floated Pallet are compared relative to each other. The format for this comparison is a tabular listing giving the advantages and disadvantages of each of the systems investigated. Comparison between system weight and the pallet/telescope interface stiffness requirements is also presented. However, before presenting the comparison tables some general comments on the systems investigated are in order.

The one main disadvantage of the IOG system is its extreme sensitivity to payload characteristics. This payload sensitivity manifests itself in three ways:

a. Severe stiffness requirements are placed upon the telescope structural design. These stiffness requirements apply to the total telescope structure including the instrument and subsystem compartment behind the actual telescope (i.e., optical bench), which traditionally does not require a stiff structural design. Hence telescope structural design will be driven to a great degree by IOG stability and performance needs rather than the requirements primarily placed upon its design from the scientific mission it is to perform. Compensation for telescope flexibility can be designed in order to alleviate the requirements for structural rigidity. However, if this approach is adopted, a phase stabilization technique would be required in order to maintain the 2 Hz control loop bandwidth required to meet pointing performance. This would necessitate accurate knowledge of telescope and interface flexibility characteristics, which can possibly require on-board measurement, and the capability of varying compensator characteristics as a function of these measurements.

b. Sensors required for IOG control should be mounted on the telescope in order to minimize the interface and telescope structural stiffness required for system stability. This detracts from the IOG as a general purpose experiment accommodator and requires a mechanical and an additional electrical interface.

c. Pedestal rotations, translations, and isolator elongation as a function of telescope mass, inertia characteristics, and slew profiles. This sensitivity probably will not allow the slewing of telescopes larger than 1,000 $kg\text{-}m^2$, even for earth point tracking, in order to maintain pedestal motion and isolator elongations within tolerable limits.

The advantage of the IOG system is that it does not require payload mass balancing, thus making it ameanable to changing telescope instrument packages as desired without telescope rebalancing. In addition, the IOC is the lowest weight system of

options investigated. The IOG will also be the minimum cost option of the Instrument Pointing Systems considered, however, in light of the payload sensitivity described above it is not apparent that minimum overall program cost would result.

The SEPB does not exhibit the degree of payload sensitivity as the IOG, however, it does place relatively severe gimbal to telescope interface stiffness requirements in order to meet telescope pointing stability performance. However, there is one significant difference between the SEPB and IOG. Since the SEPB is a center of mass mount (i.e., telescope CM must be constrained to a "small" radius sphere with respect to the gimbal intersection point), it can conveniently be attached to the telescope optical bench. The optical bench is normally made quite stiff due to thermal and dimensional stability considerations. Thus the stiffness required to meet pointing stability will probably not drive telescope structural design. In addition, the stiffness requirements for the SEPB is to meet pointing performance and is not required for absolute system stability. This means that the interface stiffness does not have to be designed with any safety margins. Also from structural considerations the stiffness requirements across the interface are minimized if the sensors are mounted on the SEPB inner or inertial gimbal. This eliminates a mechanical and electrical interface and makes the SEPB a piece of general experiment accommodation equipment.

The SEPB exhibits the best slewing capability of the three systems investigated. There is no restriction on the size of telescope used or the slew profile that could be performed from a dynamic viewpoint. The only restriction is that the gimbal torquer has sufficient torque to execute a desired slew profile for a particular telescope being considered.

There are two primary disadvantages to the SEPB systems. These are:

a. The need for telescope mass balancing in order to achieve satisfactory pointing performance. This would complicate the logistics of changing telescope experiment packages thus detracting from its role as an overall experiment accommodator.

b. It is projected to be the heaviest of the systems considered particularly when considering multiple telescope operations.

There are two principal disadvantages to the Floated Pallet system:

a. The Floated Pallet requires a control moment gyro system.

b. It would not be feasible to maneuver the total orbiter in order to perform telescope slewing due to control moment gyro system size and torque considerations. Hence a separate gimballing system would be required in order to perform accurate telescope slewing. If there are slew requirements for many of the projected Spacelab experiments, this would require the use of essentially redundant Instrument Pointing Systems.

The three prime advantages of the Floated Pallet concept are:

a. The total pallet is stabilized to ± 1 sec thus making it an ideal experiment carrier or base for all types of experiments requiring precise pointing accuracy.

b. The Floated Pallet is not sensitive to payload characteristics making it an ideal piece of experiment accommodation equipment. There are virtually no requirements on telescope structural integrity that would probably not be met by standard structural design. In addition, all control gear would be mounted on the pallet thus eliminating mechanical and electrical interfaces with the various pallet mounted experiments.

c. Use of the Floated Pallet system will eliminate the contaminants due to maintaining the orbiter attitude with the presently defined hypergolic reaction control system. It should be noted that if contamination considerations require the use of CMGs in order to eliminate the contamination effects of the orbiter RCS, one of the prime objections to the Floated Pallet concept, both from a cost and complexity viewpoint, is removed. The additional effort required to float the pallet does not appear to be appreciably, hence it would be a real contender for the Spacelab Instrument Pointing System. Even if separate gimballing systems would be required to perform accurate telescope slewing, the Floated Pallet should still be considered for development once CMGs become a necessity from a contamination viewpoint. This would eliminate the interface and telescope structural stiffness requirements that would otherwise be present in gimballing concepts, thus yielding payload insensitive performance characteristics.

Table 6-1 shows the weight comparison between the IOG, SEPB, and Floated Pallet concepts. Table 6-2 shows the comparison between the structural interface stiffness requirements for the systems considered. Tables 6-3, 6-4, and 6-5 summarize the overall advantages and disadvantages of the Spacelab Instrument Pointing Systems.

Table 6-1. Instrument Pointing System Weight Summary

Inside-Out Gimbal System (IOG)		
Weight of Gimbal and Pedestal = 488 kg (1,076 lb)		
Standard Experiment Pointing Base (SEPB)		
Weight of SEPB = 962 kg (2,121 lb)		
Floated Pallet		
Suspension Weight	[11 kg/corner (24.25 lb)]	44 kg (97 lb)
Retention System Weight	[4 kg/mechanism (8.818 lb)]	20 kg (44.09 lb)
CMG Mounting Rack	(Four CMGs)	90 kg (198.4 lb)
CMG Weight	[190 kg/CMG (418.9 lb)]	760 kg (1,676 lb)
CMG Electronics	[9.07 kg/box (20 lb)]	18.14 kg (40 lb)
Total Floated Pallet Weight		932.1 kg (2,055 lb)

Table 6-2. Effects of Flexibility on Instrument Pointing System

SYSTEM	INTERFACE STIFFNESS FOR STABILITY WITH FLEXIBLE INTERFACE BETWEEN SENSORS AND ACTUATORS	INTERFACE STIFFNESS FOR STABILITY WITH SENSORS AND ACTUATORS MOUNTED ON RIGID STRUCTURE	INTERFACE STIFFNESS TO MEET POINTING STABILITY REQUIREMENT OF ±1 SEC PEAK
Inside-Out Gimbal System (IOG) 2 Hz Control Loop 2.5×10^3 kg-m^2 Instrument	1st Cantilever Mode f_n=2.846 Hz k=1.647×10^6 n-m/rad Should at least be increased by a factor of 2 (5.692 Hz) to achieve adequate system response	1st Cantilever Mode f_n=7.967 Hz k=1.291×10^7 n-m/rad	Not Applicable
Standard Experiment Pointing Base (SEPB) 1 Hz Control Loop 2.5×10^3 kg-m^2 Instrument	f_n=6 Hz k=3.599×10^6 n-m/rad	f_n=0.5 Hz k=2.499×10^4 n-m/rad	f_n=3 Hz k=8.996×10^5 n-m/rad
Floated Pallet 1 Hz Control Loop	f_n=8 Hz k=1.73×10^8 n-m/rad K=2.313×10^6 n/m	None required as long as rigid (i.e., 8 Hz) section corresponds to approximately 30 percent of the total pallet inertia	f_n=4 Hz k=2.93×10^7 n-m/rad K=5.784×10^5 n/m

Table 6-3. Inside-Out Gimbal System (IOG)

ADVANTAGES	DISADVANTAGES
• Projected to be the minimum weight option. • Does not require payload mass balance. • Projected to be minimum cost option. However, it is not at all apparent that the IOG would result in overall minimum program cost. • Does not require a stiff pallet. • Does not require pallet suspension. • Shuttle attitude can be maintained by RCS. • Does not require accurate roll (i.e., about telescope line-of-sight) stabilization if consistant with experiment requirements.	• Sensors should be mounted on telescope in order to minimize the telescope and gimbal/interface stiffness requirements for stability. This would force an IPS/experiment mechanical and electrical interface detracting from the IOG utility as a piece of experiment accommodation equipment. • Severe stiffness requirements on the total telescope structure and telescope gimbal interface result, even if sensors are mounted on the telescope. • High gimbal/pallet and telescope stiffness required for stability. Hence, must be designed with proper margins. • If flexible body compensation is to be employed in order to achieve stability while alleviating telescope and gimbal stiffness requirements, the resulting design would have to be performed for each payload individually, thus making the IOG extremely payload sensitive. • Since loop bandwidths of 2 Hz or better are required for meeting system performance, phase stabilization techniques would be needed for flexible body compensation. This requires an accurate knowledge of flexible body characteristics which can possibly necessitate an on-board measuring system. • Slewing payloads in excess of 10^3 kg-m^2 to perform earth point tracking is not feasible if pedestal motions and isolator elongations are to be kept within tolerable limits. • Since the IOG mounts to the back end of the telescope, large volumes are swept out as the telescope is positioned, making the mounting of multiple telescopes difficult.

Table 6-3. Inside-Out Gimbal System (IOG) (Concluded)

ADVANTAGES	DISADVANTAGES
	• Acquisition star trackers would be required for each telescope since accurate location of one telescope with respect to the other would be difficult in light of the IOG shockmount. This is aggravated as the shockmount is made softer, as is presently indicated (i.e., the shockmount stiffness should be reduced by a factor of 20 to 30 from the present nominal stiffness value of 10^4 n/m). • Separate servos and retention/releasing mechanism would be required for each IOG. • Shuttle attitude would be maintained by a hypergolic RCS, thus maximizing the possibility of experiment contamination. • As mission time increases, an increasing RCS weight penalty results.

Table 6-4. Standard Experiment Pointing Base (SEPB)

ADVANTAGES	DISADVANTAGES
• Does not require stiff pallet. • Does not require pallet suspension. • Shuttle attitude can be maintained by RCS. • Sensors and actuators can be and should be mounted on the SEPB inner gimbal, thus eliminating an electrical/mechanical interface present for the IOG. • Although a 3 Hz interface stiffness is required for the gimbal and the gimbal-to-telescope interface, the attach point to the telescope is at the cm. It is therefore relatively simple to attach to the telescope truss structure which is usually very stiff from optical, thermal, and dimensional stability consideration. • Would not require separate acquisition star trackers. • Telescope slewing easily achieved for a large variety of payloads and slew profiles. • Sweeps out minimum volume when positioning telescope. • System not as payload sensitive as IOG. • Does not require accurate roll (i.e., about the telescope line-of-sight) if consistant with experiment requirements.	• Requires experiment mass balance. • Projected to be heaviest of the systems considered, particularly when considering multiple telescopes. • Each telescope requires a separate SEPB. This will only allow the mounting of two telescopes without exceeding the pallet weight capability. • Shuttle attitude would be maintained by hypergolic RCS, maximizing the possibility of experiment contamination. • As mission time is extended, an increasing RCS fuel weight penalty is paid.

Table 6-5. Floated Pallet

ADVANTAGES	DISADVANTAGES
• Stabilizes total pallet to 1 sec accuracy, thus making total pallet a stable experiment carrier. • Requires only positioning gimbals for the various telescopes mounted on the pallet. Gimbals do not have to be actively servoed. This only applies to experiments that require pointing and not those that require slewing. • Does not require separate acquisition star trackers for each telescope. • Will result in minimum gimbal/telescope interface stiffness requirements (i.e., between 0.5 and 1 Hz). • Minimizes experiment contamination probability since shuttle attitude is maintained via CMGs. • As mission duration is increased, the weight penalty due to the addition of CMGs decreases. • Experiment mass balancing is not required. • System is essentially payload insensitive and is adaptable to a wide variety of payloads.	• Requires CMGs for pallet/shuttle stabilization. • Requires stiff pallet (4 Hz first significant bending mode). • Requires pallet suspension/retention system. • Requires separate servoed gimballing system to perform experiment slewing and tracking. • Requires accurate (i.e., $< \pm 1$ $\widehat{\text{sec}}$) three axis stabilization.

7. RECOMMENDED FUTURE EFFORT

The following tasks are recommended to continue and extend the investigations performed in this study to better evaluate, specify, and compare the IOG, SEPB, and Floated Pallet systems.

a. Determine the stability of the IOG system as a function of the following system parameters:

1) Suspension characteristics (i.e., stiffness and damping).

2) Telescope look angle.

3) Telescope mass and inertia characteristics.

4) Variation in telescope cm location.

5) Sensor and actuator characteristics.

6) Interface stiffness.

7) Control law structure.

The interrelationship between these parameters and their effect on IOG stability should be determined.

b. Determine the adaptability of the IOG in accommodating various projected payload performance requirements. Establish whether one suspension design would be adequate to meet the requirements for the projected payloads or multiple suspension designs would be required.

c. Establish the effects of gimbal friction, wire torques, and other pertinent gimbal nonlinearities on IOG and SEPB pointing and slewing performance.

d. Determine the effect of wire torques on the pointing performance of the Floated Pallet.

e. Determine the effects of sensor and actuator noise on the pointing performance of the IOG, SEPB, and Floated Pallet. Establish the allowable levels of these noise sources consistent with meeting ± 1 $\widehat{\text{sec}}$ pointing stability.

f. Determine the effects of sampling and quantization on the pointing performance of the IOG, SEPB, and Floated Pallet. Establish the required sampling rate and quantization levels that would yield satisfactory system performance.

g. Define in detail the hardware complement required for the IOG, SEPB, and Floated Pallet concepts. Particular emphasis should be given to determining the hardware needed for multiple telescope operation. In addition, the modifications to the pallet structure required to yield the needed stiffness for satisfactory Floated Pallet stability and pointing performance be defined in enough detail to make an accurate evaluation of the level of effort involved.

h. Perform a detailed cost analysis of the IOG, SEPB, and Floated Pallet systems in order to enable the optimum choice or possible choices of Instrument Pointing Systems.